Characterization of Metabolic Glycoengineering in Mesenchymal Stromal Cells for its Application in thermoresponsive Bioinks

Charakterisierung von *Metabolic Glycoengineering* in mesenchymalen Stromazellen für die Anwendung in thermoresponsiven Biotinten

Doctoral Thesis for a Doctoral Degree
at the Graduate School of Life Sciences,
Julius-Maximilians-Universität Würzburg,
Section Biomedicine

submitted by

Stephan Altmann

from

Berlin

Würzburg 2022

Submitted on: ……..……..

Office stamp

Members of the Thesis Committee

Chairperson:	**Prof. Dr. Carmen Villmann**
Primary Supervisor:	**Prof. Dr. Regina Ebert**
Second Supervisor:	**Prof. Dr. Jürgen Seibel**
Third Supervisor:	**Prof. Dr. Stephan Gekle**

Date of Public Defence: ……..……..

Date of Receipt of Certificates: ……..

Table of Content

Summary III

Zusammenfassung V

Introduction 1

Mesenchymal Stromal Cells and their Potential for medical Applications 1

Glycocalyx as Target Structure for specific Modifications 2

Metabolic Glycoengineering as versatile Tool to modify the Cell Glycocalyx 4

3D Bioprinting for the Generation of functional Tissues 7

Shear Stress as a potential Threat for Cell Viability during Bioprinting 9

Galectin 1 as Target for tailored Ligands in Biofabrication Approaches 11

Aims of this Work 13

Materials & Methods 14

General 14

Cell Culture 14

Cell Viability & Apoptosis Assays 14

Live/Dead Assay 15

Immunocytochemical Staining 15

Adipogenic & Osteogenic Differentiation 16

Histochemical Staining 16

RNA Isolation, Reverse Transcription & qPCR Analysis 17

Qualitative PCR Analysis & Gel Electrophoresis 17

Introduction of Target Molecules into the Cell Glycocalyx via Click Reaction 18

Fluorescence Imaging after Click Reaction on the Cell Surface 20

Shear Flow Deformation Cytometry 20

Bioprinting 21

Luciferase Assay 21

Data Processing 22

Results 23

Impact of Click Reagents on the Cell Viability 23

Impact of Modified Monosaccharides on Mesenchymal Differentiation and Gene Regulation 26

Evaluation of Modified Monosaccharides regarding their Incorporation and Retention in the Glycocalyx 29

Detection of Galectin 1 as Binding Target for artificial Ligands 35

Effects of Metabolic Glycoengineering on biophysical Cell Features 36

Impact of the Bioprinting Process on the Cell Behavior 36

Discussion 41
Primary hMSC revealed superior Cell Viability upon Incubation with Click Sugars than hMSC-TERT 41
Metabolic Glycoengineering does not alter the Phenotype of hMSC-TERT 42
Modified Mannose Sugars showed superior Potential for Metabolic Glycoengineering in hMSC or hMSC-TERT 43
Incorporation of Target Molecules into the Glycocalyx increases the Cell Stiffness 47
Stable Galectin 1 Expression in hMSC or hMSC-TERT supports the Application of tailored Galectin 1 Ligands 48
Thermoresponsive Bioinks exhibit good Cytocompatibilities with hMSC-TERT after Bioprinting 49
Thermoresponsive Bioinks induced minimal Mechanotransduction in hMSC-TERT 50
Conclusion 52
Bibliography 54
Annex 68
List of Figures 68
List of Tables 69
Statement on Copyright & Self-Plagiarism 70
Affidavit 71
Acknowledgements 72

Summary

This work developed during the first funding period of the subproject B05 in the framework of the interdisciplinary research consortium TRR 225 'From the Fundamentals of Biofabrication toward functional Tissue Models' and was part of a cooperation between the Orthopedic Department represented by Prof. Dr. Regina Ebert and the Institute of Organic Chemistry represented by Prof. Dr. Jürgen Seibel.

This project dealed with cellular behavior during the bioprinting process and how to influence it by modifying the cell glycocalyx with functional target molecules. The focus was on the impact of potential shear stress, that cells experience when they get processed in thermoresponsive bioinks, and a way to increase the cell stiffness via metabolic glycoengineering to attenuate shear forces. For the characterization of the metabolic glycoengineering, four different peracetylated and four non-acetylated modified monosaccharides (two mannose and two sialic acid sugars) were tested in primary human mesenchymal stromal cells (hMSC) and telomerase-immortalized hMSC (hMSC-TERT). Viability results demonstrated a dose-dependent correlation for all sugars, at which hMSC-TERT seemed to be more susceptible leading to lower viability rates. The assessment of the incorporation efficiencies was performed by click chemistry using fluorescent dyes and revealed also a dose-dependent correlation for all mannose and sialic acid sugars, while glucose and galactose variants were not detected in the glycocalyx. However, incorporation efficiencies were highest when using mannose sugars in the primary hMSC. A subsequent analysis of the temporal retention of the incorporated monosaccharides showed a constant declining fluorescence signal up to 6 d for azido mannose in hMSC-TERT, whereas no signal could be detected for alkyne mannose after 2 d. Investigation of the differentiation potential and expression of different target genes revealed no impairment after incubation with mannose sugars, indicating a normal phenotype for hMSC-TERT. Following the successful establishment of the method, either a coumarin derivative or an artificial galectin 1 ligand were incorporated into the cell glycocalyx of hMSC-TERT as functional target molecule. The biophysical analysis via shear flow deformation cytometry revealed a slightly increased cell stiffness and lowered fluidity for both molecules. A further part of this project aimed to control lectin-mediated cell adhesion by artificial galectin 1 ligands. As that hypothesis was settled in the work group of Prof. Dr. Jürgen Seibel, this work supported with an initial characterization of galectin 1 as part of the hMSC biology. A stable galectin 1 expression at gene and protein level in both hMSC and hMSC-TERT could be confirmed, at which immunocytochemical stainings could detect the protein only in the glycocalyx. The treatment of hMSC-TERT with a galectin 1 ligand in different concentrations did not show an altered gene expression of galectin 1. However, these first data in addition to the investigation of stiffness confirmed the applicability of specific and artificial

galectin 1 ligands in biofabrication approaches to alter cell properties of hMSC. To conclude, metabolic glycoengineering has been successfully implemented in hMSC and hMSC-TERT to introduce glycocalyx modifications which reside there for several days. A proof of concept was carried out by the increase of cell stiffness and fluidity by the incorporation of a coumarin derivative or an artificial galectin 1 ligand.

For the characterization of shear stress impact on cells after printing in thermoresponsive bioinks, the processing of hMSC-TERT (mixing or additionally printing) with Pluronic F127 or Polyoxazoline-Polyoxazine (POx-POzi) polymer solution was investigated. While there were no changes in viability when using POx-POzi bioink, processing with Pluronic F127 indicated slightly lower viability and increased apoptosis activity. Assessment of cellular responses to potential shear stress showed no reorganization of the cytoskeleton independent of the bioink, but highly increased expression of the mechanoresponsive proto-oncogene c Fos which was more pronounced when using Pluronic F127 and just mixed with the bioinks. Interestingly, processing of the mechanoresponsive reporter cell line hMSC-TERT-AP1 revealed slightly elevated mechanotransduction activity when using POx-POzi polymer and just mixed with the bioinks as well. In conclusion, hMSC-TERT embedded in thermoresponsive bioinks might shortly experience shear stress during the printing process, but that did not lead to remarkable cell damage likely due to the rheological properties of the bioinks. Furthermore, the printing experiments also suggested that cells do not sense more shear stress when additionally printed.

Zusammenfassung

Diese Arbeit entstand aus dem Projekt B05 während der ersten Förderperiode im Rahmen des interdisziplinären Sonderforschungsbereiches TRR 225 „Von den Grundlagen der Biofabrikation zu funktionalen Gewebemodellen“ und beinhaltete eine Kooperation zwischen dem Lehrstuhl für Orthopädie repräsentiert durch Prof. Dr. Regina Ebert und dem Institut für Organische Chemie repräsentiert durch Prof. Dr. Jürgen Seibel.

Das Projekt beschäftigte sich mit den Auswirkungen des 3D Drucks auf Zellen während und nach dem Druck mit thermoresponsiven Biotinten. Hierbei lag der Fokus auf Scherkräften, die Zellen während des Drucks erfahren, und der Möglichkeit, deren nachteilige Auswirkungen durch gezielte Erhöhung der Zellsteifigkeit via *Metabolic Glycoengineering* zu minimieren. Zur Etablierung dieser Methode wurden vier azetylierte sowie vier nicht-azetylierte modifizierte Einfachzucker (zwei Mannosen und zwei Sialinsäuren) hinsichtlich ihrer Zellkompatibilität und Einbaurate in primären humanen mesenchymalen Stromazellen (hMSC) und Telomerase-immortalisierten hMSC (hMSC-TERT) charakterisiert. Bei der Viabilität zeigte sich für alle untersuchten Zucker ein konzentrationsabhängiges Verhalten, wobei die hMSC-TERT generell empfindlicher reagierten. Eine Untersuchung von verschiedenen Zielgenen nach Zuckerinkubation gab keine Hinweise auf biologisch veränderte Expressionsmuster und auch das phänotypische Differenzierungspotenzial (adipogen und osteogen) blieb erhalten. Der Einbau der modifizierten Zucker in Proteoglykane sowie Glykoproteine der Glykokalyx wurde mikroskopisch mittels Fluoreszenzfarbstoffen charakterisiert. Dabei zeigte sich ebenfalls ein konzentrationsabhängiges Verhalten für alle Mannosen und Sialinsäuren, wohingegen die Glukose- und Galaktosevarianten nicht nachgewiesen werden konnten. Die Mannosezucker zeigten die höchsten Einbauraten, welche in primären hMSC noch stärker ausfielen als in hMSC-TERT. Ein Langzeitversuch zur Beurteilung der zeitlichen Stabilität der Glykokalyxmodifikation konnte für die azetylierte Azidomannose ein abnehmendes Fluoreszenzsignal bis zum sechsten Tag nach der Klickreaktion ermitteln. Im Gegensatz dazu konnte die azetylierte Alkinmannose bereits ab dem zweiten Tag nicht mehr nachgewiesen werden. Nach der erfolgreichen Optimierung der Methodik wurde der Effekt eines Kumarinderivates oder eines künstlichen Galektin 1 Liganden auf die Zellsteifigkeit sowie die -fluidität mit Hilfe der Deformationszytometrie untersucht. Die Modifikation der Glykokalyx mit beiden untersuchten Molekülen führte zu einer leichten Erhöhung der Steifigkeit in Kombination mit einer leicht erniedrigten Fluidität. In einem weiteren Teil des Projekts sollte die Lektin-vermittelte Adhäsion von Zellen an Polymerstränge initiiert werden, indem sie mit künstlichen Galektin 1 Liganden modifiziert werden. Da diese Hypothese in der Forschungsgruppe von Prof. Dr. Jürgen Seibel bearbeitet wurde, unterstützte diese Arbeit mit einer anfänglichen Charakterisierung von Galektin 1 als Teil der hMSC Zellbiologie. In hMSC und hMSC-TERT konnte eine

stabile Expression auf Gen- und Proteinebene nachwiesen werden, wobei das Lektin in der Glykokalyx lokalisiert war. Ein Inkubationsversuch mit einem spezifischen Liganden zeigte in hMSC-TERT unabhängig von der Konzentration keine veränderte Galektin 1 Genexpression. In Verbindung mit den Steifigkeitsuntersuchungen bestätigt diese anfängliche Charakterisierung die Anwendbarkeit von künstlichen Galektin 1 Liganden in der Biofabrikation um hMSC zu modifizieren. Somit konnte gezeigt werden, dass *Metabolic Glycoengineering* sich für die gezielte Einbringung von Molekülen in die Zellglykokalyx von primären hMSC sowie der entsprechenden TERT-Zelllinie zur mittelfristigen Modifikation eignet. Dies wurde durch einen funktionellen Ansatz bestätigt, indem die Zellsteifigkeit und -fluidität durch den Einsatz zwei verschiedener Moleküle erwartungsgemäß beeinflusst wurden.

Für die Charakterisierung der Scherstressauswirkungen auf Zellen nach 3D Druck in thermoresponsiven Biotinten wurden hMSC und hMSC-TERT in Pluronic F127 oder Polyoxazolin-Polyoxazin (POx-POzi) Polymerlösung prozessiert (gemischt oder zusätzlich verdruckt) und direkt danach analysiert. Während letztere die Viabilität nicht verschlechterte, zeigten hMSC-TERT nach Verarbeitung in Pluronic F127 eine leicht erniedrigte Viabilität sowie leicht erhöhte Apoptoseraten. Im Zuge von Analysen der Mechanotransduktion und deren Auswirkungen konnte unabhängig von der Biotinte sowie der Behandlung kein Umbau des Zytoskeletts immunzytochemisch nachgewiesen werden. Im Gegensatz dazu zeigten Genexpressionsanalysen eine starke Hochregulierung des mechanoresponsiven Proto-Onkogens c Fos unter allen Bedingungen, wobei diese stärker ausfiel bei Verwendung der Pluronic F127 Biotinte und nur nach Mischen (gilt für beide Biotinten). Um den Scherstress quantitativ zu beurteilen, wurde die Reporterzelllinie hMSC-TERT-AP1 verwendet, welche das Auslesen der Mechanotransduktion durch eine gekoppelte Luziferase-Proteinexpression ermöglicht. Interessanterweise zeigte sich eine leicht erhöhte Luziferaseaktivität nur nach Verarbeitung mit der POx-POzi Polymerlösung, welche stärker ausfiel wenn die Zellen mit der Biotinte lediglich gemischt wurden. Zusammengenommen bestätigten die Ergebnisse die zelluläre Wahrnehmung von Scherstress in thermoresponsiven Biotinten, allerdings scheint dieser nur schwache Auswirkungen auf die Zellen zu haben, was auf die rheologischen Eigenschaften beider untersuchten Biotinten zurückgeführt werden kann. Die Druckergebnisse legten außerdem nahe, dass die Zellen nicht mehr Scherstress erfahren, wenn sie zusätzlich verdruckt wurden.

Introduction

Mesenchymal Stromal Cells and their Potential for medical Applications

Human mesenchymal stromal cells (hMSC) are a heterogeneous population of adult precursor cells, which have self-renewal [1] and multilineage differentiation capacities. Minimal criteria to define hMSC *in vitro* [2] comprise their plastic adherence, the expression of specific mesenchymal surface markers as well as the absence of hematopoietic surface markers [3,4], and their capacity to differentiate toward the osteogenic, adipogenic, and chondrogenic lineage [5,6]. These cell characteristics point to a strong potential for regeneration and repair processes within the body besides the contribution toward tissue maturation. In addition to a direct cell-to-cell contact, hMSC initialize many modulatory biological effects by secreting bioactive molecules [7] often packed in extracellular vesicles as carriers [8]. In that way, hMSC contribute to tissue maturation and regeneration by adapting to their microenvironment resulting in specific modes of action (**Figure 1**).

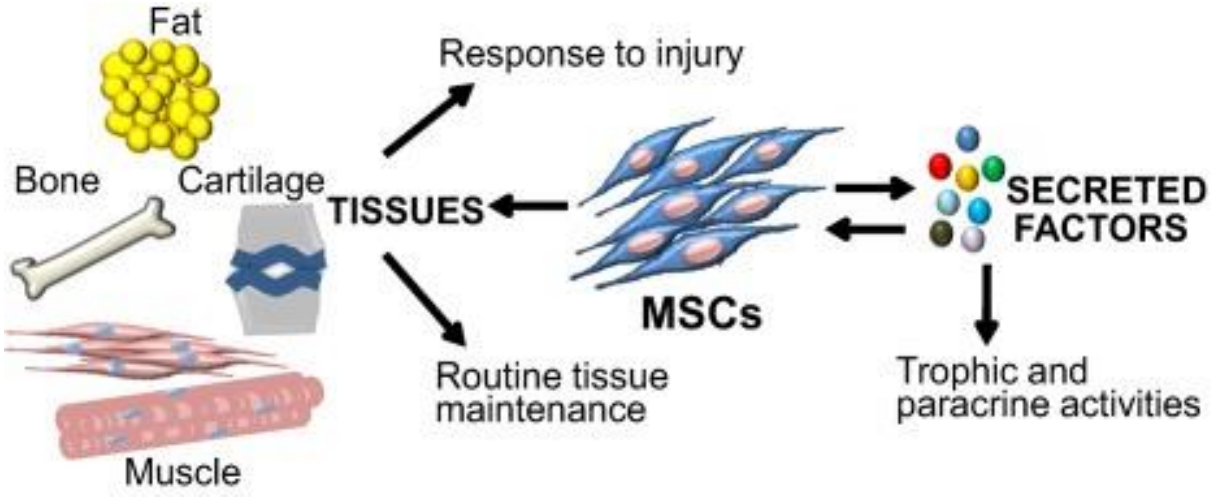

Figure 1: Mesenchymal Stromal Cells (MSC) as Interface between Tissue Maturation, Regeneration, and Repair. In addition to their mesodermal commitment to build up musculoskeletal tissues, MSC are competent to influence other cells as well through their secretome, which acts in auto- and paracrine ways. This figure was reproduced from Samsonraj *et al*. [9], which was published as an open access article under the terms of the Creative Commons Attribution-NonCommercial-NoDerivatives 4.0 License.

Especially this regenerative potential raised widespreaded interest of clinical researchers in medical applications of hMSC and their extracellular vesicles. Thus, a plethora of clinical trials and animal studies demonstrated immunosuppressive properties (*e. g*. hMSC ameliorated graft-versus-host disease after allogeneic transplantation of hematopoietic stem cells [10-12] or knockdown of galectin 1 in hMSC partially restored proliferation of T cells [13]) and anti-inflammatory properties (*e. g*. hMSC modulated leukocytes and cytokine levels attenuating inflammation response in murine lung cells after injury [14-16]). Furthermore, anti-apoptotic properties (*e. g*. hMSC inhibited expression of proapoptotic genes in corneal epithelial cells after injury [17,18]), anti-oxidative properties (*e. g*. hMSC

increased activity of anti-oxidative enzymes in murine lung cells after injury [19]) as well as proangiogenic effects (*e. g*. hMSC-derived conditioned medium stimulated directed migration of human endothelial cells [20]) have been shown.

However, working with primary cell material from patients or animals comes with some uncertainties as geno- and phenotypes on single cell level might vary due to heterogeneity of the cell population, which is influencing the reproducibility of experimental outcomes. In addition to this donor-derived heterogeneity determined by sex, age, and health status [21], cultivation period of primary hMSC is limited due to the normal process of replicative senescence when cultured *in vitro* [22-24]. These conditions increase effort and demand more time especially for the establishment of standardized procedures. A possible and well established alternative to primary cell material is the use of an appropriate cell line, in this case telomerase-immortalized hMSC (hMSC-TERT). The overexpression of telomerase overrides replicative senescence and the cells display a high proliferation rate while maintaining their mesenchymal differentiation capacity [25]. This work used mainly hMSC-TERT accompanied by primary hMSC from surgery if available and additionally hMSC-TERT-AP1 as mechanoresponsive reporter cell line [26] for bioprinting experiments.

Glycocalyx as Target Structure for specific Modifications

The glycocalyx (also pericellular matrix) is a highly versatile molecular network mainly comprising proteoglycans and glycoproteins covering the whole cell membrane (**Figure 2**). The former are composed of membrane core proteins like syndecan, or glypican, and covalently bound glycosaminoglycan chains typically linked to serine residues [27,28]. The group of glycosaminoglycans contain hyaluronan, chondroitin sulfate, heparan sulfate, and keratan sulfate, which are long linear heteropolysaccharides consisting of repeated disaccharide units comprising a hexosamine and an uronic acid (or galactose in case of keratan sulfate) [29-32]. Heparan sulfate has shown to be the most abundant glycosaminoglycan in the glycocalyx [33] and is heavily sulfated like chondroitin sulfate and keratan sulfate as well providing them an overall negative charge. Although hyaluronan is not covalently bound to the cell surface, its tethering is possible mostly mediated through cluster of differentiation 44 receptors [34]. In contrast to the molecular composition, the glycocalyx ultrastructure is not fully understood yet. An early model assumes the core proteins as bush-like structures to be arranged in a regular hexagonal pattern with spacings of 100 nm [35], while the thickness may vary from some hundred nanometers up to several micrometers [36-40]. Further investigations indicate a non-uniform glycosaminoglycan distribution at the vertical level [36] and a more dense and rigid sublayer of the glycocalyx [36,41] suggesting that hyaluronan chains play a cushioning role by distributing shear forces over the glycocalyx [42]. Besides proteoglycans,

glycosylation pattern of glycoproteins contribute to the glycocalyx structure as well, since studies revealed co-localization of clustered *N*-acetylglucosamine (GlcNAc)-glycosylated transmembrane proteins with lipid rafts [43] or a positively correlation of mucin rigidity with the glycosylation degree [44].

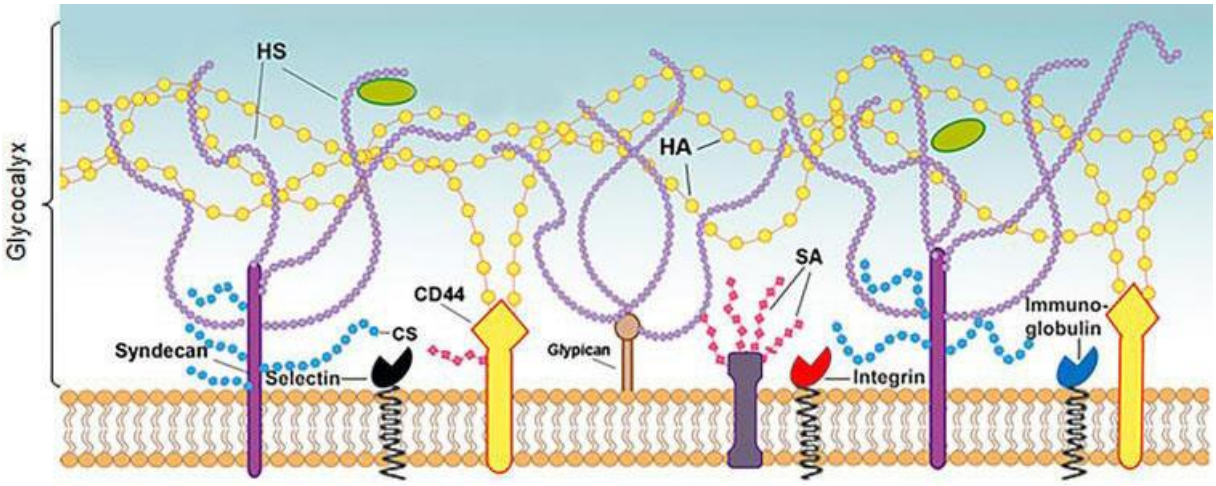

Figure 2: Schematic Model of the Cell Glycocalyx. Glycosaminoglycans like hyaluronan (HA), heparan sulfate (HS) or chondroitin sulfate (CS) are more or less covalently bound to core proteins forming proteoglycans and interact with free extracellular molecules (green ellipses) in the periphery, while the base is covered with functional glycoproteins that are highly covered with sialic acid (SA) residues. The depicted selectin (black structure) points to an endothelial or hematopoietic cell origin. CD 44: Cluster of differentiation 44. This figure was reproduced and adapted from Harding *et al*. [45] with permission from IOS Press (http://dx.doi.org/10.3233/BIR-180205).

As the outermost layer of the cell, the glycocalyx exhibits different important functions related to interactions with the cell environment. Thus, it functions as an additional physical barrier [46,47] providing a sieving effect for extracellular molecules [46], which becomes most prominent in endothelial cells constantly exposed to a plethora of macromolecules. This property also regulates endocytotic processes [48-50] and highly affects cell adhesion [51,52] since studies showed glycocalyx-mediated steric hindrance regarding cell-cell contacts [53-55]. The glycocalyx further plays a strong role in immunogenicity and –modulation [56], which are mainly mediated through sialic acid residues. Especially tumor cells are known to evade immunosurveillance by the expression of specific glycosylation patterns on their cell surface [57,58]. As example for signaling, the transduction of shear stress toward the underlying cytoskeleton demonstrates the glycocalyx as a fine-tuned sensory system. This system plays an important role in the regulation of blood pressure, as endothelial cells control vasodilation by the release of nitric oxide in response to higher shear forces [59-62]. These functions and the glycocalyx characteristics are strongly influenced by the specific cell environment, resulting in very variable states adapted to the local physicochemical conditions (*e. g*. nutrition supply [63] or matrix stiffness [64]). Due to its biochemical importance and its ease of accessibility for experimental manipulations, the cell glycocalyx offers great potential as target for questions in basic and biomedical research.

Metabolic Glycoengineering as versatile Tool to modify the Cell Glycocalyx

Metabolic glycoengineering represents an easy-to-use and versatile tool for the investigation or modification of glycosylated macromolecules *in situ* and involves two different steps. The first one is the incorporation of monosaccharides bearing unnatural functional groups such as azides or alkynes into macromolecules as part of the glycosylation process (**Figure 3**). In detail, incubation of the target cells with these modified sugars lead to their active uptake via membrane transporters [65,66] into the cytosol, where an activation with nucleotides is necessary for the relocation into the Golgi apparatus via nucleotide sugar transporters [67-69]. The cellular uptake can be enhanced by the use of acylated sugars as the resulting increased lipophilicity promotes passive membrane diffusion [70,71]. Intracellularly, unspecific esterases remove the *O*-linked short chain fatty acids [72] enabling the monosaccharides to enter enzymatic processes. In case of mannose sugars, they are primarily converted to sialic acid [73] via three enzymatic steps and its activation by linkage with a cytidine monophosphate residue takes place in the nucleus [74]. After initiation of the glycosylation process in the endoplasmic reticulum, several glycosidases as well as glycosyltransferases [75] proceed the work in the Golgi apparatus by removing sugar moieties from or transferring them onto glycoconjugates resulting in their maturation. According to the binding site in case of proteins, some of them remain in the cytosol or cell organelles [76], while the majority gets transferred to the cell membrane, where they are secreted or become parts of the glycocalyx. Although there are different sites for modified monosaccharides to enter the sialic acid pathway (**Figure 3**), their design should also consider natural restrictions related to substrate specificity, which is especially important for the two enzymes glucosamine (UDP-*N*-acetyl)-2-epimerase/*N*-acetylmannosamine kinase (GNE) [77] and *N*-acetylneuraminic acid synthase (NANS) [78] as control points in the sialic acid pathway. For the latter, analyses with different *N*-acetylmannosamine analogs revealed an impaired conversion for longer or bigger *N*-acyl side chains demonstrating a steric hindrance issue [79]. Although the glycosylation process cannot be controlled *per se*, parameters such as the incorporation efficiency or cell viability can be optimized by adjusting the methodic conditions [80]. This is even more important when glycoengineered cells are used for *in vivo* purposes, in which the quality of the glycoengineering affects subsequent cell behavior in specific environments or situations.

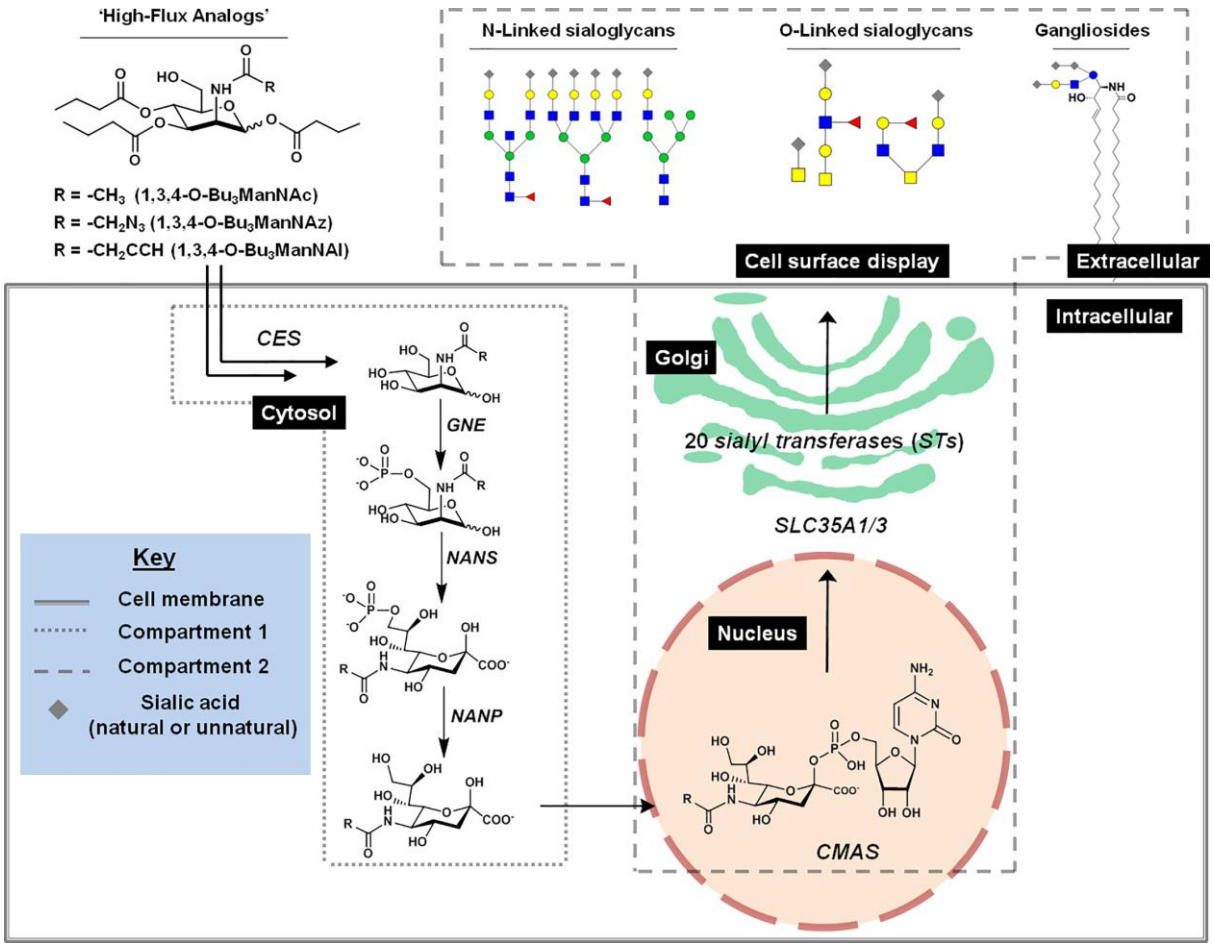

Figure 3: Principle of Metabolic Glycoengineering. The cells are incubated with modified monosaccharides (*e. g*. tributyl *N*-acetylmannosamine (Bu_3ManNAc) analogs), which are intracellularly processed in different cell compartiments and finally integrated via the glycosylation pathway into the cell glycocalyx as part of glycoconjugates. CES: Carboxylesterases, GNE: Glucosamine (UDP-*N*-acetyl)-2-epimerase/*N*-acetylmannosamine kinase, NANS: *N*-acetylneuraminic acid synthase, NANP: *N*-acylneuraminate-9-phosphatase, CMAS: Cytidine monophosphate *N*-acetylneuraminic acid synthetase, SLC35A1/3: Solute carrier family 35 member A1 (CMP-sialic acid transporter). This figure was reproduced from Saeui *et al*. [81], which was published as an open access article under the terms of the Creative Commons Attribution License.

Once incorporated into the cell glycocalyx, these modified monosaccharides are accessible for click chemistry, which allows the conjugation of target molecules dependent on the respective scientific question in the second step. The term 'click chemistry' comprises a class of chemical reactions that are simple, stereospecific, and efficient yielding high product amounts with low byproduct rate. This reaction type typically aims for the conjugation of biomolecules with reporter or target molecules, introducing specific functionalities to the biological system. Defined by the setting, the reaction must work under physiological conditions and should be highly specific to avoid any interference with other biomolecules *in situ*, referred as 'bioorthogonal'. The latter is achieved by using unnatural chemical groups, which do not impair the natural activity of the coupled biomolecule. Out of the pool of molecular pairs suitable for click reactions, azido and alkyne groups are widely used due to some advantages like their size or rarity in biological systems. The respective click reaction represents an

azide-alkyne 1,3-dipolar cycloaddition, which results in a stable triazole (**Figure 4**). However, physiological conditions require catalysis to initiate the reaction. The copper-catalyzed azide-alkyne cycloaddition uses a mixture comprising a Cu^{II} salt and a reducing agent to provide reactive Cu^{I} species [82]. The addition of a chelating ligand further stabilizes them, resulting in much shorter reaction times and dispose reactive oxygen species [83]. To circumvent Cu-mediated cytotoxicity [84] and enable *in vivo* applications, cycloalkynes were designed providing sufficient ring strain to initiate the reaction without the need for catalysts [85,86], referred as strain-promoted azide-alkyne cycloaddition (SPAAC).

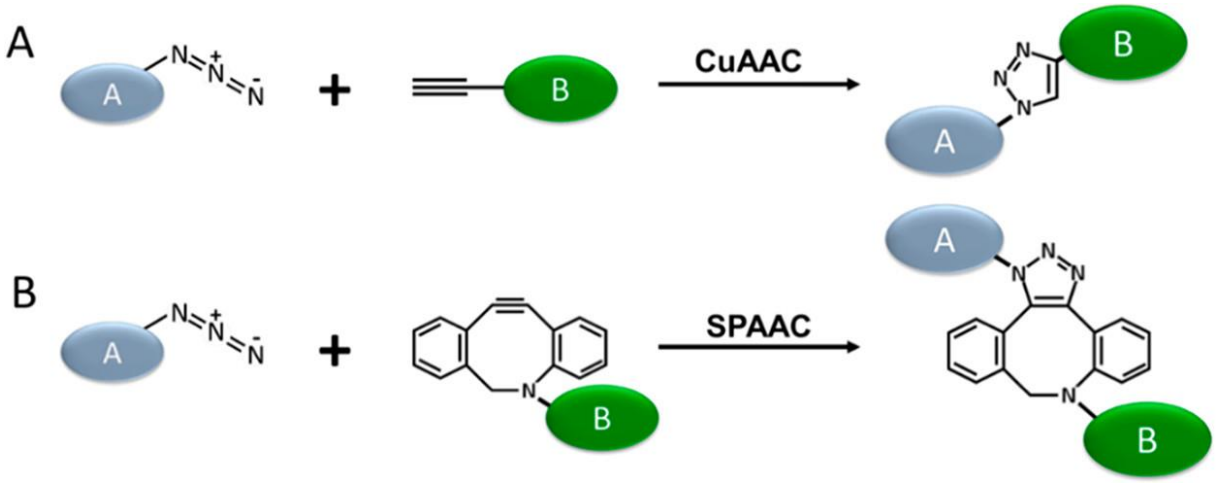

Figure 4: Principle of Azide-Alkyne 1,3-dipolar Cycloaddition (AAC) Click Reaction. (A) The Cu-mediated reaction of azides with terminal alkynes requires catalyzation via Cu^{I} ions, which are stabilized through a complexing ligand (both not shown). **(B)** The strain-promoted (SP) reaction works solely via ring strain provided by the dibenzocyclooctyne and is therefore also applicable *in vivo*. This figure was reproduced from Gutmann *et al*. [87] with permission from the American Chemical Society (https://pubs.acs.org/doi/10.1021/acsbiomaterials.8b00865).

Metabolic glycoengineering can be a useful tool in both basic and applied research. Its potential to further unravel the glycosylation pathway (*e. g*. *de novo* glycan biosynthesis during embryogenesis in zebrafish [88]) and the role of glycans (*e. g*. regulation of pluripotency in murine embryonic stem cells by *O*-GlcNAcylation of a specific transcription factor [89]) seems quite obvious and is widely used in combination with molecular imaging and glycoproteomic analyses. The medical research applies metabolic glycoengineering to alter cell characteristics or their products (*e. g*. extra cellular matrix components [90] or recombinant antibodies [91]) for different purposes. From simple cell tracking (*e. g*. surface modification of human adipose-derived stromal cells enabled the monitoring and tracking of cell fate in mice [92]) to control of cell behavior (*e. g*. the attachment capability of glycoengineered macrophages resulted in a better *in situ* cellularization of a tissue scaffold implanted in mice [93] or surface modification of the bacterium *Staphylococcus aureus* reduced adhesion to tumor cells [94]), the new features finally depend on the conjugated target molecules. In cell therapy-based

research, metabolic glycoengineering can support treatment of tumors in different ways. Either glycoengineered cells equipped with drugs deliver them to the cancer cells (*e. g*. paclitaxel-conjugated hMSC showed enhanced tumor homing and its growth inhibition in mice [80] and cetuximab-conjugated natural killer cells inhibited tumor growth in mice [95]) or cancer cells get modified and take up glycoengineered drugs (*e. g*. subsequent intratumorally injections of peracetylated *N*-azidoacetylmannosamine and dibenzocyclooctyne-functionalized RNase A inhibited tumor growth in mice [96]).

A strong advantage over genetic cell engineering is the fact, that the altered cells return to their native cell state after a while omitting any artificial modifications. However, a certain stability of the introduced new functions is necessary to define the time window for further processing of glycoengineered cells. Even though metabolic glycoengineering allows the simple incorporation of every possible target molecule, their surface exposition might lead to unwanted interferences with other biomolecules requiring a sophisticated and careful proceeding.

3D Bioprinting for the Generation of functional Tissues

In the field of tissue engineering and regenerative medicine, biofabrication represents a promising and innovative technology to generate tissue constructs in a precise and adaptable way. Classic approaches in tissue engineering use prefabricated scaffolds providing cells a suitable environment for proliferation and development. However, a main drawback poses the lack of structural hierarchy as given in natural tissues thus limiting the applicability of respective cell constructs. The extrusion-based biofabrication can overcome this issue by the use of 3D printers offering several advantages. The most obvious and important feature represents the spatial-controlled layer-by-layer fabrication of the construct allowing printing resolutions at μm range in x-, y- and z-direction. The complexity of printed constructs can be extended through additional printing heads enabling the addition of other cell types, bioinks, and specific reagents or through altered printer components like coaxial nozzles allowing the generation of tubular structures [97,98]. The basis for printing cells is their resuspension in biocompatible polymer solutions called ‘bioinks’. Natural polymers like alginate [99], hyaluronan [100], gelatin [101], or spider silk [102] as well as artificial designed ones like poloxamers (Pluronic F127 for example) or Polyoxazoline-Polyoxazine [103] are used as bioinks exhibiting similar properties. They must be viscous, incorporate water to form a ‘hydrogel’ by swelling, and should be physicochemically stable for long-term incubation post-print. The latter can be achieved by cross-linking the polymer network via ions [104-106] or photons [101] partially during the printing process or afterwards. The bioink features can be improved by the addition of specific reagents [107-111] or mixing with other polymers

resulting in blends [112-114]. Further, the polymers can be functionalized with target molecules for modifying their properties [99,115] or their interactions with the cells [116,117].

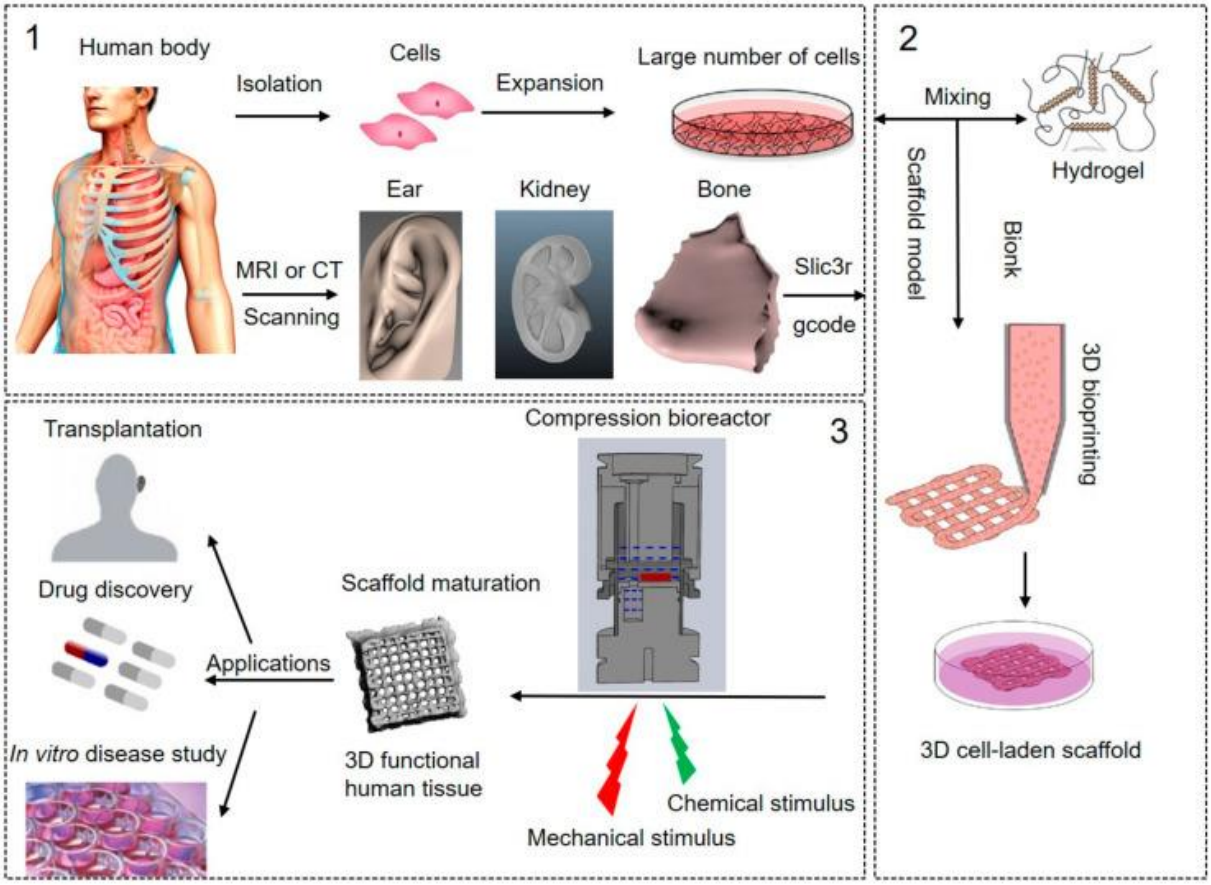

Figure 5: Biofabrication Steps in Tissue Engineering. (1) Preparation of cells and printing model. MRI: Magnetic resonance imaging, CT: Computed tomography. **(2)** Bioprinting process. **(3)** Maturation of tissue construct and its different applications. This figure was reproduced from Zhang *et al.* [118], which was published as an open access article under the terms of the Creative Commons Attribution License.

For individual therapy approaches involving tissue engineering, patients' cells are isolated, expanded and eventually modified *in vitro* prior to the cell loading of a scaffold and its subsequent maturation. The biofabrication principally works the same way, just adding the step of 3D printing replacing prefabricated scaffolds (**Figure 5**). The maturated cell constructs can either be transplanted into the patient or serve for personalized *in vitro* studies like drug testing. Besides treatment of patients, printed cell constructs offer a great potential in research to replace 2D cell models as well as animal models improving experimental outcomes [119] and ethical standards. The field of biofabrication is still in its early years, thus the research focus is on the design of suitable bioinks, optimization of printing process parameters, and characterization of printed constructs with simple geometry and less cell types; leaving fully functional tissue constructs exhibiting an organ-like hierarchy as a future goal. Currently, several biofabrication studies aim to generate disease (*e. g.* composite hydrogel lung model allowed for investigation of pathogenic mechanism of an influence A virus strain [120]) or tumor

models (*e. g*. breast cancer cells MDA-MB-231 remodeled the extracellular matrix within a printed adipose tissue construct [121]). Bioprinted cell constructs have already been used as simple transplants to imitate specific tissue functions (*e. g*. transplantation of a printed hepatorganoid prolonged survival of fumaroylacetic acid hydrolase-deficient mice suffering chronic liver injury without intervention [122]). Furthermore, they can support different biological processes like regeneration or immunosurveillance by serving as repositories for bioactive substances (*e. g*. composite hydrogel supported neomeniscal regeneration in rabbits by release of chemokines and chondroinductive kartogenin [123] or impaired bacterial infection in mice after craniotomy by release of antibiotics [124]). A big challenge in biofabrication is still the printing of fine and branched capillaries ensuring the nutrition and oxygen supply of encapsulated cells within the hydrogel as blood vessels do in organs. Since size and proliferation of currently printed cell constructs are mainly limited by diffusion capacity of vital molecules, it is not surprising that a plethora of researchers only concentrate on the generation of vessel-like structures [97,98,125,126].

Shear Stress as a potential Threat for Cell Viability during Bioprinting

While the bioinks influence cell behavior through their physicochemical properties, the printing process *per se* adds a further challenge regarding viability by the occurence of mechanical forces. Upon the application of pressure within the printing nozzle, the bioink develops a laminar plug fluid flow profile at the front dependent on its rheological properties and the applied pressure (**Figure 6**). In that, flow velocity is highest in the center and decreases when getting closer to the edge [127]. The shear stress being the product of shear rate and viscosity exhibits a similar mathematical behavior, but in a linear fashion meaning no stress in the center and the maximum at the edge [128]. Thus, embedded cells get deformed and compressed dependent on their radial location experiencing mechanical forces of different magnitudes, which in the worst case leads to disruption of their plasma membranes. To minimize shear stress during printing and preserve cell viability, some measures can be taken. On the level of materials, bioinks have been adapted in their rheology to feature stronger shear-thinning behavior resulting in a lower viscosity when printed [127] and characterized by a more aligned flow velocity profile over the radial axis. Low polymer and cell concentrations also diminish the impact of shear forces, but might impair the final outcome attributed to bad printability or delayed cell maturation due to lacking paracrine signaling. On the technical level, printing nozzles have been adapted in their shape depicting cones resulting in a shorter residence time of cells near the edges. Additionally, the use of lower printing pressures effectively decreases shear stress, but is highly dependent on the bioink rheology and the printing nozzle geometry [129-131]. A recent approach applied multidimensional vibrations to the printing cartouche, which resulted in an evenly distributed bioink viscosity within and lower shear stress [132].

Interestingly, mechanical forces during printing can have beneficial effects. Studies demonstrated better orientation of C2C12 muscle precursor cells within the polymer network due to higher shear forces [133] or a shear force-mediated alignment of collagen fibrils of a printed cornea transplant [134]. Despite these exceptions, shear stress deriving from the printing process is generally considered to be adverse for cell viability and thus should be minimized. Most studies investigating shear stress in bioprinting focus on low concentrated alginate (< 3 % (*w*/*v*)) as well as low cell concentrations (often 1×10^6 cells/mL) [129,130,135,136] applied by many other researchers in the field of biofabrication. However, due to the evolution of the field, the materials and technologies improve, which is subsequently increasing the amount of available applications. To further elucidate shear stress in other bioinks, this work investigates its role in thermoresponsive bioinks using harsher printing conditions and higher cell concentrations.

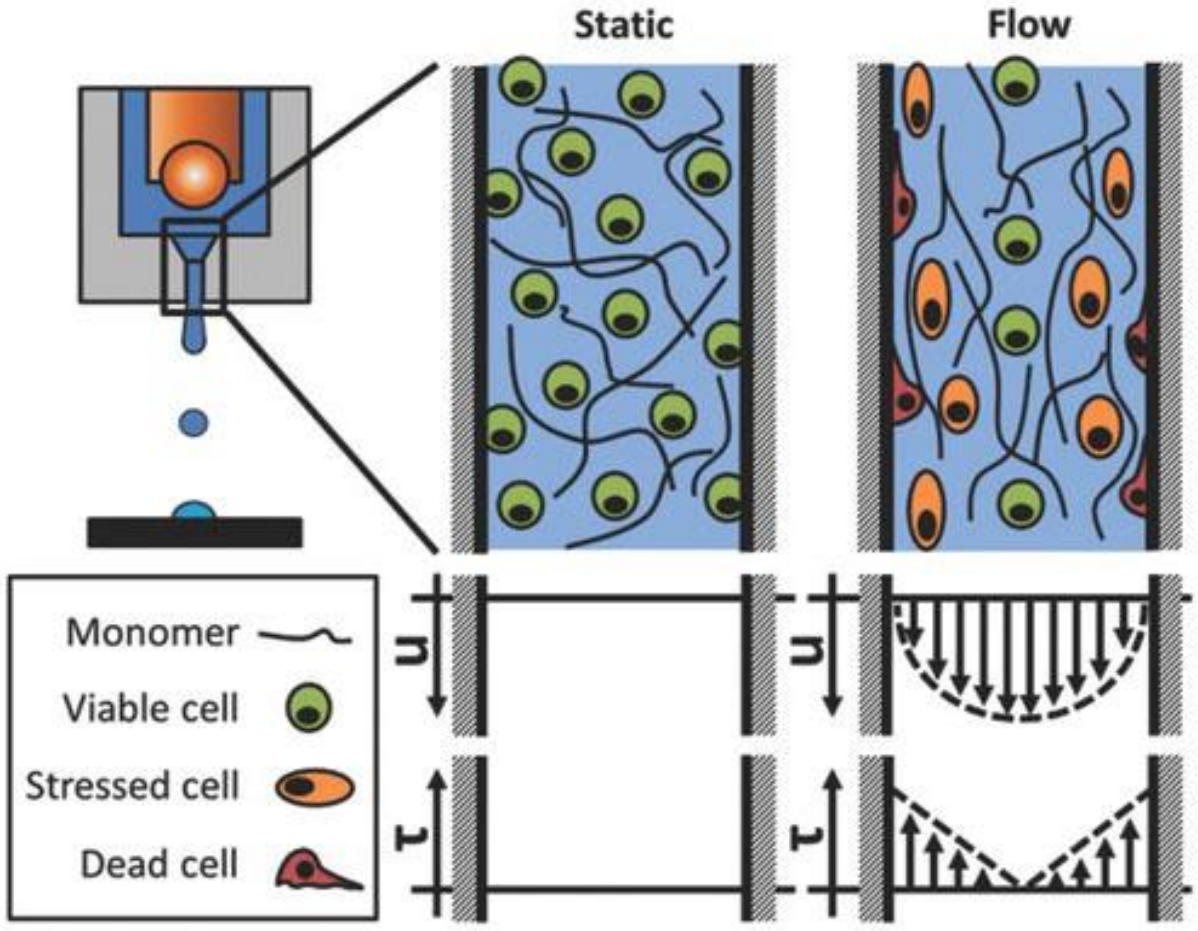

Figure 6: Shear Forces in a cylindrical Bioprinter Nozzle. Flow velocity (u) of bioink and respective shear stress (τ) acting on cells. The depicted cell behavior is also true for printing needles. This figure was reproduced from Blaeser *et al*. [135] with permission from John Wiley & Sons (https://onlinelibrary.wiley.com/doi/10.1002/adhm.201500677).

Galectin 1 as Target for tailored Ligands in Biofabrication Approaches

Upon bioprinting, the adhesion and spreading of the embedded cells in the hydrogel is important for their proliferation and subsequent maturation of the tissue construct. Not all bioinks promote cell adherence *in situ* and thus specific modifications are introduced to tackle this issue. The conjugation of the polymers with RGD peptide sequences would be the common way to increase integrin-mediated adhesion, but studies revealed that modification of bioinks with RGD peptide motifs promotes differentiation (*e. g.* osteogenesis of hMSC [137] or chondrogenesis of murine cell line ATDC5 [138]), which is not desired in this setup. Hence, alternative targets extend the possibilities and allow for additional control points in the biofabrication process. One such alternative represents galectin 1, a homodimeric protein [139], which belongs to a family that cross-links biomolecules by preferentially binding to galactosides via their carbohydrate recognition domain [140]. Although galectin 1 gets secreted in contrast to some other members, it can bind to surface glycans in the depth of the glycocalyx and reside there [141].

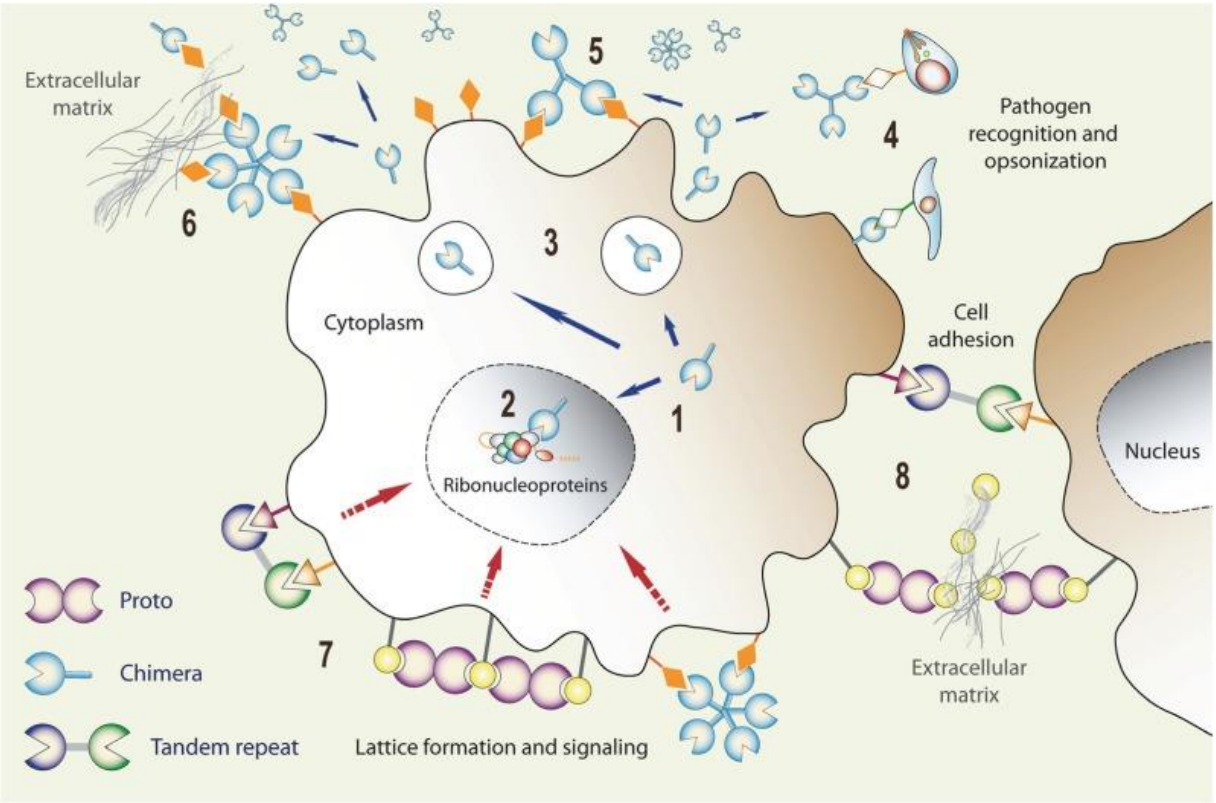

Figure 7: Binding Sites for Galectins and possible Functions. After their expression (1) and transport to the nucleus (2) or cell surface (3), galectins can recognize pathogens (4), bind to glycocalyx components, and initiate signaling cascades (5+7) or mediate interactions with extracellular matrix components (6) or other cells (8). Galectin 1 belongs to the proto type subfamily. This figure was reproduced from Vasta *et al*. [142], which was published as an open access article under the terms of the Creative Commons Attribution License.

Galectin 1 is involved in many different biological processes and functions at every developmental stage (**Figure 7**). It has been shown to promote formation (*e. g*. knockdown of a galectin 1 ortholog

impaired muscle development in zebrafish [143] and mice [144]) and regeneration of skeletal muscle tissue (*e. g*. injury of skeletal muscles led to high galectin 1 expression levels in mice [145]). Also more general processes as proliferation [146], apoptosis [147-151], differentiation [152], angiogenesis [153], hemostasis [154,155], or mRNA splicing [156] are mediated by galectin 1. Furthermore, this lectin shows strong immunomodulatory properties regarding normal cell-based [157-160] and humoral [161] immune response. However, at the same time galectin 1 seems to play a prooncogenic role identifying it as a potential target for tumor therapy. Studies showed that galectin 1 promotes tumor angiogenesis [162], interacts with oncogenic factors [163], and supports immunoevasion [164,165].

Due to its cross-linking activity, galectin 1 is strongly involved in several adhesion processes. Via interaction with cell surface receptors, it can promote [166-168] or inhibit [169] cell-cell adhesion as well as cell spreading and migration through cross-linking with extracellular matrix components like laminin [170-172], or fibronectin [173-175]. As pathogens also exhibit surface glycans, galectin 1 facilitates adsorption of viruses (*e. g*. human immunodeficiency virus [176,177]) or bacteria (*e. g. Porphyromonas* [178] or *Streptococcus* [179]) to host cells. It is this ambivalent nature, being involved in vital and abnormal processes, that identifies galectin 1 as interesting target in medical research and the framework of this project aims to expand its potential by the implementation of lectin-controlled adhesion in biofabrication approaches conducted by the work group of Prof. Dr. Jürgen Seibel.

Aims of this Work

Being set in the field of biofabrication, this biochemical work wants to investigate the role of shear stress during bioprinting in thermoresponsive bioinks and how to improve cell behavior by altering their glycocalyx via metabolic glycoengineering. In that way, two different target molecules are assessed for biological functionality.

1. Thus, the first part deals with the establishment of the glycoengineering technique in primary hMSC and hMSC-TERT and the characterization of different click sugars. The method shall be optimized in terms of experimental conditions resulting in best cell viabilities and highest incorporation efficiencies of the modified monosaccharides. Following, hMSC-TERT get modified with either a coumarin derivative or a galectin 1 ligand with subsequent characterization of the cell stiffness.

2. Since the project plans to use galectin 1 ligands for controlled adhesion in the hydrogel after printing in the future, a further part of this work provides a first characterization of galectin 1 as part of the hMSC biology by analysis of the expression of galectin 1 in primary hMSC and hMSC-TERT and its localization. Furthermore, an artificial galectin 1 ligand is tested for a potential impact on the galectin 1 gene expression of hMSC-TERT.

3. The second part investigates shear stress during the bioprinting process with thermoresponsive bioinks and its impact on cell behavior. Viabilities and expression of mechanoresponsive genes of printed hMSC-TERT are compared after printing in Pluronic F127 or POx-POzi bioink. Additionally, printing of the mechanoresponsive reporter cell line hMSC-TERT-AP1 shall elucidate the structural impact of both different bioinks on the mechanotransduction.

Materials & Methods

General

Cell culture flasks for cell cultivation were used from Thermo Fisher Scientific (Waltham, USA) and well plates for experiments from Greiner Bio-One GmbH (Frickenhausen, Germany). All chemicals were purchased from Sigma-Aldrich Chemie GmbH (Munich, Germany) if not stated otherwise.

Cell Culture

Telomerase-immortalized human mesenchymal stromal cells (hMSC-TERT) were established from a 33-year-old male donor by the work group of Prof. Dr. Moustapha Kassem (Odense University Hospital, Department of Endocrinology, Denmark). These cells show high proliferation rates, while maintaining their mesenchymal differentiation capacity *in vitro* and *in vivo* [180,181]. Cells were cultured in Eagle's Minimum Essential Medium (MEM) (Thermo Fisher Scientific, Waltham, USA) supplemented with 10 % (*v*/*v*) heat-inactivated fetal calf serum (FCS) (Bio & Sell, Ulm, Germany) [182], 50 μg mL^{-1} gentamicin sulfate, and 100 nM sodium selenite [183] at 37 °C in a 95 % humidified air and 5 % CO_2 atmosphere. hMSC-TERT-AP1 were cultured the same way, but medium was additionally supplemented with 50 μg mL^{-1} hygromycin B (Thermo Fisher Scientific, Waltham, USA). This cell line was stably transfected with a mechanoresponsive AP1 luciferase reporter gene construct [26]. Primary hMSC were isolated from patients undergoing hip joint surgery and cultured in Dulbecco's Modified Essential Medium (DMEM/F-12 (1:1) + GlutaMAX) (Thermo Fisher Scientific, Waltham, USA) supplemented with 10 % (*v*/*v*) heat-inactivated FCS (Bio & Sell, Ulm, Germany), 100 units mL^{-1} penicillin, 100 μg mL^{-1} streptomycin (both Thermo Fisher Scientific, Waltham, USA), 50 μg mL^{-1} L-ascorbic acid 2-phosphate sesquimagnesium hydrate, and 100 nM sodium selenite at 37 °C in a 95 % humidified air and 5 % CO_2 atmosphere. The procedure was approved by the local Ethics Committee of the University of Würzburg (241/17) while informed consent was obtained by the patients.

Cell Viability & Apoptosis Assays

To examine cell viability and apoptosis, hMSC-TERT or hMSC were seeded in a 96-well plate (1×10^3 cells per well) to adhere at 37 °C and 5 % CO_2 overnight. Cells were treated with peracetylated *N*-azidoacetylglucosamine (Ac_4GlcNAz), peracetylated *N*-azidoacetylgalactosamine (Ac_4GalNAz), peracetylated *N*-azidoacetylmannosamine (Ac_4ManNAz) (Jena Bioscience GmbH, Jena, Germany), peracetylated *N*-alkyneacetylmannosamine (Ac_4ManNAl), *N*-azidoacetylmannosamine (ManNAz), *N*-alkyneacetylmannosamine (ManNAl), *N*-azidoacetylneuraminic acid (hereinafter SiaNAz), or *N*-alkyneacetylneuraminic acid (hereinafter SiaNAl) (the last five monosaccharides were

provided by the work group of Prof. Dr. Jürgen Seibel, Institute of Organic Chemistry, University of Würzburg) (**Figure 8**) in different concentrations for 48 h or 72 h. For negative controls, cells were treated with either medium or with dimethyl sulfoxide (DMSO) (0.2 % *v*/*v*) (AppliChem GmbH, Darmstadt, Germany) as solvent for the peracetylated sugars. Viability and apoptosis rates were assessed using the CellTiter-Glo Luminescent Cell Viability Assay and the Caspase-Glo 3/7 Assay, respectively (both Promega GmbH, Mannheim, Germany), according to the manufacturer's instructions. Luminescence was measured with an Orion II Microplate Luminometer (Berthold Detection Systems, Pforzheim, Germany). Each reaction was performed in technical triplicates and luminescence values were averaged.

Live/Dead Assay

To evaluate the ratio of viable to dead cells, hMSC-TERT were seeded in a 24-well plate (40×10^3 cells per well) to adhere at 37 °C and 5 % CO_2 overnight. For preparation of the click mixture, Dulbecco's phosphate-buffered saline (DPBS) (AppliChem GmbH, Darmstadt, Germany) was supplemented with $CuSO_4$ (Merck KGaA, Darmstadt, Germany) in different concentrations, the respective 5-fold concentration of tris(3-hydroxypropyl-triazolylmethyl)amine (THPTA) (Carl Roth GmbH + Co. KG, Karlsruhe, Germany) as well as 2.5 mM sodium ascorbate and incubated at 37 °C for 10 min. Meanwhile, cells were washed with DPBS followed by a treatment of one well with 70 % (*v*/*v*) isopropanol (AppliChem GmbH, Darmstadt, Germany) for 5 min as negative control. Cells were incubated with the mixture at 37 °C and 5 % CO_2 for 5 min and washed three times with DPBS. After staining by using the LIVE/DEAD Cell Imaging Kit according to the manufacturer's instructions (Thermo Fisher Scientific, Waltham, USA), cells were imaged with a LEICA DMi8 fluorescence microscope (Leica Camera AG, Wetzlar, Germany) using a 10 × 0.3 NA objective.

Immunocytochemical Staining

Cells were seeded in 24-well plates (40×10^3 cells per well) provided with circular cover slips and incubated at 37 °C and 5 % CO_2 overnight to adhere. For fixation, cells were treated with a mixture of 2 % (*v*/*v*) formaldehyde (Merck KGaA, Darmstadt, Germany) and 2.5 % (*v*/*v*) glutaraldehyde at 4 °C for 10 min, followed by three washing steps with DPBS each for 30 s on a shaker. To permeabilizing the membranes, cell layers were incubated with 0.05 % (*v*/*v*) Tween 20 (AppliChem GmbH, Darmstadt, Germany) in DPBS for 15 min and washed three times. For blocking unspecific binding sites, cells were incubated with 3 % (*w*/*v*) bovine serum albumin (BSA) (AppliChem GmbH, Darmstadt, Germany) in DPBS for 30 min and washed one time, followed by an incubation with the primary antibody (**Table 1**) (diluted 1:50 in DPBS with 1 % (*w*/*v*) BSA) at 4 °C overnight or with

one unit phalloidin (diluted 1:40 in DPBS with 1 % (*w*/*v*) BSA) (Biotium, Fremont, USA) for 20 min protected from light. After three washing steps with DPBS each for 5 min on a shaker, antibody treated cell layer were incubated with secondary antibody (**Table 1**) (diluted 1:400 in DPBS with 1 % (*w*/*v*) BSA) for 1 h protected from light. After three washing steps with DPBS each for 5 min on a shaker, the cover slips were put on glass slides with Vectashield mounting medium with 4',6-diamidino-2-phenylindole (DAPI) (Vector Laboratories, Burlingame, USA) and analyzed with a ZEISS Axio Observer 7 fluorescence microscope (Carl Zeiss AG, Oberkochen, Germany) using a 10 × 0.3 NA objective.

Table 1: Antibodies (class G) used for immunocytochemical Analyses. Ig: Immunoglobulin, FITC: Fluorescein isothiocyanate.

Name	Manufacturer
Galectin-1/LGALS1 (D6O8T) Rabbit mAB	Cell Signaling Technology Inc., Danvers, USA
Goat anti-rabbit IgG-FITC: sc-2012	Santa Cruz Biotechnology Inc., Dallas, USA

Adipogenic & Osteogenic Differentiation

hMSC-TERT were differentiated by seeding 200 x 10^3 cells per well in 6-well plates, cultivated until confluence and incubated in either adipogenic differentiation medium consisting of DMEM High Glucose (Thermo Fisher Scientific, Waltham, USA), 10 % FCS (*v*/*v*), one unit mL^{-1} penicillin, 100 μg mL^{-1} streptomycin, 1 μM dexamethasone, 0.5 mM 3-isobutyl-1-methylxanthine, 1 μg mL^{-1} insulin, and 100 μM indomethacin or osteogenic differentiation medium consisting of DMEM High Glucose, 10 % FCS (*v*/*v*), one unit mL^{-1} penicillin, 100 μg mL^{-1} streptomycin (all Life Technologies GmbH), 50 μg mL^{-1} L-ascorbic acid 2-phosphate sesquimagnesium hydrate, 0.1 μM dexamethasone, and 10 mM β-glycerophosphate. After two weeks, the cells were harvested for RNA isolation and staining of intracellular lipid droplets or mineralized matrix. Cells cultured in expansion medium served as negative control and medium was changed twice a week.

Histochemical Staining

For the detection of intracellular lipid vesicles, adipogenic monolayer cultures were stained with Oil Red O solution (Merck, Darmstadt, Germany) according to the manufacturer's instructions. For the detection of calcium hydrogen phosphate and hydroxylapatite in the extracellular matrix, hMSC-TERT were fixed in methanol, stained with alkaline Alizarin Red S (1 % *w/v*) (Chroma-Schmidt GmbH, Stuttgart, Germany) for 2 min and air dried according to the manufacturer's instructions. Images were taken with an EX Z150 digital camera (Casio Computer Co, Tokyo, Japan).

RNA Isolation, Reverse Transcription & qPCR Analysis

For gene expression analyses, hMSC-TERT were seeded in 6-well plates (200×10^3 cells per well) to adhere at 37 °C and 5 % CO_2 overnight and treated with 20 μM or 50 μM of Ac_4ManNAz or Ac_4ManNAl, or with DMSO (0.2 % *v*/*v*) as negative control for 72 h. Total RNA was isolated by using NucleoSpin RNA II kit (Macherey-Nagel, Düren, Germany) according to the manufacturer's instructions. For mRNA reverse transcription, 1 μg of total RNA was used for first strand cDNA synthesis with MMLV reverse transcriptase (Promega GmbH, Mannheim, Germany) in 25 μL total volume. cDNA was diluted 1:10, and 2 μL were used for real-time qPCR with the GoTaq qPCR Master Mix (Promega GmbH, Mannheim, Germany) in 20 μL total volume. Primers were obtained from Biomers GmbH (Ulm, Germany) or in case of unknown primer sequences from Qiagen (Hilden, Germany) (see **Table 2**) for primer sequences and annealing temperatures). qPCR conditions were as follows: 95 °C for 3 min; 40 cycles: 95 °C for 10 s; respective annealing temperature for 10 s; 72 °C for 10 s; followed by melting curve analysis for specificity of the qPCR products by using the qPCR thermal cycler Professional Thermocycler Biometra (Analytik Jena AG, Jena, Germany). Each reaction was performed in technical triplicates and Ct values were averaged. Relative gene expression was calculated with the efficiency-corrected Ct model [184] using cytochrome c oxidase subunit 4 isoform 1 (COX4I1) or acidic ribosomal protein P0 (RPLP0) as reference gene.

Qualitative PCR Analysis & Gel Electrophoresis

cDNA from different hMSC donors or hMSC-TERT was used for PCR with 20 mM $MgCl_2$, 20 mM dNTP, 10 μM each sense and antisense primer (see **Table 2**) and one unit GoTaq G2 Flexi polymerase (Promega GmbH, Mannheim, Germany) in a total volume of 50 μL. PCR conditions were as follows: 94 °C for 4 min; 40 cycles: 94 °C for 30 s, respective annealing temperature for 30 s, 72 °C for 30 s; 72 °C for 10 min. Eukaryotic translation elongation factor 1 alpha 1 (EEF1A1) was used as reference gene. Amplificates were separated in an agarose gel (2 % *w/v*) (Biozym Scientific GmbH, Hessisch Oldendorf, Germany) at 120 V for 45 min using an electrophoresis chamber (PEQLAB Biotechnologie GmbH, Erlangen, Germany) and detected with a Fusion SL Vilber Lourmat Gel Documentation System (VWR International GmbH, Darmstadt, Germany).

Table 2: Primers used for Gene Expression Analyses. First sequence is sense, second is antisense.

Gene name	Gene ID	Sequence (5' - 3')	Annealing temp. [°C]	Product size [bp]
Galectin 1	LGALS1	GGAACATCCTCCTGGACTCA CAGGTTGTTGCTGTCTTTGC	60	149
Eukaryotic translation elongation factor 1 alpha 1	EEF1A1	unknown	60	unknown
Cytochrome c oxidase subunit 4 isoform 1	COX4I1	unknown	60	unknown
Acidic ribosomal protein P0	RPLP0	TGCATCAGTACCCCATTCTATCAT AGGCAGATGGATCAGCCAAGA	60	122
Alkaline phosphatase	ALPL	GTACGAGCTGAACAGGAACAACG CTTGGCTTTTCCTTCATGGTG	58	151
Bone gamma carboxyglutamate protein	BGLAP	TGACCACATCGGCTTTCAG AAGGGGAAGAGGAAAGAAGG	60	126
Fatty acid binding protein	FABP	TACTGGGCCAGGAATTTGAC GACACCCCCATCTAAGGTTATG	60	77
Peroxisome proliferator activated receptor gamma	PPARG	GTAAATCTGCGGGATGATGG TGACCTGCGCAAAGTGTATC	60	200
Fibronectin	FN1	CTGAAAGACCAGCAGAGGCA GTGTAGGGGTCAAAGCACGA	59	110
Integrin subunit alpha V	ITGAV	ATGTCACCTGGGGCATTCAG TGTTCTTGAGGTGGCCG	59	154
Heparan sulfate proteoglycan	HSPG2	GGCAAGGACTTCATCAGCCT ACTTGGATGGAACCTCTGCG	59	161
Laminin subunit gamma 2	LAMC2	CATTAGACGGCCTCCTGCAT CGCAGTTGGCTGTTGATCTG	60	115
Thrombospondin 1	THBS1	TTTGGCCAGTCCAGCAG AGAAAGGCCCGAGTATCCCT	60	108
Signal transducer and activator of transcription 1	STAT1	TGGGCTTCAGCAAGGAG GTAGGGTTCAACCGCATGGA	60	167
Epidermal growth factor receptor	EGFR	AAGGCACGAGTAACAAGC AGGGCAATGAGGACATAA	60	170
Proto-oncogene c Fos	FOS	unknown	57	unknown
Prostaglandin-endoperoxide synthase 2	PTGS2	unknown	59	unknown

Introduction of Target Molecules into the Cell Glycocalyx via Click Reaction

For the microscopic evaluation of metabolic glycoengineering, hMSC from different donors or hMSC-TERT from different passages were seeded in a 24-well plate (40×10^3 cells per well or 10×10^3 cells per well for the long-term experiments) to adhere at 37 °C and 5 % CO_2 overnight and incubated afterwards in growth medium with Ac_4GlcNAz, Ac_4GalNAz, Ac_4ManNAz, Ac_4ManNAl,

ManNAz, ManNAl, SiaNAz or SiaNAl (**Figure 8**) at different concentrations, or with DMSO (0.2 % *v*/*v*) as negative control for 48 h or 72 h.

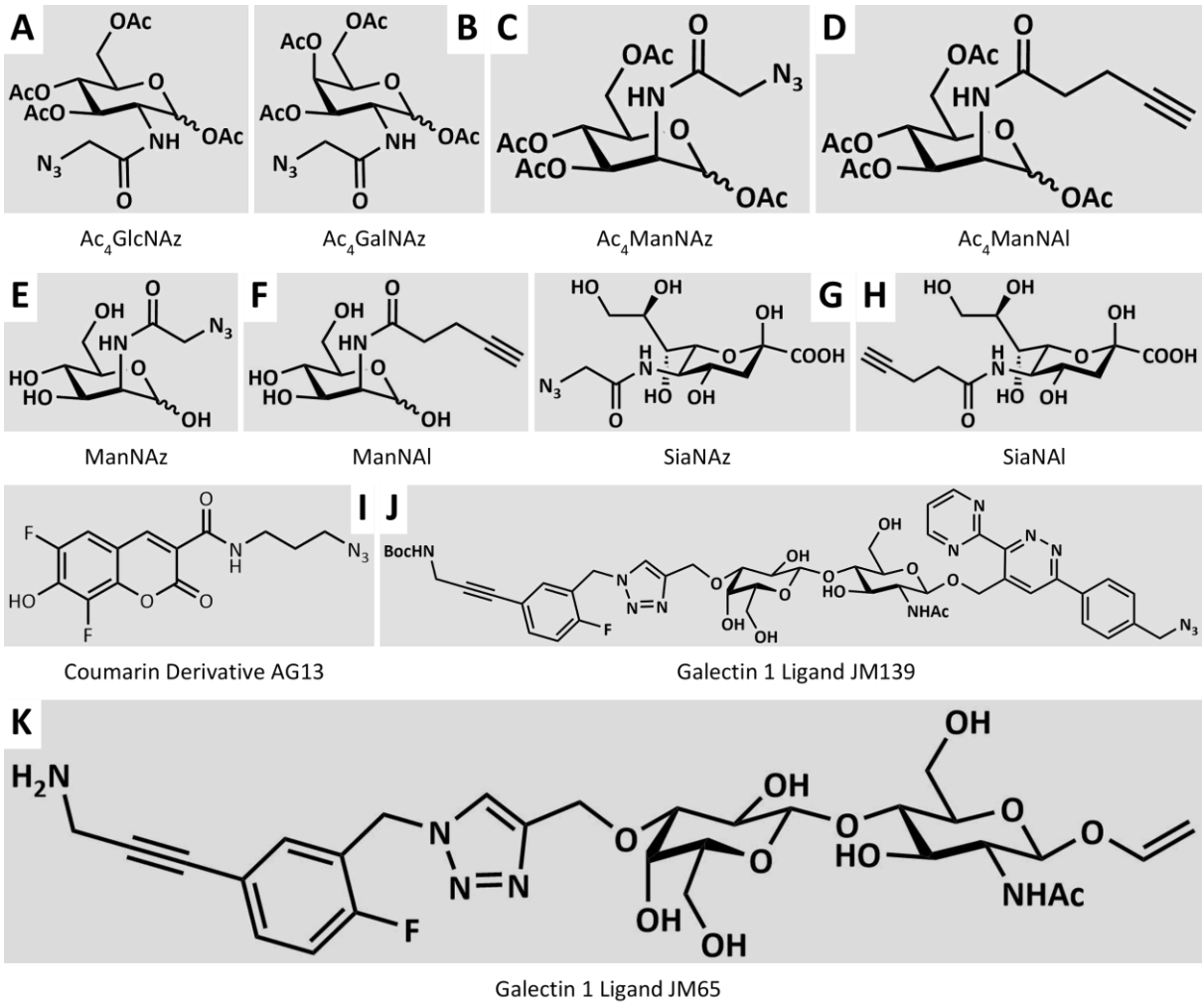

Figure 8: **Modified Monosaccharides and Target Molecules for Metabolic Glycoengineering used in this Project**. **(A-D)** Peracetylated modified monosaccharides, **(E-H)** modified mannose and sialic acids, **(I)** fluorescent target molecule, **(J+K)** glycoconjugates. Ac: acetyl group, Boc: tert-butyloxycarbonyl group, Ac4GlcNAz: peracetylated *N*-azidoacetylglucosamine, Ac4GalNAz: peracetylated *N*-azidoacetylgalactosamine, Ac4ManNAz: peracetylated *N*-azidoacetylmannosamine, Ac4ManNAl: peracetylated *N*-alkyneacetylmannosamine. The molecules D-K were provided by the work group of Prof. Dr. Jürgen Seibel (Institute of Organic Chemistry, University of Würzburg).

For the copper-catalyzed azide–alkyne cycloaddition (CuAAC) click reaction, DPBS was supplemented with 50 μM $CuSO_4$ (Merck KGaA, Darmstadt, Germany) and 250 μM THPTA (Carl Roth GmbH + Co. KG, Karlsruhe, Germany), as well as 2.5 mM sodium ascorbate (Sigma-Aldrich Chemie GmbH, Munich, Germany), and incubated at 37 °C for 10 min. Subsequently, 20 μM alkyne-sulfo-Cy 3 or azido-sulfo-Cy 5 [185] (provided by the work group of Prof. Dr. Jürgen Seibel) were added and cells were treated with the mixture at 37 °C and 5 % CO_2 for 5 min after removal of the medium and one washing step with DPBS. After the click reaction, cells were washed three times with DPBS and incubated with growth medium for 30 min, 2 d, 4 d, or 6 d. For the SPAAC click reaction, DPBS was

supplemented with 1 % (*v*/*v*) FCS and 20 μM dibenzocyclooctyne-Cy 3 and cells were treated with the mixture at 37 °C and 5 % CO_2 for 60 min after removal of the medium and one washing step with DPBS.

To assess the impact of target molecules on cell stiffness or mechanoresponsive luciferase expression, hMSC-TERT or hMSC-TERT-AP1 were grown in 75 cm^2 culture flasks to 80 % confluence and incubated in growth medium supplemented with 20 μM Ac_4ManNAl or with DMSO (0.2 % *v*/*v*) as negative control for 72 h. After cell detachment with 15 mM sodium citrate in DPBS, cells were centrifuged at 250 x g for 5 min, washed with DPBS and filtered using a 40 μm cell strainer (Greiner Bio-One GmbH, Frickenhausen, Germany) followed by a centrifugation step. Click reaction was carried out in suspension as written above with the coumarin derivative AG13 (synthesized by Adrian Graef from the work group of Prof. Dr. Jürgen Seibel), the galectin 1 ligand JM139 (synthesized by Jürgen Mut from the work group of Prof. Dr. Jürgen Seibel) (**Figure 8I + J**), or in case of the negative control without any target molecule.

Fluorescence Imaging after Click Reaction on the Cell Surface

For fluorescence imaging, cells were washed once with DPBS, incubated with a mixture of 2 % (*v*/*v*) formaldehyde (Merck KGaA, Darmstadt, Germany) and 2.5 % (*v*/*v*) glutaraldehyde at 4 °C for 10 min, washed three times with DPBS, and followed by an incubation with 300 nM DAPI in DPBS at room temperature for 10 min for nuclei staining and three washing steps with DPBS. Images were taken with a ZEISS Axio Observer 7 fluorescence microscope (Carl Zeiss AG, Oberkochen, Germany) using a 10 × 0.3 NA objective, while exposure time and gain for Cy 3 or Cy 5 fluorescence were kept constant. For qualitative comparison, brightness and contrast of Cy 3/5-related fluorescence signals were adjusted according to the sample with the highest signal intensity. For indirect quantitation, grey values of unaltered Cy 3/5-related fluorescence signals from three different visual fields per micrograph were measured using Fiji [186] and averaged.

Shear Flow Deformation Cytometry

To evaluate the cell stiffness of glycoengineered cells, 1×10^6 cells were resuspended in 1 mL sodium alginate solution (1.5 % *w*/*v*) (VIVAPHARM alginate PH176) (JRS PHARMA GmbH & Co. KG, Rosenberg, Germany) after the click reaction and shortly centrifuged to remove air bubbles. The subsequent biophysical measurements were conducted according to Gerum *et al*. [187]. Briefy, the bioink was pumped through a microfluidic channel using air pressure at 1, 2 or 3 bar. Micrographs were taken in bright field mode with a LEICA DMIL microscope (Leica Camera AG, Wetzlar, Germany)

using a CMOS acA720-520um camera (Basler AG, Ahrensburg, Germany) and a 40 × 0.6 NA objective. Cell stiffness and fluidity were calculated using a computational model according to Gerum *et al*. [187]. These measurements were conducted in cooperation with Jennifer Elsterer from the work group of Prof. Dr. Ben Fabry (Department of Physics, University of Nürnberg-Erlangen).

Bioprinting

For bioprinting, 5×10^6 cells were resuspended in 100 μL DPBS and carefully mixed with 900 μL Methyl-(2-n-proply-2-oxazine)$_{100}$-*block*-(2-methyl-2-oxazoline)$_{100}$-ethylisonipecotate diblock copolymer solution (27.8 % *w*/*v*) (hereinafter as POx-POzi) [103] (provided by Lukas Hahn from the work group of Prof. Dr. Robert Luxenhofer) or (Ethylene glycol)$_{100}$-*block*-(propylene glycol)$_{65}$-*block*-(ethylene glycol)$_{100}$ triblock copolymer solution (27.8 % *w*/*v*) (hereinafter as Pluronic F127) (**Figure 9**) on ice obtaining a final concentration of 25 % *w*/*v*. A 3 mL printing cartridge was carefully filled with half of the bioink, locked with a 30 Gauge printing needle (160 μm in diameter, 12.7 mm in length) (Cellink, Boston, USA) and horizontally incubated for 10 min at 37 °C to increase the viscosity. The printing cartridge was inserted into a preheated printing head (37 °C) of an Inkredible Plus bioprinter (Cellink, Boston, USA) and the bioink was pneumatically extruded at 2.5 bar. For cell isolation, 1 mL DPBS was added and the cells were incubated for 5 min at 4 °C. The diluted bioink solution was resuspended and centrifuged for 5 min at 250 × g, resulting in a cell pellet which was used for analyses of cell viability, F-actin formation and expression of mechanoresponsive genes.

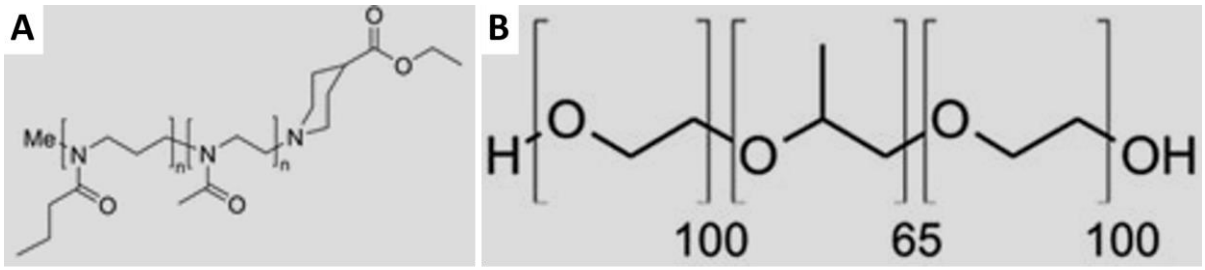

Figure 9: Bioinks used in this Project. POx-POzi structure according to Lorson *et al*. [103] with n=100 (reproduced with permission from the American Chemical Society).

Luciferase Assay

To measure the activity of luciferase, 30×10^3 cells (hMSC-TERT-AP1) were seeded in a 24-well plate after mixing or additionally bioprinting with the above mentioned bioinks and incubated at 37 °C and 5 % CO_2 for 24 h. Cells were washed three times with DPBS and resuspended in 150 μL Pierce Luciferase Cell Lysis buffer (Thermo Fisher Scientific, Waltham, USA). Luminescence was measured in 20 μL cell lysate after addition of luciferase buffer (**Table 3**) using an Orion II Microplate Luminometer

(Berthold Detection Systems, Pforzheim, Germany). For correlation of luciferase activity to the whole protein amount, the absorption of 20 μL cell lysate in 200 μL Roti-Nanoquant solution (Carl Roth GmbH + Co. KG, Karlsruhe, Germany) was measured at 600 nm using a Glomax Multi Detection System (Promega GmbH, Mannheim, Germany). Each reaction was performed in technical duplicates and the averaged absorption values were compared to a BSA standard curve (2 μg μL^{-1}) (AppliChem GmbH, Darmstadt, Germany) to obtain the protein amount.

Table 3: Composition of Luciferase Buffer. Reagents are solved in Aqua dest. and the pH value was set to 7.8**.**

Reagent	Concentration [mM]	Manufacturer
$MgSO_4$ x H_2O	2.67	Carl Roth GmbH + Co. KG, Karlsruhe, Germany
Na_2-EDTA x 2 H_2O	0.1	AppliChem GmbH, Darmstadt, Germany
Tricine	20	Sigma-Aldrich Chemie GmbH, Munich, Germany
DTT	2	
ATP	5	
D-Luciferin (free acid)	0.47	PJK GmbH, Kleinblittersdorf, Germany

Data Processing

Numerical data were evaluated with Office Excel 2016 (Microsoft Corporation, Redmond, USA) and graphs were created in Prism 7 (GraphPad Software, San Diego, USA), while image processing was performed with Fiji 1.53c (National Institutes of Health, Bethesda, USA) [186] and ScientiFig [188]. For statistical analysis, datasets were compared to DMSO- or untreated controls for significance in Prism 7 using two-tailed paired *t*-tests, at which *p*-values less than 0.05 were considered to be statistically significant.

Results

Impact of Click Reagents on the Cell Viability

Prior to the characterization of metabolic glycoengineering, the impact of click reagents on the cells' properties was tested to define the optimal experimental conditions. Starting with three commercially available peracetylated azido monosaccharides, preliminary toxicity tests were carried out using a recommended incubation time of 48 h. In human mesenchymal stromal cells (hMSC), viability showed only a slight decrease for peracetylated *N*-azidoacetylglucosamine (Ac_4GlcNAz) and peracetylated *N*-azidoacetylmannosamine (Ac_4ManNAz) at 50 μM (89 % to 93 %) (**Figure 10A**) and more pronounced declines for the apoptosis rates of Ac_4GlcNAz as well as the other two monosaccharides at 50 μM (67 % to 77 %). In contrast, viability in telomerase-immortalized hMSC (hMSC-TERT) dropped for Ac_4GlcNAz to 69 % at 25 μM and 38 % at 50 μM while it fluctuated around 78 % for peracetylated *N*-azidoacetylgalactosamine (Ac_4GalNAz) and dropped to 68 % only at the higher concentration when using the mannose variant. The apoptosis rates were slightly increased for Ac_4GalNAz at 50 μM and Ac_4ManNAz at 25 μM, but much more for the higher concentration and the azido glucose (in the range of 2.4- to 3.3-fold).

During the implementation of the method, the incubation time and concentration were adapted according to the literature [80,189] to increase the incorporation yield. The cells were incubated now on for 72 h and a peracetylated *N*-alkyneacetylmannosamine (Ac_4ManNAl) was analyzed in addition. In hMSC-TERT, all four investigated modified monosaccharides showed only slightly increased apoptosis rates, except Ac_4ManNAz, which was 3.6-fold higher compared to the control and significantly decreased viability rates (40 % to 60 %) at 50 μM concentrations (**Figure 10B**). The results for the 20 μM concentration showed viability rates above 90 % for Ac_4GlcNAz and Ac_4GalNAz and 67 % for both mannose sugars, while there was no remarkably increased apoptosis.

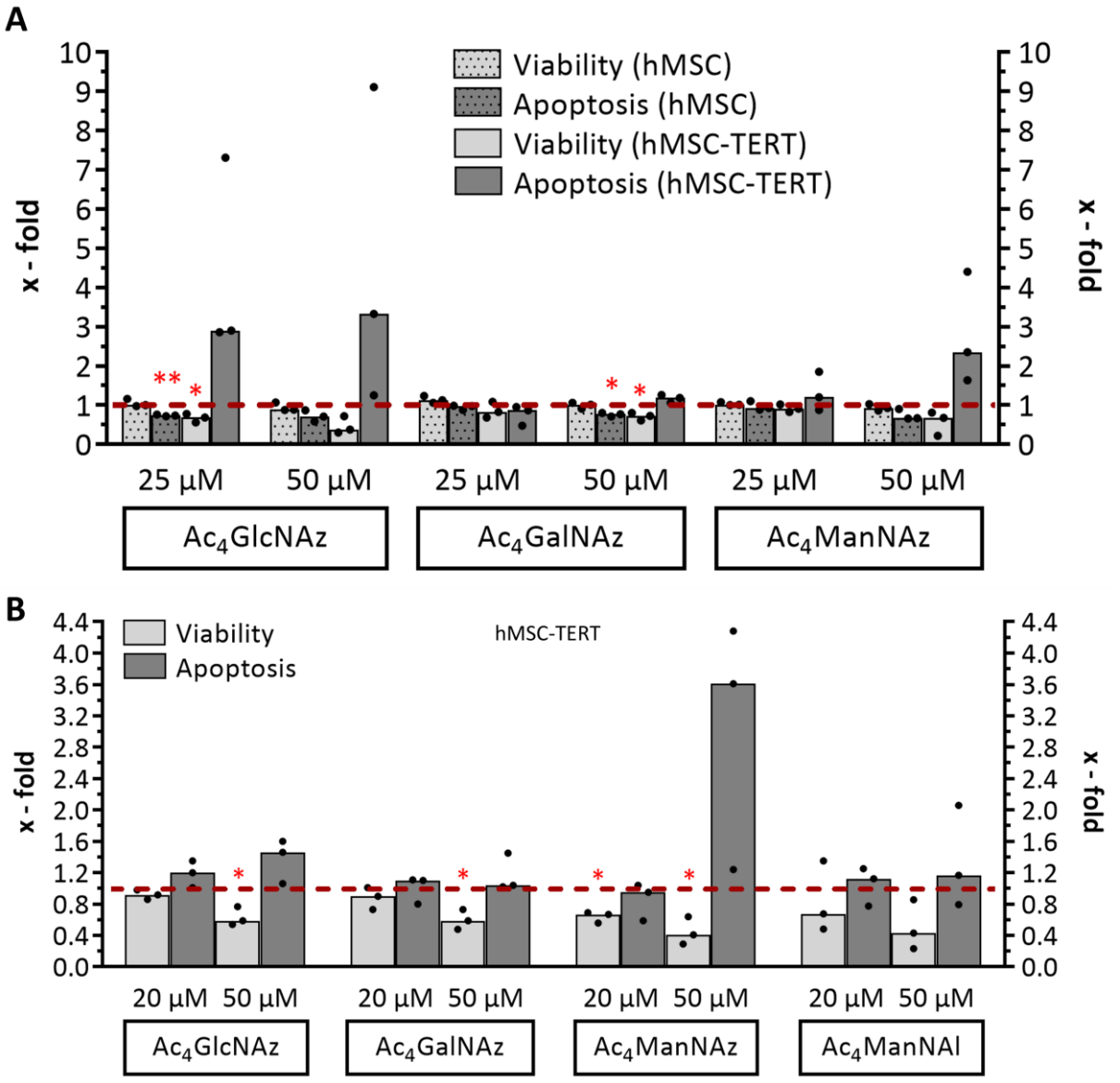

Figure 10: Cell Viability of human Mesenchymal Stromal Cells (hMSC) and Telomerase-immortalized hMSC after Treatment with peracetylated modified Monosaccharides. (A) Viability and apoptosis rates of hMSC and hMSC-TERT after 48 h incubation with peracetylated azido monosaccharides relative to dimethyl sulfoxide (DMSO)-treated control (dashed line). Datasets of three independent experiments (median with individual values depicted as points and three individual donors in case of primary hMSC) were tested for significance using two-tailed paired *t*-test ($p < 0.05$ depicted as *, $p < 0.01$ depicted as **). **(B)** Viability and apoptosis rates of hMSC-TERT after 72 h incubation with peracetylated azido/alkyne monosaccharides relative to DMSO-treated control (dashed line). Datasets of three independent experiments (median with individual values) were tested for significance using two-tailed paired *t*-test ($p < 0.05$ depicted as *). Ac_4GlcNAz: peracetylated *N*-azidoacetylglucosamine, Ac_4GalNAz: peracetylated *N*-azidoacetylgalactosamine, Ac_4ManNAz: peracetylated *N*-azidoacetylmannosamine, Ac_4ManNAl: peracetylated *N*-alkyneacetylmannosamine. This diagram was adapted from Altmann *et al*. which was published as an open access article under the terms of the Creative Commons Attribution License in the International Journal of Molecular Sciences.

To avoid potential chemical side reactions due to binding of the C_1-acetyl group to cysteine residues of membrane proteins [190] and to assess potentially higher incorporation efficiencies of sialic acids, four non-acetylated azido/alkyne monosaccharides were investigated as well. In hMSC, all four sugars showed a viability over 90 % for concentrations up to 1 mM (except *N*-azidoacetylneuraminic

acid (hereinafter SiaNAz) at 1 mM) (**Figure 11A**). At 2 mM, viability dropped significantly to 80 % to 85 % (except *N*-alkyneacetylneuraminic acid (hereinafter SiaNAl) with 68 %). The apoptosis rates for both azido sugars, ManNAl at both the lowest concentrations and SiaNAl at 250 μM revealed no to slight changes (86 % to 105 %), while the higher concentrations of both alkyne sugars showed small increases from 1.1- to 1.3-fold (even significant for ManNAl). In hMSC-TERT, ManNAz and SiaNAl exhibited a significant similar viability trend from 86 % to 90 % at 250 μM to 18 % to 31 % at 2 mM (**Figure 11B**).

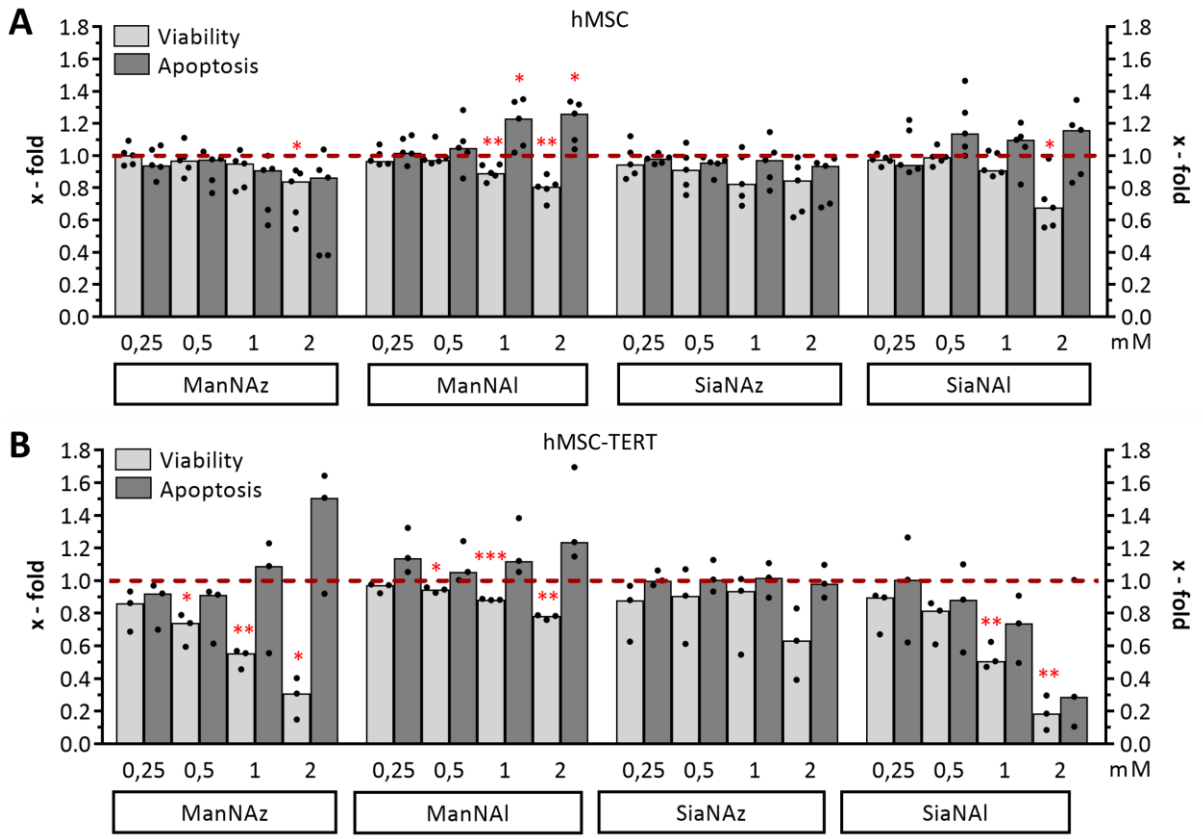

Figure 11: Cell Viability of human Mesenchymal Stromal Cells (hMSC) and Telomerase-immortalized hMSC after Treatment with non-acetylated modified Monosaccharides. (A) Viability and apoptosis rates of hMSC after 72 h incubation with azido/alkyne monosaccharides relative to untreated control (dashed line). Datasets of three independent experiments (median with individual values) (five individual donors in case of primary hMSC) were tested for significance using two-tailed paired *t*-test ($p < 0.05$ depicted as *). **(B)** Viability and apoptosis rates of hMSC-TERT after 72 h incubation with azido/alkyne monosaccharides relative to untreated control (dashed line). Datasets of three independent experiments (median with individual values) were tested for significance using two-tailed paired *t*-test ($p < 0.05$ depicted as *). ManNAz: *N*-azidoacetylmannosamine, ManNAl: *N*-alkyneacetylmannosamine, SiaNAz: *N*-azidoacetylneuraminic acid, SiaNAl: *N*-alkyneacetylneuraminic acid.

While ManNAl also showed a significant but less pronounced concentration-dependent decrease from 97 % to 78 %, viability for SiaNAz fluctuated around 91 % up to 1 mM and dropped to 63 % at 2 mM. The apoptosis rate did not change for SiaNAz at any concentration, but evenly decreased for SiaNAl to 74 % at 1 mM and dropped further to 29 % at the highest concentration. The two lower

concentrations of ManNAz led to less diminished apoptosis rates (92 %), which increased to 1.1-fold (1 mM) and 1.5-fold (2 mM), respectively. The values fluctuated around 1.1-fold for ManNAl with a small and steady increase from 0.5 mM to 2 mM.

The copper-catalyzed azide–alkyne cycloaddition (CuAAC) click reaction is catalyzed by Cu^{I} ions, which are stabilized by the tris(3-hydroxypropyl-triazolylmethyl)amine (THPTA) ligand. Although the 5-fold ligand amount should bind all free Cu^{I} species, it was analyzed whether potential residual free cytotoxic Cu^{I} species have an impact on cell viability [84]. Live/dead staining of hMSC and hMSC-TERT mostly showed living cells directly after incubation with the click reaction mixture (containing different concentrations of $CuSO_4$, the respective 5-fold concentration of THPTA, and 2.5 mM sodium ascorbate), with almost no dead cells for all chosen concentrations (**Figure 12**). Despite a potentially higher reaction efficiency, 50 μM were used for all further experiments to keep Cu^{I} ion-mediated cytotoxicity as low as possible.

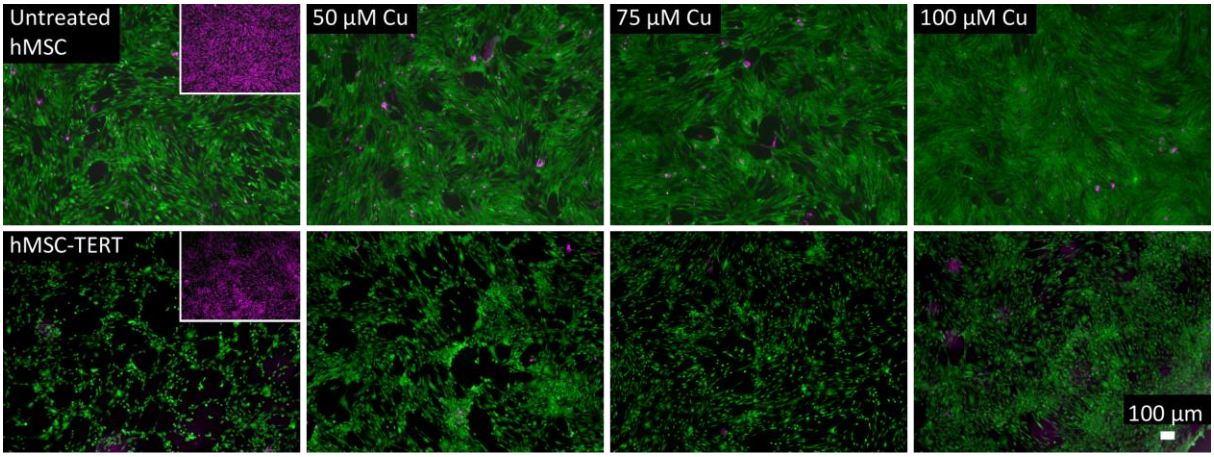

Figure 12: Cell Viability of human Mesenchymal Stromal Cells (hMSC) and Telomerase-immortalized hMSC after Treatment with Cu. Live/dead staining after 5 min incubation with Cu^{I}-containing click reaction mixture. Green: fluorescence signal of living cells, magenta: fluorescence signal of dead cells. The insets depict isopropanol-treated cells. Representative images of three independent experiments are shown. Parts of this figure were adapted from Altmann *et al*., which was published as an open access article under the terms of the Creative Commons Attribution License in the International Journal of Molecular Sciences.

Impact of Modified Monosaccharides on Mesenchymal Differentiation and Gene Regulation

Sugars are involved in many metabolic pathways; therefore, the influence of Ac_4ManNAz or Ac_4ManNAl on the mesenchymal differentiation potential of hMSC-TERT as well as their impact on gene expression were analyzed. Alizarin Red staining revealed the formation of calcium phosphate aggregates for both modified monosaccharides (**Figure 13A, left**) after two weeks of osteogenic differentiation (it was less pronounced for Ac_4ManNAz at 50 μM). Oil Red staining resulted in evenly

distributed lipid droplet formations in all samples (**Figure 13A, right**) under adipogenic conditions. Gene expression analyses of differentiation marker genes (alkaline phosphatase (ALPL) and bone gamma carboxyglutamate protein (BGLAP) (osteogenic markers), as well as fatty acid binding protein (FABP) and peroxisome proliferator activated receptor gamma (PPARG) (adipogenic markers)) showed fold changes in the range from 0.4 to 1.3 after 72 h incubation with modified monosaccharides and subsequent differentiation (**Figure 13B**). In detail, stimulation with Ac_4ManNAz led to an increase of up to 1.3-fold for BGLAP (20 μM), ALPL, and both adipogenic marker genes (50 μM), as well as for ALPL after incubation with 20 μM Ac_4ManNAl. On the contrary, stimulation with Ac_4ManNAl resulted in decreased gene expression after osteogenic differentiation (0.6- to 0.8-fold for ALPL and BGLAP at 50 μM, or the latter at 20 μM) or adipogenic differentiation (0.4- to 0.6-fold for FABP and PPARG at both concentrations). Additionally, stimulation with Ac_4ManNAz (20 μM) revealed a decrease of 0.6- to 0.7-fold for both adipogenic marker genes (20 μM) or BGLAP at 50 μM. Overall, the fold changes were scattered in all but two cases.

In addition, a set of seven genes responsible for different cell functions were analyzed for fold changes after incubation with Ac_4ManNAz or Ac_4ManNAl as the treatment of endothelial progenitor cells with the former sugar led to downregulation of genes related to different functional areas in an earlier study [189]. In this work, functional areas were thematically covered by fibronectin (FN1), laminin subunit gamma 2 (LAMC2), and heparan sulfate proteoglycan (HSPG2) linked to extracellular matrix components, integrin subunit alpha V (ITGAV) and thrombospondin 1 (THBS1) linked to cell–cell interactions, as well as signal transducer and activator of transcription 1 (STAT1) and epidermal growth factor receptor (EGFR) linked to cell survival and signal transduction. Although most conditions did not result in significant fold changes compared to the DMSO-treated control, the expression of three genes was slightly increased by using both modified monosaccharides (**Figure 13C**). In detail, FN1 showed a slight increase of 1.3-fold (Ac_4ManNAz at 50 μM and Ac_4ManNAl at 20 μM), HSPG2 an increase of 1.4- to 1.5-fold (Ac_4ManNAz) or 2.6-fold for Ac_4ManNAl at 20 μM, and STAT1 an increase of 1.3-fold (Ac_4ManNAz). Additionally, ITGAV (1.2-fold for Ac_4ManNAz) and EGFR (1.4-fold for Ac_4ManNAl) were slightly increased at 50 μM. Decreased gene expressions were seen for LAMC2 (0.9-fold for Ac_4ManNAz and 0.6- to 0.8-fold for Ac_4ManNAl), ITGAV (0.6- to 0.7-fold at 20 μM or 0.4-fold for Ac_4ManNAl at 50 μM), and THBS1 (0.6- to 0.8 fold for Ac_4ManNAz). Furthermore, gene expression of STAT1 with 0.9-fold for Ac_4ManNAl at 50 μM as well as EGFR (0.7- to 0.8-fold for Ac_4ManNAz or 0.4-fold as a consequence of incubation with Ac_4ManNAl used at 20 μM) were diminished. Although the data showed high variances, it should be noted that there were often grouped single values with one or two outliers representing natural biological variation.

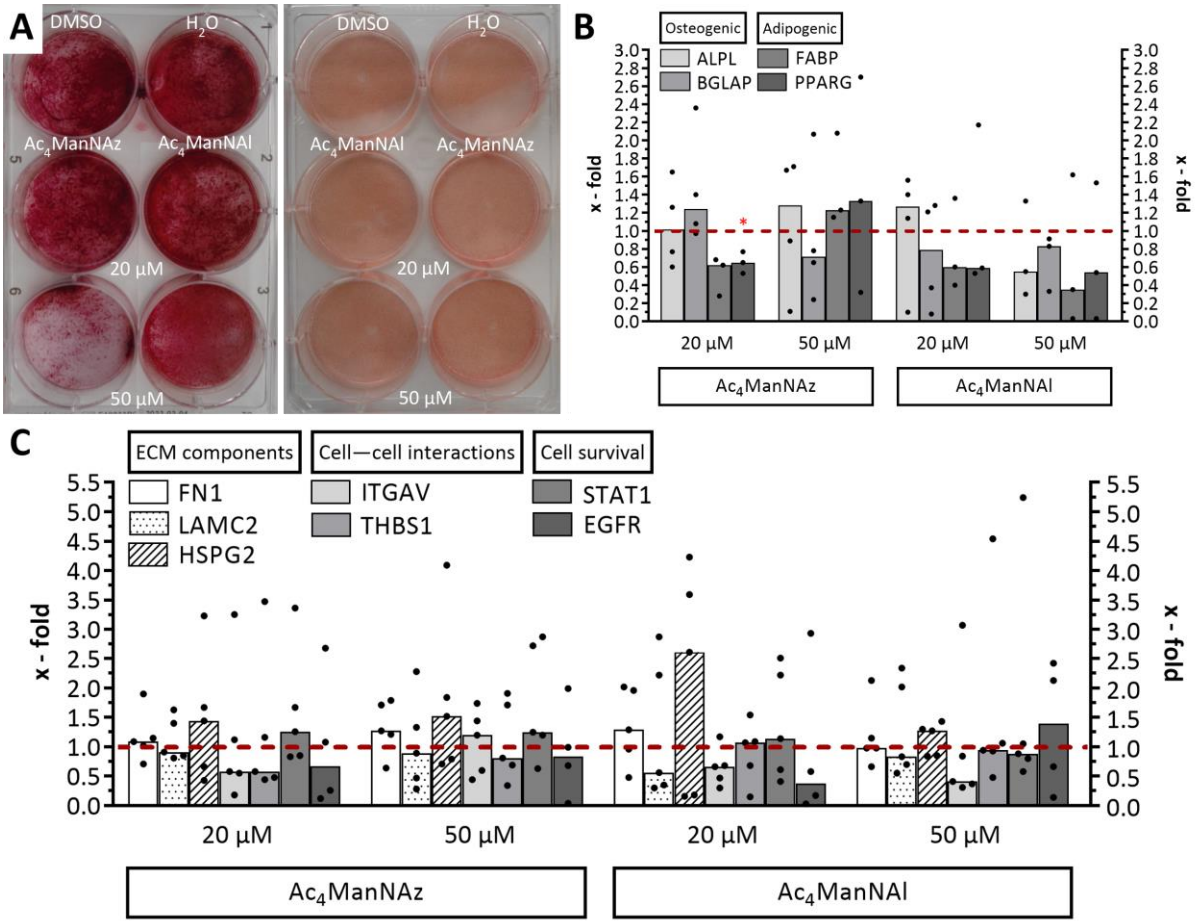

Figure 13: Differentiation Capacity and Gene Expression of Telomerase-immortalized human Mesenchymal Stromal Cells (hMSC-TERT) after 72 h Incubation with peracetylated *N*-azidoacetylmannosamine (Ac$_4$ManNAz) or peracetylated *N*-alkyneacetylmannosamine (Ac$_4$ManNAl). (A) Alizarin Red and Oil Red staining after two weeks of osteogenic or adipogenic differentiation. DMSO: dimethyl sulfoxide. Representative images of three independent experiments are shown. **(B)** Gene expression analysis of alkaline phosphatase (ALPL) and bone gamma carboxyglutamate protein (BGLAP) (osteogenic markers) as well as fatty acid binding protein (FABP) and peroxisome proliferator activated receptor gamma (PPARG) (adipogenic markers) relative to DMSO-treated control (dashed line). Datasets of three independent experiments (median with individual values) were tested for significance using two-tailed paired *t*-tests ($p < 0.05$ depicted as *). Acidic ribosomal protein P0 (RPLP0) was used as reference gene. **(C)** Gene expression analysis of fibronectin (FN1), laminin subunit gamma 2 (LAMC2), heparan sulfate proteoglycan (HSPG2), integrin subunit alpha V (ITGAV), thrombospondin 1 (THBS1), signal transducer and activator of transcription 1 (STAT1), and epidermal growth factor receptor (EGFR) relative to DMSO-treated control (dashed line). ECM: Extracellular matrix. Datasets of five independent experiments (median with individual values) were tested for significance using two-tailed paired *t*-test. RPLP0 was used as reference gene. This figure was adapted from Altmann *et al.*, which was published as an open access article under the terms of the Creative Commons Attribution License in the International Journal of Molecular Sciences.

Evaluation of Modified Monosaccharides regarding their Incorporation and Retention in the Glycocalyx

To assess the efficiency of metabolic glycoengineering of hMSC and hMSC-TERT, eight modified monosaccharides (four of them peracetylated) (**Figure 8A - H**) in different commonly used concentrations were tested for their potential to incorporate into the glycocalyx by clicking a detectable fluorescent dye using either strain-promoted azide–alkyne cycloaddition (SPAAC) or CuAAC click reaction. First experiments with Ac_4ManNAz revealed a successful incorporation into the cell glycocalyx independent on the click reaction type (**Figure 14** and **Figure 15**). Due to similar incorporation efficiencies at shorter incubation times compared to SPAAC click reaction shown by Gutmann *et al*. in HEK 293-F cells [191] and simpler functionalization steps in organic synthesis of target molecules, it was decided to just use the CuAAC click reaction from now on.

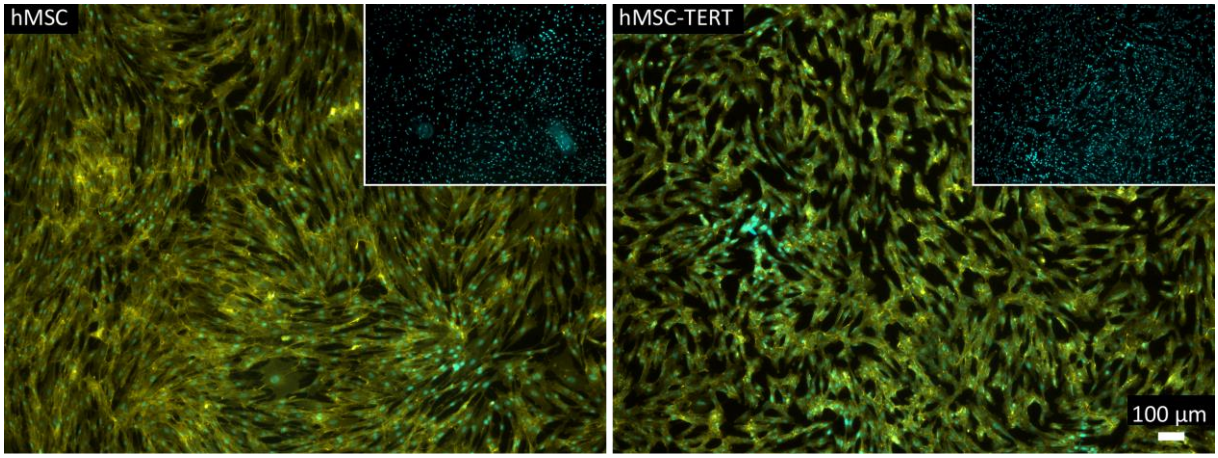

Figure 14: Incorporation of peracetylated *N*-azidoacetylmannosamine (Ac_4ManNAz) (25 μM) into the Glycocalyx of primary human Mesenchymal Stromal Cells (hMSC) and Telomerase-immortalized hMSC after 48 h Incubation. Yellow: fluorescence signal of Cy 3 after strain-promoted azide–alkyne cycloaddition (SPAAC) click reaction, cyan: fluorescence signal of nuclei. The insets depict dimethyl sulfoxide (DMSO)-treated controls. Representative fluorescence images of three independent experiments are shown.

When using the peracetylated sugars in hMSC-TERT, there was no detectable fluorescence upon incubation with Ac_4GlcNAz or Ac_4GalNAz compared to the DMSO-treated control. In contrast, after the click reaction the mannose sugars showed a 2.4- to 3.2-fold (Ac_4ManNAz) or a 1.9- to 2.4-fold (Ac_4ManNAl) higher fluorescence intensity (**Figure 15**). Therefore, it was decided to use both mannose sugars for further experiments and to refrain from applying Ac_4GlcNAz or Ac_4GalNAz.

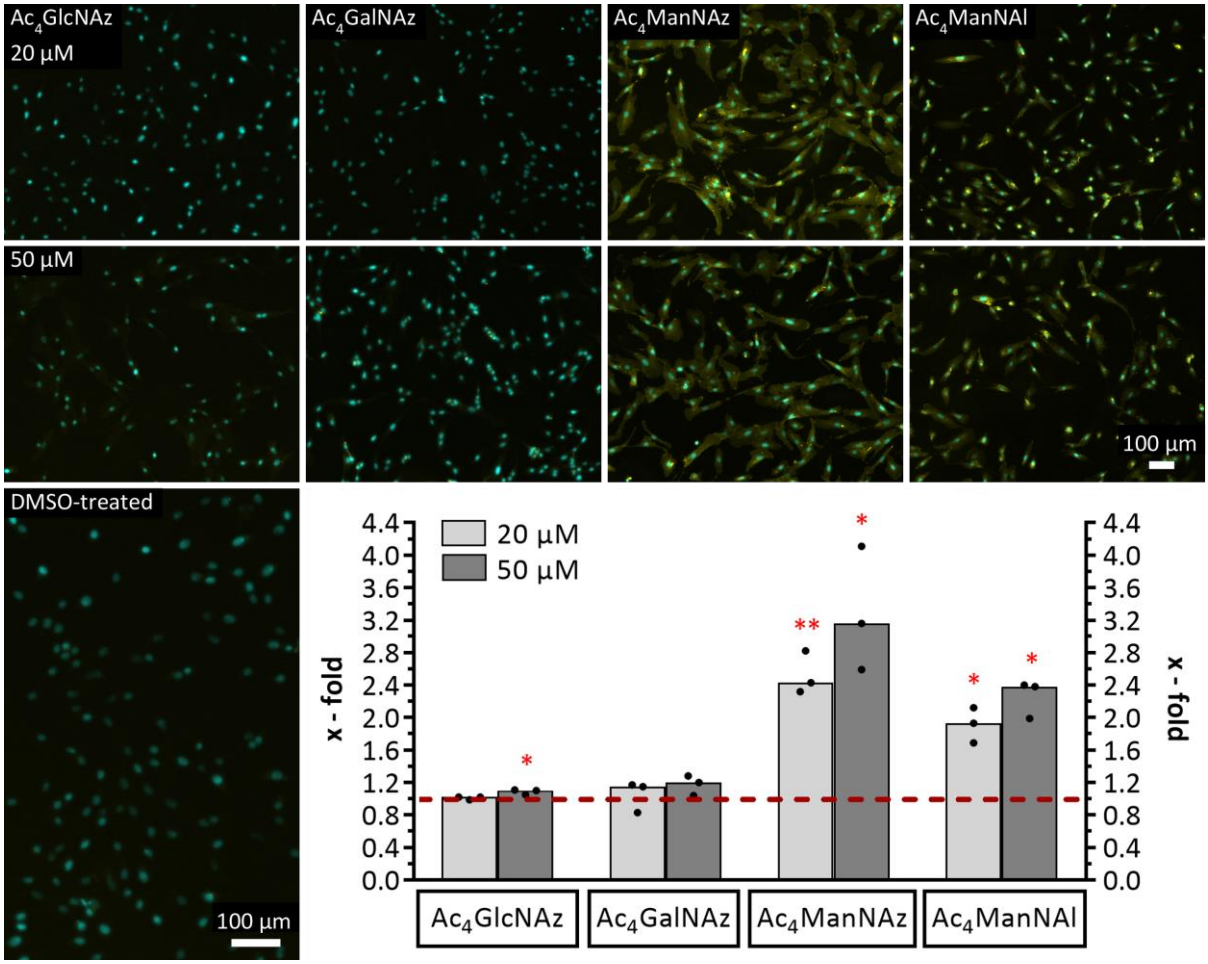

Figure 15: Incorporation of peracetylated Azido/Alkyne Monosaccharides into the Glycocalyx of Telomerase-immortalized human Mesenchymal Stromal Cells (hMSC-TERT) after 72 h Incubation. Yellow: fluorescence signal of Cy 3/5 after copper-catalyzed azide–alkyne cycloaddition (CuAAC) click reaction, cyan: fluorescence signal of nuclei. Representative fluorescence images of three independent experiments are shown. The diagram shows the quantitative analysis of fluorescence micrographs from three independent experiments. Cy 3/5 fluorescence signal as mean grey value is depicted relative to dimethyl sulfoxide (DMSO)-treated control (dashed line). Datasets (median with individual values) were tested using two-tailed paired *t*-test for significance ($p < 0.05$ depicted as *, $p < 0.01$ depicted as **). Ac_4GlcNAz: peracetylated *N*-azidoacetylglucosamine, Ac_4GalNAz: peracetylated *N*-azidoacetylgalactosamine, Ac_4ManNAz: peracetylated *N*-azidoacetylmannosamine, Ac_4ManNAl: peracetylated *N*-alkyneacetylmannosamine. This figure was adapted from Altmann *et al*., which was published as an open access article under the terms of the Creative Commons Attribution License in the International Journal of Molecular Sciences.

The cell glycocalyx is subject to permanent turnover and remodeling due to intrinsic biosynthetic processes and extrinsic influences such as shear forces [192]; therefore, the question came up how stable the chemical modifications, that were introduced by click reactions, are over time. For that reason, the glycocalyx state was evaluated at several time points up to 6 d.

Although both mannose sugars revealed an initially strong decrease in fluorescence intensity after 2 d (48 % for Ac_4ManNAz and 93 % for Ac_4ManNAl), their subsequent temporal course was different (**Figure 16**). In contrast to the missing fluorescence of Ac_4ManNAl, the azido mannose still showed a fluorescence signal, which continuously and evenly declined until day six (from 1.8-fold to 1.4-fold). Interestingly, cells incubated for 2 d or longer revealed small focal aggregates within the cytoplasm (section of Ac_4ManNAz 20 μM 2 d in **Figure 16**).

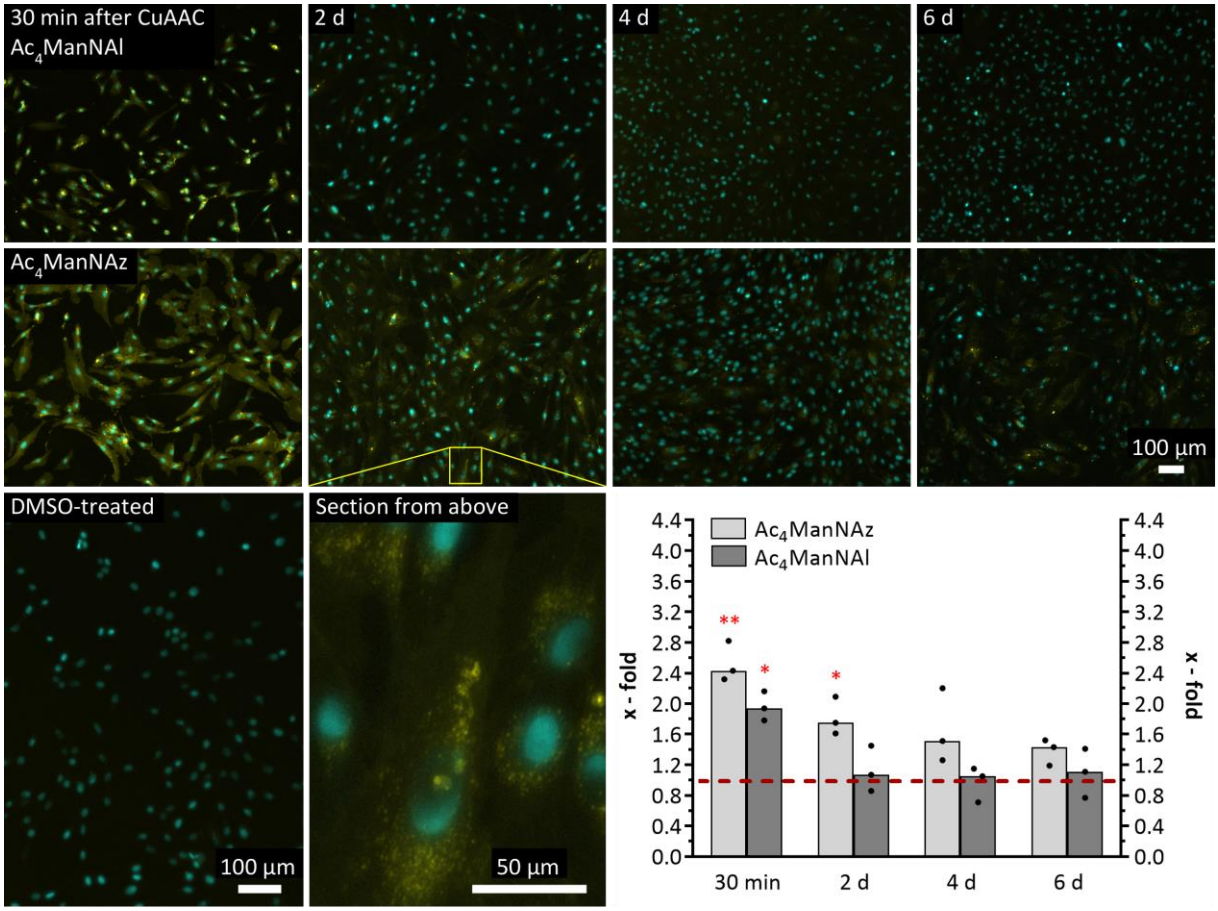

Figure 16: Temporal Course of the Decline of Glycocalyx Modification in Telomerase-immortalized human Mesenchymal Stromal Cells (hMSC-TERT) after 72 h Incubation with peracetylated *N*-azidoacetylmannosamine (Ac_4ManNAz) or peracetylated *N*-alkyneacetylmannosamine (Ac_4ManNAl) (20 μM). Yellow: fluorescence signal of Cy 3/5 after copper-catalyzed azide–alkyne cycloaddition (CuAAC) click reaction, cyan: fluorescence signal of nuclei. Representative fluorescence images of three independent experiments are shown. The diagram shows the quantitative analysis of fluorescence micrographs from three independent experiments. Cy 3/5 fluorescence signal as mean grey value is depicted relative to dimethyl sulfoxide (DMSO)-treated control (dashed line). Datasets (median with individual values) were tested for significance using two-tailed paired *t*-test ($p < 0.05$ depicted as *, $p < 0.01$ depicted as **). This figure was adapted from Altmann *et al.*, which was published as an open access article under the terms of the Creative Commons Attribution License in the International Journal of Molecular Sciences.

The investigation of the four non-acetylated azido/alkyne monosaccharides focused on sialic acids and their precursor mannose sugars. The absence of acetyl groups exclude potential unwanted chemical side reactions [190] and sialic acids are expected to increase the incorporation efficiency due to their entry site in the sialic acid pathway (**Figure 3**). In hMSC, both mannose variants showed a significant similar increase of incorporation efficiency from 2-fold at 250 μM to 7.6-fold at 2 mM in a linear manner from 500 μM on (**Figure 17**). Also both modified sialic acids showed partly significant increases, but less pronounced (from 1.4-fold at 250 μM (SiaNAl) or 500 μM (SiaNAz) to 2.6-fold at 1 mM (SiaNAl) or 2 mM (SiaNAz)). The incorporation efficiency of SiaNAl with 5.9-fold at the highest concentration was more than twice as much as with SiaNAz. In hMSC-TERT, all four monosaccharides revealed almost linear courses in concentration dependence (**Figure 18**). While both azido sugars showed the highest incorporation efficiencies at 2 mM with 1.6- to 1.9-fold, the alkyne variants exhibited a similar increase from 1.4- or 1.8-fold at 250 μM to 4.6- or 5.1-fold at 2 mM, respectively, (significant for ManNAl).

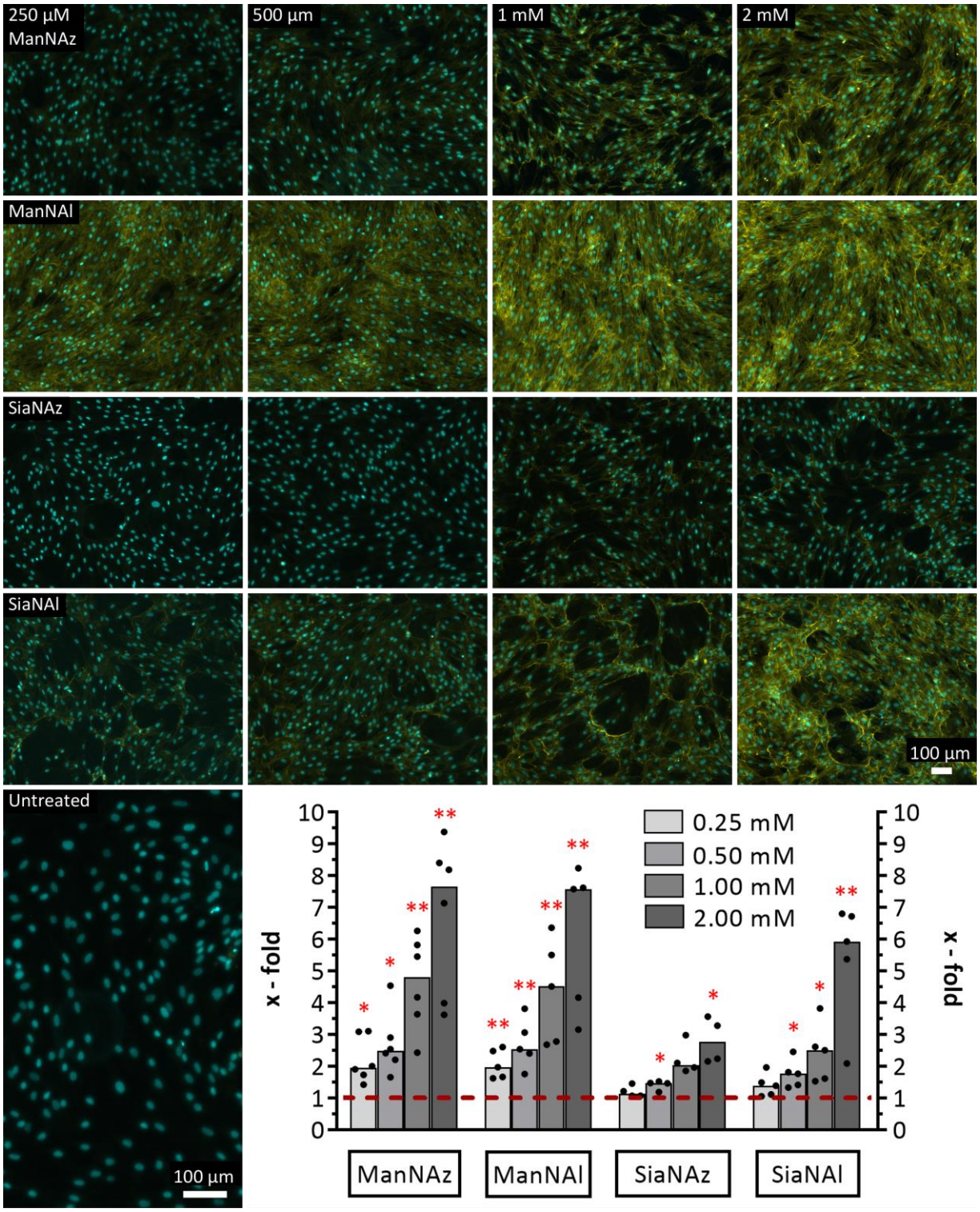

Figure 17: Incorporation of Azido/Alkyne Monosaccharides into the Glycocalyx of primary human Mesenchymal Stromal Cells (hMSC) after 72 h Incubation. Yellow: fluorescence signal of Cy 3/5 after copper-catalyzed azide–alkyne cycloaddition (CuAAC) click reaction, cyan: fluorescence signal of nuclei. Representative fluorescence images of three independent experiments are shown. The diagram shows the quantitative analysis of fluorescence micrographs from three independent experiments. Cy 3/5 fluorescence signal as mean grey value is depicted relative to untreated control (dashed line). Datasets (median with individual values) were tested using two-tailed paired *t*-test for significance ($p < 0.05$ depicted as *, $p < 0.01$ depicted as **). ManNAz: *N*-azidoacetylmannosamine, ManNAl: *N*-alkyneacetylmannosamine, SiaNAz: *N*-azidoacetylneuraminic acid, SiaNAl: *N*-alkyneacetylneuraminic acid.

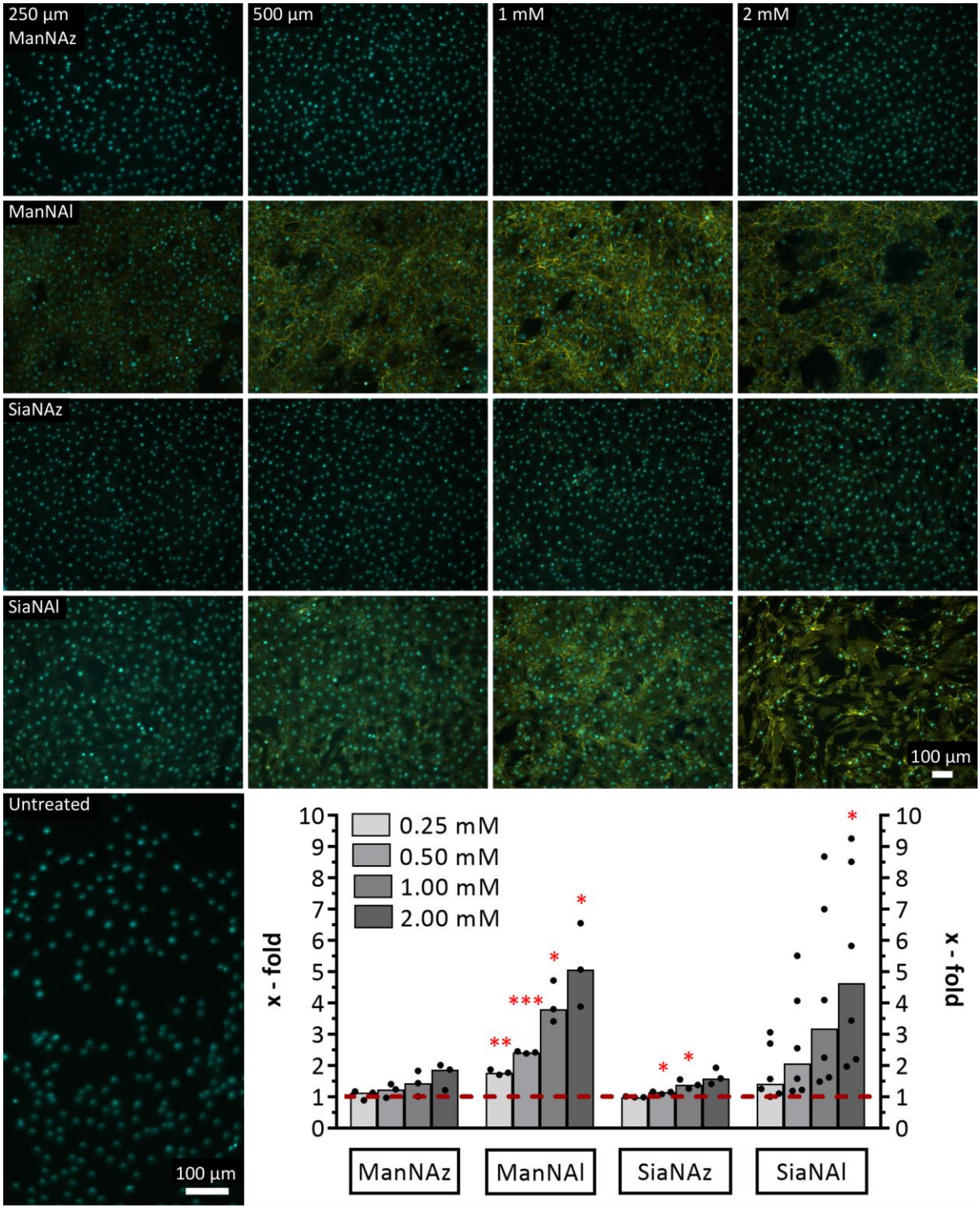

Figure 18: Incorporation of Azido/Alkyne Monosaccharides into the Glycocalyx of Telomerase-immortalized human Mesenchymal Stromal Cells (hMSC-TERT) after 72 h Incubation. Yellow: fluorescence signal of Cy 3/5 after copper-catalyzed azide–alkyne cycloaddition (CuAAC) click reaction, cyan: fluorescence signal of nuclei. Representative fluorescence images of three independent experiments are shown. The diagram shows the quantitative analysis of fluorescence micrographs from three independent experiments. Cy 3/5 fluorescence signal as mean grey value is depicted relative to untreated control (dashed line). Datasets (median with individual values) were tested using two-tailed paired *t*-test for significance ($p < 0.05$ depicted as *, $p < 0.01$ depicted as **, $p < 0.001$ depicted as ***). ManNAz: *N*-azidoacetylmannosamine, ManNAl: *N*-alkyneacetylmannosamine, SiaNAz: *N*-azidoacetylneuraminic acid, SiaNAl: *N*-alkyneacetylneuraminic acid.

Detection of Galectin 1 as Binding Target for artificial Ligands

As one future aim of this project focus on the manipulation of the cell adherence behavior in the hydrogel using galectin 1 ligands, the presence of galectin 1 in hMSC and hMSC-TERT was checked followed by stimulation tests with an artificial potential ligand (**Figure 8K**) to provide a first insight into the galectin 1 biology of hMSC .

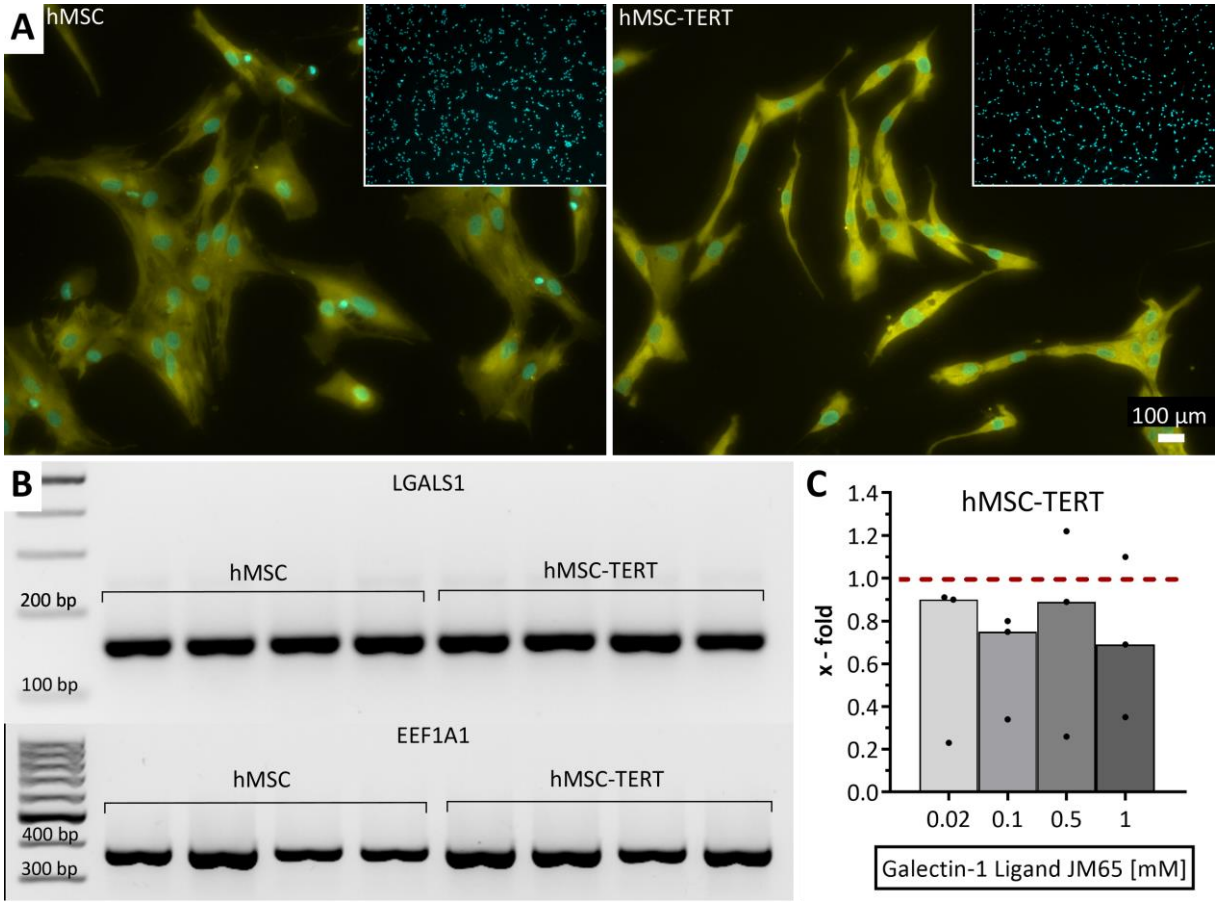

Figure 19: Galectin 1 Expression in human Mesenchymal Stromal Cells (hMSC) and Telomerase-immortalized hMSC (hMSC-TERT). (A) Immunocytochemical detection of galectin 1 protein expression in hMSC and hMSC-TERT. Yellow: fluorescence signal of galectin 1 – antibodies complex, cyan: fluorescence signal of nuclei. Insets depict controls without primary antibody incubation. Representative images of three independent experiments are shown. **(B)** Detection of galectin 1 (LGALS1) gene expression in hMSC and hMSC-TERT of different donors or passages, respectively. Eukaryotic translation elongation factor 1 alpha 1 (EEF1A1) was used as reference gene. Representative images of three independent experiments are shown. **(C)** Galectin 1 gene expression in hMSC-TERT after 24 h incubation with galectin 1 ligand JM65 relative to untreated control (dashed line). Datasets of three independent experiments (median with individual values) were tested for significance using two-tailed paired *t*-test. Cytochrome c oxidase subunit 4 isoform 1 (COX4I1) was used as reference gene.

To confirm the applicability of galectin 1 ligands, the expression of galectin 1 at different levels was investigated. Endpoint PCR analyses showed strong bands in hMSC as well as hMSC-TERT of different donors or passages at a size of 150 bp corresponding to the expected amplificate length of galectin 1 (**Figure 19B**). On protein level, immunocytochemistry revealed a strong fluorescence signal in both hMSC and hMSC-TERT, which was evenly distributed over the cell membrane (**Figure 19A**).

Stimulation of the cells with an artificial galectin 1 ligand for 24 h led to small decreases of gene expression (10 % at 0.02 mM and 0.5 mM or 25 % to 30 % at 0.1 mM and 1 mM) (**Figure 19C**).

Effects of Metabolic Glycoengineering on biophysical Cell Features

To evaluate biophysical cell features like stiffness and fluidity after glycocalyx modification, shear flow deformation cytometry [187] was used to measure potential changes in cooperation with Jennifer Elsterer from the work group of Prof. Dr. Ben Fabry (Department of Physics, University of Nürnberg-Erlangen). As target molecules, the coumarin derivative AG13 or the artificial galectin 1 ligand JM139 (**Figure 8I + J**) were introduced into the glycocalyx of hMSC-TERT via CuAAC click reaction in suspension. While incorporation of Ac_4ManNAl alone did not show any changes (except for 1.8- to 2.0-fold increase of stiffness in one experiment), additional surface covering with a target molecule resulted in higher stiffness and lower fluidity (**Figure 20**). In detail, conjugation with the coumarin derivative AG13 led to an increase in stiffness of 1.1- to 1.4-fold concomitant with a lowered fluidity of 77 % to 87 %. Conjugation with the galectin 1 ligand JM139 showed stronger shifts in both parameters (1.4- to 1.8-fold increase of stiffness and a lower fluidity of 63 % to 84 %).

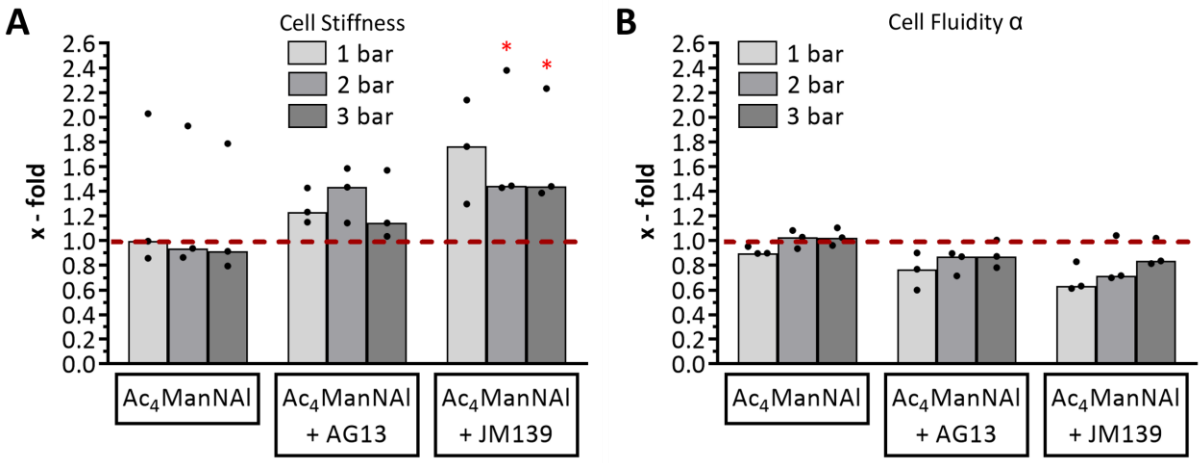

Figure 20: Biomechanical Features of Telomerase-immortalized human Mesenchymal Stromal Cells (hMSC-TERT) after Introduction of Target Molecules Coumarin Derivative AG13 or Galectin 1 Ligand JM139 into the Glycocalyx via Copper-catalyzed Azide–Alkyne Cycloaddition (CuAAC) Click Reaction. (A) Cell stiffness of hMSC-TERT relative to untreated control (dashed line). Datasets of three independent experiments (median with individual values) were tested for significance using two-tailed paired *t*-tests ($p < 0.05$ depicted as *). **(B)** Cell fluidity α of hMSC-TERT relative to untreated control (dashed line). Datasets of three independent experiments (median with individual values) were tested for significance using two-tailed paired *t*-tests. Ac_4ManNAl: peracetylated *N*-alkyneacetylmannosamine.

Impact of the Bioprinting Process on the Cell Behavior

The bioprinting experiments focused on potential influences deriving from the bioink or the printing process *per se* on cell viability or reactions to biophysical stress on cellular level as part of mechanotransduction. Cells were mixed or additionally printed with the thermoresponsive bioinks

Pluronic F127 or Polyoxazoline-Polyoxazine (hereinafter POx-POzi) and immediately isolated for subsequent analyses.

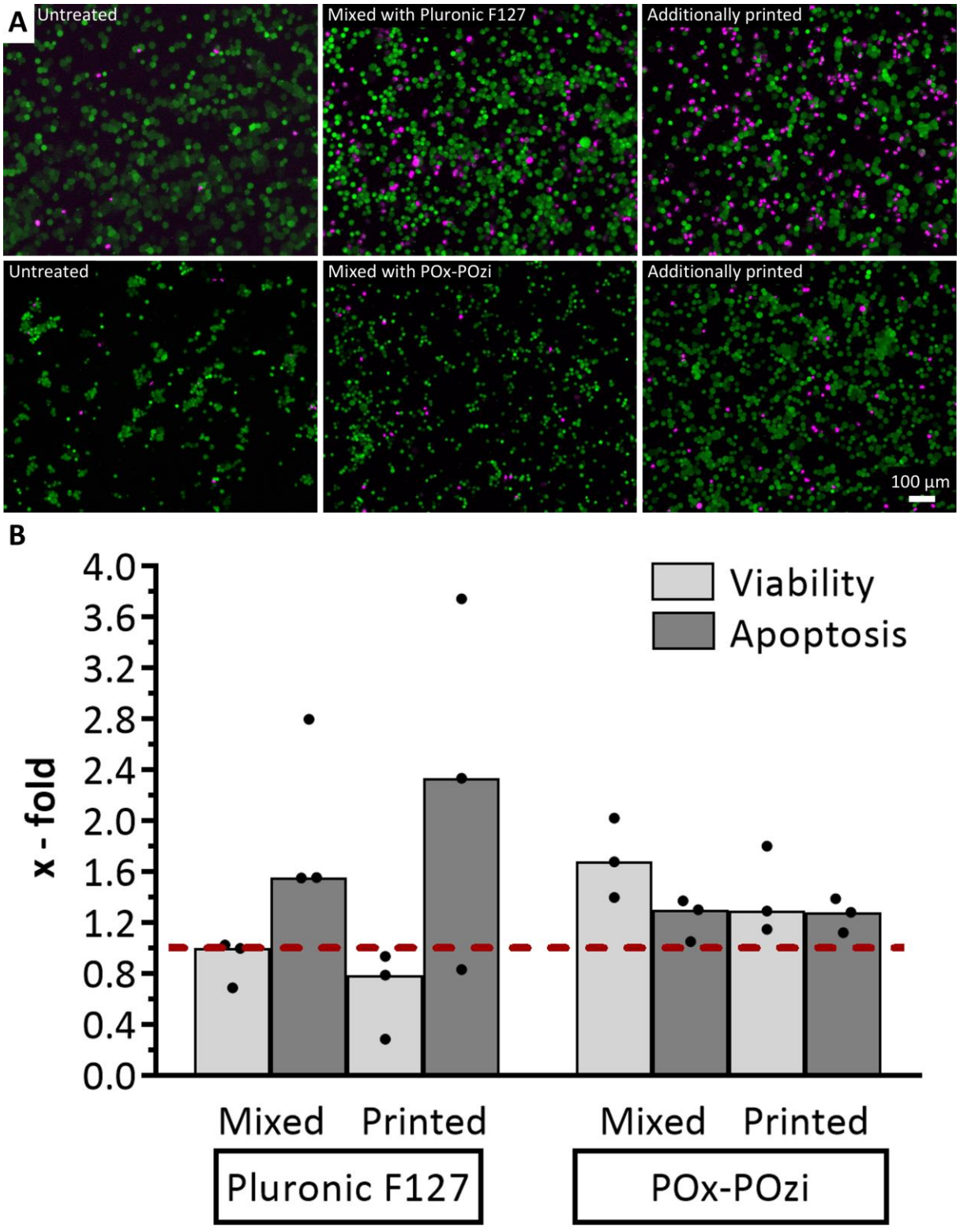

Figure 21: Viability of Telomerase-immortalized human Mesenchymal Stromal Cells (hMSC-TERT) after Processing in Pluronic F127 or POx-POzi Bioink. (A) Live/dead staining of hMSC-TERT. Green: fluorescence signal of living cells, magenta: fluorescence signal of dead cells. Representative images of three independent experiments are shown. **(B)** Viability and apoptosis rates of hMSC-TERT after processing followed by 24 h recovery relative to untreated control (dashed line). Datasets of three independent experiments (median with individual values) were tested for significance using two-tailed paired *t*-test.

Live/dead staining of hMSC-TERT after mixing with Pluronic F127 showed considerably more dead cells compared to the untreated control cells and still more after the printing (**Figure 21A**). In contrast, mixed and printed samples of hMSC-TERT in POx-POzi revealed a high fraction of living cells and sporadic dead cells, which are less in number than in Pluronic F127. The viability did not change after mixing with Pluronic, but dropped to 79 % when printed (**Figure 21B**). The apoptosis rate increased to 1.6-fold after mixing and doubled to 2.3-fold when printed. Treatment of hMSC-TERT with POx-POzi led to increased values for viability and apoptosis independent of the process step (1.3-fold except viability after mixing with 1.7-fold).

To get an impression of the impact deriving from shear forces due to the printing process, the cytoskeleton as well as expression of mechanoresponsive genes in hMSC-TERT were investigated. Phalloidin staining revealed spreaded cells with evenly distributed fluorescence signal throughout their cytoplasm in all samples (**Figure 22**).

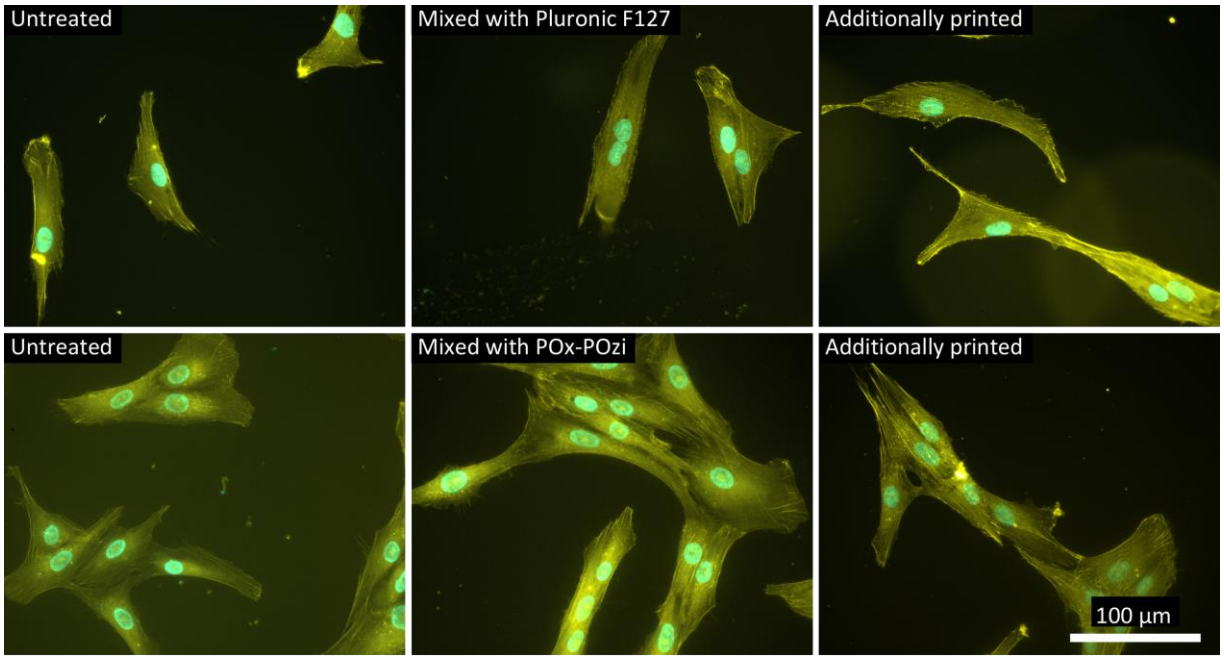

Figure 22: Cytoskeleton Formation in Telomerase-immortalized human Mesenchymal Stromal Cells (hMSC-TERT) after Processing in Pluronic F127 or POx-POzi Bioink. Phalloidin staining of F-actin filaments after processing followed by 24 h recovery. Yellow: fluorescence signal of phalloidin – F-actin complex, cyan: fluorescence signal of nuclei. Representative images of three independent experiments are shown.

For gene expression analyses, mRNA of mechanoresponsive genes proto-oncogene c Fos (FOS) and prostaglandin-endoperoxide synthase 2 (PTGS2) were assessed 30 min after processing with the bioinks under different conditions. Treatment of 5 x 10^6 cells per mL with both bioinks led to an increase of FOS expression after mixing (28.6-fold for Pluronic F127or 6.1-fold for POx-POzi), which was weaker when printed using a cylindrical needle and a pneumatic pressure of 2.5 bar (18.5-fold for Pluronic F127 or 3.8-fold for POx-POzi) (**Figure 23A**). In contrast, PTGS2 expression was significantly diminished under these conditions; this time more pronounced after printing (11 % for Pluronic F127 or 43 % for POx-POzi) compared to mixing (20 % for Pluronic F127 or 68 % for POx-POzi). When using more 'cell-friendly' conditions (data were provided by Maria Danz from the work group of Prof. Dr. Regina Ebert), processing with POx-POzi revealed opposed results. While FOS expression was diminished (40 % when mixed or 50 % after additional printing), PTGS2 expression showed a slight increase (1.1-fold) after mixing, which increased up to 1.6-fold due to additional printing (**Figure 23B**). Additional analyses with the genetically modified reporter cell line hMSC-TERT-AP1 allowed a read-out of shear stress by linking its transduction to the expression of luciferase. When using Pluronic F127, mixing showed a 1.2-fold increase of luciferase activity and a lower decrease to 0.9-fold when additionally printed (**Figure 23C**). Mixing of cells with POx-POzi led to an increase of 1.7-fold and 1.3-fold after additional printing.

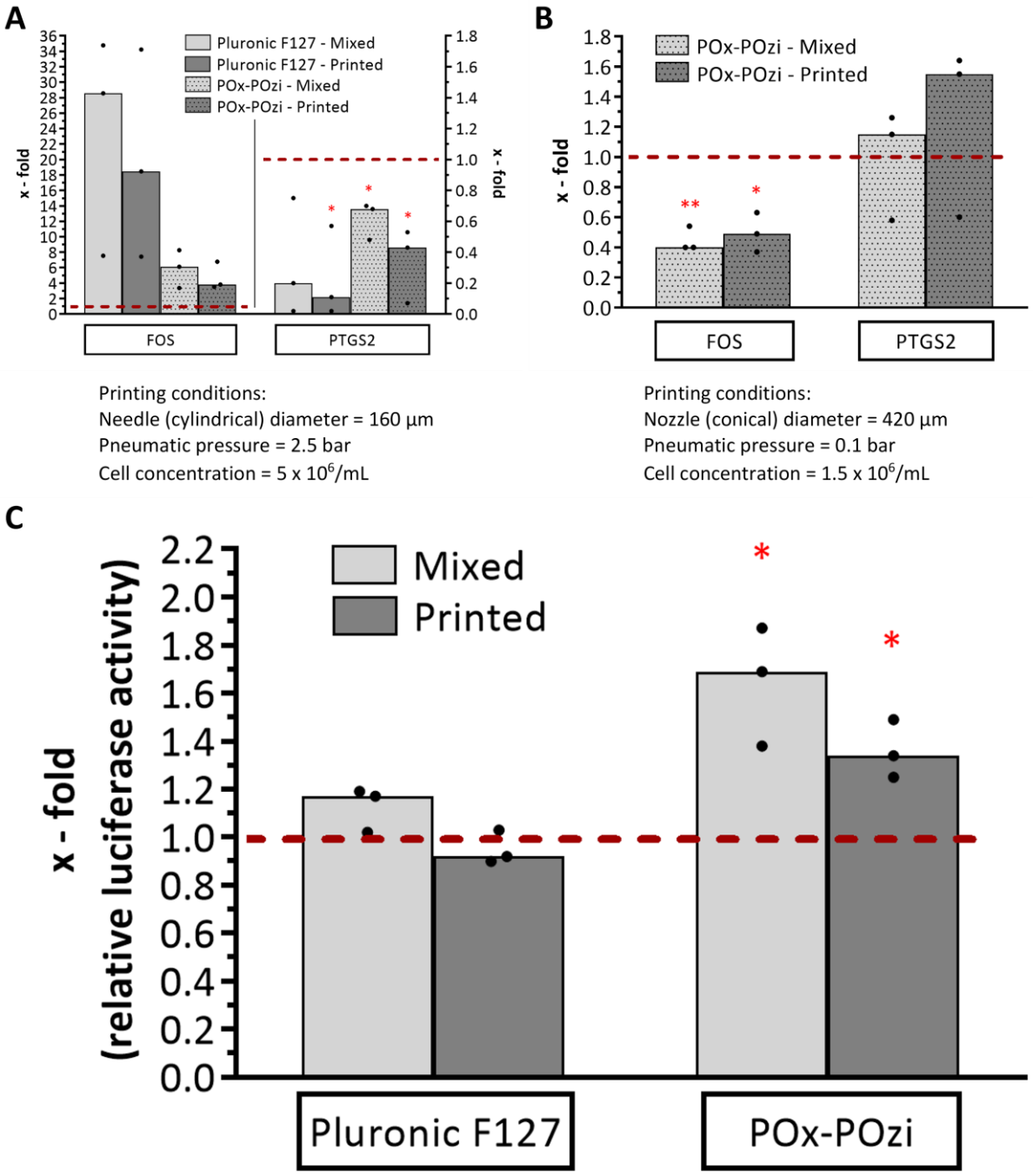

Figure 23: Expression of mechanoresponsive Genes in Telomerase-immortalized human Mesenchymal Stromal Cells (hMSC-TERT) or Luciferase Activity in hMSC-TERT-AP1 after Processing in Pluronic F127 or POx-POzi Bioink. (A) Gene expression analysis of proto-oncogene c-Fos (FOS) and prostaglandin-endoperoxide synthase 2 (PTGS2) in hMSC-TERT relative to untreated control (dashed line). Datasets of three independent experiments (median with individual values) were tested for significance using two-tailed paired *t*-tests ($p < 0.05$ depicted as *). Acidic ribosomal protein P0 (RPLP0) was used as reference gene. **(B)** Gene expression analysis of FOS and PTGS2 in hMSC-TERT relative to untreated control (dashed line) using more 'cell-friendly' conditions. Datasets of three independent experiments (median with individual values) were generated by Maria Danz from the work group of Prof. Dr. Regina Ebert and tested for significance using two-tailed paired *t*-tests ($p < 0.05$ depicted as *, $p < 0.01$ depicted as **). Cytochrome c oxidase subunit 4 isoform 1 (COX4I1) was used as reference gene. **(C)** Luciferase activity after shear stress-mediated luciferase expression in hMSC-TERT-AP1 relative to untreated control (dashed line). Datasets of three independent experiments (median with individual values) were tested for significance using two-tailed paired *t*-tests ($p < 0.05$ depicted as *).

Discussion

Primary hMSC revealed superior Cell Viability upon Incubation with Click Sugars than hMSC-TERT

To set up the optimal methodic conditions for metabolic glycoengineering prior to the click experiments, the impact of modified monosaccharides on the cell viability of primary human mesenchymal stromal cells (hMSC) and telomerase-immortalized hMSC (hMSC-TERT) were assessed. Incubation of hMSC with up to 50 μM peracetylated azido monosaccharides for 48 h did not remarkably alter viability (**Figure 10A**), showing no increased apoptosis, and viability rates still over 88 %. Interestingly, hMSC-TERT responded differently to the sugar treatment showing dose-dependent diminished viabilities and increased apoptosis rates for peracetylated *N*-azidoacetylglucosamine (Ac_4GlcNAz) and peracetylated *N*-azidoacetylmannosamine (Ac_4ManNAz) at 50 μM. A closer look reveals two differences between the cells: the genetically enhanced expression of telomerase and the higher cell 'age' of the hMSC-TERT used in this project as the cells were already cultured for at least 45 passages prior to the experiments. According to Abdallah *et al*., the hMSC-TERT maintain growth rate, surface markers, and differentiation potential for up to three years [180], concluding that cell age should not be problematic for experimental use. However, the authors witnessed some phenotypic drifts in late passages and did not investigate glycosylation or sugar-mediated pathways at all. Although the phenotypic stability of the hMSC-TERT could be proven by them, one cannot exclude unwanted genetic modifications by the retroviral transfection as shown in hematopoietic stem cells by Montini *et al*. [193,194]. The authors demonstrated a higher oncogenic risk for mice to develop myeloid cancer after transplantation of retroviral transfected tumor-prone hematopoietic stem cells compared to lentiviral transfected cells and observed an intrinsic integration-site bias toward cancer genes for retroviral vectors. When the incubation time of the click sugars were extended to 72 h according to the literature [80], cell viability of hMSC-TERT was tested again revealing a better outcome regarding Ac_4GlcNAz, but worse outcome when using the galactose or mannose variant (**Figure 10B**). Additionally, the apoptosis rates were quite different now for Ac_4GlcNAz and Ac_4ManNAz, which does not support the assumption of programmed cell death due to lacking data consistency. If this viability assay is considered as proliferation, one could suggest a correlation between decreased proliferation rates and enhanced glycosylation, which has been shown by a study in 2004. Kim *et al*. revealed a correlation between diminished cell growth and enhanced sialic acid production after the treatment of Jurkat cells with 500 μM peracetylated *N*-acetylmannosamine (Ac_4ManNAc), while cell viability was similar to untreated cells [71]. However, a much lower concentration of modified ManNAc analogs was used in this project and the viability assay measured the intracellular ATP content. It is known, that formation of the apoptosome [195,196]

and subsequent activation of the caspase cascade [197] is highly dependent on ATP, which might explain the mostly unchanged or highly scattered apoptosis rates of hMSC-TERT (**Figure 10**). Modulation of both intrinsic and extrinsic apoptosis pathways, such as via death receptors, cannot be excluded as a reason for this phenomenon, although the influence of glycans and glycosylation patterns on cell death induction is incompletely understood [198]. Taken together, the hMSC-TERT viability data suggest a dose-dependent cell cytotoxicity resulting in necrosis. The additional investigation of peracetylated *N*-alkyneacetylmannosamine (Ac_4ManNAl) featuring an alkyne group showed similar results as the respective azido sugar excluding an impact of both bioorthogonal groups on the cell viability.

The different biochemical responses between primary hMSC and hMSC-TERT in regard to viability were also present when using non-acetylated modified monosaccharides, but less pronounced for each sugar (**Figure 11**). Interestingly, viability rates differ this time when using azido or alkyne sugars suggesting an impact of the bioorthogonal group. However, this effect is not consistent as viability for ManNAl at 2 mM is still over 77 %, while it drops to 18 % for *N*-alkyneacetylneuraminic acid (hereinafter SiaNAl) and the hMSC data do not support this assumption (**Figure 11A**). Although there are no obvious explanations, some facts need to be considered for better understanding. As the uptake of non-acetylated monosaccharides mostly depends on sugar channels [65,66] and is not driven by passive diffusion as it is the case for peracetylated monosaccharides, higher concentrations are necessary for similarly effective usage in metabolic glycoengineering (compare **Figure 15** and **Figure 18**). However, without an experimental quantitication of intracellular sugar levels, concentrations might be different. Although the modified monosaccharides are not used for energy harvesting due to missing increased ATP levels, their impact and utilization in sugar-dependent pathways other than glycosylation cannot be excluded. For that reason, cytotoxicity tests based on DNA content or doubling time might be more robust for the characterization of click sugars in metabolic glycoengineering research.

Metabolic Glycoengineering does not alter the Phenotype of hMSC-TERT

As already shown by Layek *et al*. for hMSC [80], it was additionally analyzed whether the stimulation of hMSC-TERT with modified monosaccharides has an impact on their mesenchymal differentiation capacity in this work. The assessment of the osteogenic and adipogenic differentiation potential suggests no remarkable impairment after incubation with Ac_4ManNAz or Ac_4ManNAl. The Oil Red staining results revealed a highly regular lipid accumulation regardless of the test conditions (**Figure 13A, right**), and the Alizarin Red staining also revealed positive results for all conditions, confirming a successful mineralization as well (**Figure 13A, left**). The marker gene expression data

showed no significant inhibition or increased fold changes for adipogenic and osteogenic marker genes after incubation with Ac_4ManNAz at 20 μM, suggesting that the differentiation process was not severely impaired (**Figure 13B**).

To obtain more insight into the molecular influence of both mannose sugars Ac_4ManNAz and Ac_4ManNAl, their impact on gene expression were analyzed in hMSC-TERT. Genes were selected according to a paper published by the group of Han *et al*. [189]. The authors showed that Ac_4ManNAz, if applied in concentrations higher than 20 μM, led to a downregulation of genes related to one of the following four subgroups: cell adhesion, cytokine–cytokine receptor interaction, extracellular matrix–receptor interaction, and cancer-related pathways. Seven genes were selected out of this group and analyzed for their expression in hMSC-TERT after 72 h incubation with Ac_4ManNAz or Ac_4ManNAl by qPCR. All examined gene expressions were affected by high variances for all conditions, suggesting no relevant biological conclusions for these datasets (**Figure 13C**). Considering that there were no obvious differences (not even by trend findings) deriving from the functional click group or the concentration, it can be assumed that data from this work indicate no interference of Ac_4ManNAz or Ac_4ManNAl with transcriptional processes during protein biosynthesis in hMSC-TERT, which is in contrast to the results shown in endothelial progenitor cells.

Modified Mannose Sugars showed superior Potential for Metabolic Glycoengineering in hMSC or hMSC-TERT

Prior to functional applications with glycoengineered cells, the glycoengineering technique was investigated for optimization and the proof of concept. The conjugation of incorporated modified monosaccharides and target molecules can be conducted via the strain-promoted (SP) or copper-catalyzed azide–alkyne cycloaddition (CuAAC) click reaction. Initial experiments after incubation with Ac_4ManNAz and conjugation with a fluorescent dye revealed a successful cell modification in both hMSC and hMSC-TERT independent of the reaction type (**Figure 14** and **Figure 15**). Reasons like higher reaction rates with other cell types [191] or the easier synthesis of target molecules with alkynyl groups were decisive factors to choose the CuAAC click reaction for all further experiments. As Cu ions are necessary for this reaction type, cytotoxicity was tested before. The cell viability was high, even at Cu concentrations up to 100 μM (**Figure 12**), which can be explained by the short exposure time of 5 min with subsequent washing steps removing residual Cu^{I} ions and the stable complexing through the ligand [199]. This short-time resistance against Cu^{I} ions has already been shown in viability tests for NIH 3T3 fibroblasts and HEK293-F cells. In those experiments, the cells still

showed a survival rate of approximately 80 % after 10 min incubation with up to 200 μM Cu (both cell types), and even after 20 min for the HEK293-F cells [191].

Several modified monosaccharides exist and are used for metabolic glycoengineering; therefore, peracetylated click sugars like Ac_4GlcNAz, Ac_4ManNAz, Ac_4ManNAl as alkyne analog, or peracetylated *N*-azidoacetylgalactosamine (Ac_4GalNAz) were tested for their biochemical incorporation potential into the glycocalyx of hMSC-TERT. Only Ac_4ManNAz and Ac_4ManNAl could be detected in the glycocalyx as part of glycans (**Figure 15**), however with a difference regarding their respective incorporation efficiency. It can be assumed that the different incorporation efficiencies do not result from processes prior to the glycosylation because the uptake of the modified monosaccharides into the cell regulated by the diffusion rate and their subsequent enzymatic deacetylation by unspecific esterases should work for all four molecules. Therefore, similar intracellular sugar concentrations for subsequent glycosylation pathways can be concluded. Even though enzymes exist for the interconversion of monosaccharides [200-202] and also of *N*-acteylglucosamine (GlcNAc) to ManNAc (enzyme here *N*-acylglucosamine 2-epimerase) or *N*-acetylgalactosamine (GalNAc) to UDP-GlcNAc via a three-step process, the hMSC-TERT might use the azido variants of GlcNAc and GalNAc primarily for *O*-linked GlcNAc processing [203]. This glycosylation type results in glycoproteins also residing in the nucleus and the cytosol, which cannot be targeted by the alkyne-Cy 3 dye during the click reaction, reflected by the absence of fluorescence signals (**Figure 15**). Yarema *et al*. compared the incorporation efficiencies of *N*-levulinoylglucosamine and *N*-levulinoylmannosamine in Jurkat cells, at which they found almost no usage of the glucose variant for *N*-linked glycosylation assuming a high competition with natural UDP-GlcNAc as reason [204]. By far the strongest fluorescence signals could be observed when using the mannose sugars. In contrast to the other two isomers, these monosaccharides are direct precursors of sialic acid, promoting its biosynthesis and related negative feedback loop [205,206]. Obviously, the glycosylation process does not only depend on the type of sugar which is used, but also on the cell type. Previous studies showed that the glycoengineering of neuroblastoma (SK-N-MC) and osteosarcoma (U2OS) cell membranes resulted in the highest density of labeled glycans for GalNAz glycoconjugates, followed by ManNAz-derived glycoconjugates, while GlcNAz glycoconjugates showed the lowest density with a peculiar dependence on the investigated cell type [207]. In further studies, treatment of HEK 293 cells with Ac_4GlcNAz [191] or Ac_4GalNAz [208] resulted in a proper incorporation as seen in this work for the mannose sugars, while Ac_4ManNAz showed different incorporation efficiencies for pancreatic cell lines SW1990 and PANC-C1 as well as CHO and Jurkat cells [209]. Moreover, quantification of whole cell sialic acid levels after incubation with different modified monosaccharides by Dold *et al*. [208] revealed sugar analog-dependent differences between HEK 293T and HeLa S3 cells, but also in the compartmentalization of the respective sialic

acids between cell membranes and cytosol. Interestingly, a study from 2009 showed a higher conversion of Ac_4ManNAl into the respective sialic acid than of Ac_4ManNAz in six different cell lines [210], but without any investigation regarding their compartmentalization. Taking into account the impact of the specific cell environment on the glycocalyx development in terms of physical interactions (higher shear forces by fluid flow as an example for endothelial cells [211]) and nutrition supply, these observations also suggest specific expression patterns of the enzymes in the sialic acid biosynthesis pathway leading to different metabolic fluxes.

Following the characterization of metabolic glycoengineering with peracetylated sugars, new questions were raised and led to the decision to investigate more but different modified monosaccharides (**Figure 8E - H**). The abandonment of acetyl protection groups shall avoid unwanted chemical side reactions [190] and the use of sialic acids might result in a higher incorporation efficiency as they omit the need of intracellular enzymatic synthesis and can directly enter the glycosylation pathway (**Figure 3**). An additional advantage of sialic acids is the possibility to conjugate two different target molecules providing more functionalities by one sugar unit [212]. The data of hMSC-TERT confirm the dose-dependent incorporation already seen with peracetylated click sugars (compare **Figure 18** and **Figure 15**). Interestingly, it seems that the bioorthogonal alkyne group supports the usage in *N*-linked glycosylation compared to the azido monosaccharides, but there are several facts that question this assumption. On the one hand, peracetylated mannose sugars showed the opposite effect (**Figure 15**), on the other hand, the single data points for the incorporation efficiency of *N*-alkyneacetylneuraminic acid (hereinafter SiaNAl) are quiet scattered, which impairs drawing solid conclusions at least for this monosaccharide. The additional consideration of the viability data (**Figure 11B**) might suggest a correlation between viability and incorporation efficiency as ManNAl revealed the best outcomes in both analyses. Even though only true in case of the mannose sugars, this thought seems trivial and logic as glycosylation and intracellular transport of proteins demand ATP and cell integrity. A look at the hMSC data provides differences and similarities (**Figure 17**). Although all analyses are subject to high variances deriving from the typical cell donor variability when working with primary material from patients, both mannose sugars showed the highest incorporation efficiencies up to 7.6-fold at 2 mM. These results and the respective viability rates (**Figure 11A**) clearly demonstrate a better glycosylation performance in primary cells than in hMSC-TERT when using hexosamine click sugars. Interestingly, incubation with modified sialic acids resulted in lower incorporation efficiencies similar to those in hMSC-TERT, while showing viability rates still over 80 % (except 68 % for SiaNAl at 2 mM). This difference regarding the surface sialic acid levels has also been shown in other cells like human epithelial adenocarninoma cells (Caco-2) [213]. The most plausible explanation for this observation might be trivial but critical for

the outcome as the uptake of the molecules by the cell is the precondition for any metabolic glycoengineering approach. To date, there are no evidences for plasma membrane-located sialic acid transporters in eukaryotic cells. This fact might surprise in different ways as sialic acids are highly abundant in the glycocalyx and are involved in many biological processes (see Introduction). It is long known that there exists an H^+/anion symporter called sialin in the lysosomal membrane to recover enzymatically cleaved free sialic acids [214]. However, experimental trafficking analyses revealed its intracellular localization mainly to be the lysosomal membrane [215]. Further studies investigating the sialin delivered hints for an uptake of exogenously provided sialic acids in different eukaryotic cell lines [216,217], but without identifying a specific transporter protein in the membrane. In 2012, Qin *et al*. showed an immunocytochemical colocalization of sialin and Na^+/K^+-ATPase as plasma membrane marker in salivary gland cells [218], but without additional analyses on a submolecular level its methodic explanatory power is not sufficient as a proof for the localization. Considering all these aspects, the incorporated modified sialic acids seem to derive mainly from the glycocalyx salvage process. Although modified sialic acids can be used for metabolic glycoengineering as proven in this work or others earlier [219], its significantly lower uptake compared to hexosamine click sugars poses a drawback that needs to be considered in glycoengineering approaches.

After detecting the successful incorporation of modified monosaccharides, the question came up how long these introduced modifications persist in the glycocalyx, which will be important for applications of glycoengineered cells. The microscopic results revealed an initial decrease in the fluorescence signal for both mannose sugars, meaning a loss of the introduced glycocalyx modifications (**Figure 16**). While these alterations disappeared after 2 d when using Ac_4ManNAl, the fluorescence signal of the covalently bound alkyne-Cy 3 dye slowly decreased over time, but was still detectable after 6 d. In previous studies with primary hMSC [80] or human adipose-derived stromal cells (hASC) [92], a constant decline of the fluorescence signal over a period of 7 d or even 14 d in the case of hASC could be observed, with almost no signal at the endpoint. With regard to the Ac_4ManNAz data from this work, it can be assumed that the modified hMSC-TERT will behave similarly and return to their native glycocalyx state after a while. The reason for the missing fluorescence signal after 2 d when using Ac_4ManNAl is not obvious because both functional groups (azide and alkyne) are biologically inert and small in terms of steric hindrance [220]. The only difference lies in their polarity; the azide exhibits delocated partial charges, which could interfere at least with enzymatic cleavage. Finally, the cells showed small focal signals (section of Ac_4ManNAz 20 μM 2 d in **Figure 16**) after 2 d, which persisted until day six. These structures might be internalized glycoprotein fragments as part of salvage processes in the light of glycocalyx turnover, which was also assumed by Layek *et al*. [80].

Incorporation of Target Molecules into the Glycocalyx increases the Cell Stiffness

Following the characterization of metabolic glycoengineering, functional tests were the next logical step to demonstrate its applicability for approaches in biofabrication. As shear stress poses an issue during bioprinting dependent on the process conditions, this project investigated the reinforcement of the cell glycocalyx by incorporation of two different target molecules and its impact on cell stiffness. The conjugation of alkyne-modified surface sialic acids with both the coumarin derivative AG13 (**Figure 8I**) or the galectin 1 ligand JM139 (**Figure 8J**) increased cell stiffness, while concomitantly diminishing cell fluidity of hMSC-TERT independent on the applied pneumatic pressure (**Figure 20**). Despite the variance in the stiffness data, the higher negative correlation between stiffness and fluidity suggests a slightly stronger potential for the galectin 1 ligand JM139, which should derive from its different structure featuring more functional groups than the benzopyrone structure of the coumarin derivative AG13. Mechanistic explanations could be suspected in either these additional molecular interactions with other glycocalyx components or an increased packing effect reducing the cell fluidity leading to enhanced cell stiffness. Studies investigating the glycocalyx thickness delivered some hints for the latter assumption. Gao and Lipowsky found after *in vivo* treatment of rat mesenterial endothelial cells with glucosaminoglycan-specific lyases an impaired diffusion of FITC in the glycocalyx sublayer implicating a higher density mediated through mainly hyaluronan [36]. O'Callaghan *et al*. showed in a different approach using atomic force microscopy (AFM) with help of indentation profiles, that the elastic modulus of bovine pulmonary microvascular endothelial cells (BPMEC) increased more rapidly upon indentation after enzymatic treatment with hyaluronidase or heparinase [41]. As the experimental indentation depth correlated to the thickness of the sugar layer, the authors suggested that enzymatic cleavage of glucosaminoglycans located more in the outer boundary exposed stiffer glycocalyx regions close to the cell membrane. Wiesinger *et al*. demonstrated in a later AFM study the relation between glycocalyx stiffness and glycosaminoglycan density for several cell types including human umbilical cord veins endothelial cells (HUVEC) and human PMEC [221]. Interestingly, results were independent of the used glycosaminoglycan-lyase contrasting to the spatial distribution concluded by Gao and Lipowsky.

Stable Galectin 1 Expression in hMSC or hMSC-TERT supports the Application of tailored Galectin 1 Ligands

A further future goal of this project was the optimization of cell adherence to bioinks, which is a precondition for natural proliferation and phenotype expression. In this case, experimental approaches are based on modification of the bioinks with glycoconjugates aiming for enhanced cell-polymer adhesion. As the focus was on galectin-mediated interactions, an initial biological characterization was performed to explore the applicability of this research strategy in hMSC. The expression of galectin 1 could be detected on gene and protein level in both hMSC and hMSC-TERT (**Figure 19A + B**). Although known for hMSC [222], the detection of a stable expression in hMSC-TERT is important to exclude adverse transfection-based impacts as this cell line showed different behavior in metabolic glycoengineering compared to the primary cells. In 2017, Zhang *et al*. showed that galectin 1, secreted by cocultured hMSC or exogenously added (3 μM), increased galectin 1 mRNA expression in dendritic cells [223]. Furthermore, simultaneous supplementation with the selective galectin 1 inhibitor thiodigalactoside completely prevented gene upregulation. Based on these results, a synthesized tailored galectin 1 ligand (**Figure 8K**) showing specific binding interactions with the protein [224] was tested for a potential similar effect, but did not induce an upregulation of galectin 1 mRNA expression in hMSC-TERT (**Figure 19C**) independent of the concentration. Although this assay was not meant to detect binding interactions *in vitro*, a gene activation as result would have indirectly confirmed the crystallographic binding data for this ligand. Suzuki *et al*. demonstrated in cell adhesion assays with lymphoma cells, that enzymatic cleavage of surface sialic acids or inhibition of *N*-glycosylation with the indolizidine alkaloid swainsonine enhanced cell adhesion to galectin 1 coated plastic wells [225,226]. The authors concluded a potential masking effect of respective membrane receptors by sialic acids resulting in steric hindrance. However, tumor cells exhibit a quite different glycosylation pattern on their cell surface than normal cells [227-229] and thus could interact in other ways with free galectin 1. Another effect might be important to consider when designing lectin ligands. A recent study showed that binding of FITC-galectin 1 to murine splenocytes can be significantly increased by the addition of galectin 7 [230]. Experiments with a monomeric mutant form of galectin 1 showed cell agglutination only in the presence of galectin 7 concluding that galectins function in concert. Considering these aspects for the applicability of tailored galectin 1 ligands for a controlled adherence behavior in biofabrication approaches, cell-based binding studies are necessary to unravel lectin-mediated cell adherence and to investigate the role of other involved lectins.

Thermoresponsive Bioinks exhibit good Cytocompatibilities with hMSC-TERT after Bioprinting

For the cell characterization after bioprinting, the thermoresponsive bioinks Polyoxazoline-Polyoxazine (hereinafter POx-POzi) and Pluronic F127 were used as it is quite simple to isolate cells from the hydrogel for subsequent analyses; though viability tests were performed to evaluate cytocompatibility of both polymer solutions. Live/Dead staining directly after the printing revealed a small portion of dead cells independent of the processing step when using POx-POzi, but a higher fraction when using Pluronic F127 (more pronounced after additional printing) (**Figure 21A**). Measurements of viability and apoptosis rates after 24 h recovery time provided similar data showing a better outcome for the POx-POzi bioink (**Figure 21B**). These results are in line with some other studies using that polymer. Lorson *et al*., who synthesized the POx-POzi bioink for the first time, found a high viability of murine NIH 3T3 fibroblasts which was above 91 % after printing of 1×10^6 cells/mL using a 250 μm needle at 1.2 bar [103], while a recent study by the same group demonstrated high viability of hASC using a slightly different POx-POzi variant (above 97 % after printing of 0.5×10^6 cells/mL using a 250 μm needle at presumably 1.2 bar as well) [231]. In contrast to that, Thonhoff *et al*. showed reduced cell viability of human neural stem cells upon incubation with Pluronic F127 (88 % at 20 % *w/v* polymer concentration or 46 % at 30 % *w/v* polymer concentration) [232]. However, cells were seeded as a monolayer underneath the polymer solution and incubated for 48 h, which is different from the experimental conditions in this work. Their test design hampers the discrimination whether low viability results from material cytotoxicity or a critical shortage with nutritions. The latter reason could derive from physico-chemical interactions of the nutritions with the polymer network probably leading to a retention effect. It is known that amphiphilic block copolymers form spherical micelles in aqueous media presenting a hydrophobic core and a hydrophilic shell [233], which then aggregate into a cubic lattice depending on conditions like polymer concentration for instance. Also Lorson *et al*. performed some structural analyses of their POx-POzi bioink confirming features like isothermal shear-thinning behavior and rapid recovery after shear stress exposition [103]. Interestingly, rheologic data were better fitted by a computational model describing a bicontinuous sponge-like structure than a cubic lattice leading the authors to the assumption of a distinct gel structure compared to Pluronic F127. Despite the chemical property of both polymer units to form micelles [233,234], these data suggest different supra-molecular hydrogel networks probably resulting in unequal shear loads when pneumatically printed. Additionally, it should be considered that this project used harsher printing conditions in terms of cytocompatibility (5- to 10-fold higher cell concentration, 64 % of needle diameter and 2-fold higher pneumatic pressure). Although these conditions were chosen to provoke shear stress-related cell

damage during the printing process, the viability outcomes for the POx-POzi bioink demonstrated a good cytocompatibility and confirmed the rheological characterization by Lorson *et al*. [103].

Thermoresponsive Bioinks induced minimal Mechanotransduction in hMSC-TERT

With regard to the hypothesis that deals with cellular shear stress resistance, it was necessary to investigate the impact of potential shear stress deriving from the bioprinting process on the cells to detect any protective effects of glycoengineering approaches. An immunocytochemical visualization of the cytoskeleton revealed no enhanced or altered formation of F-actin fibers independent on the processing step or the used polymer (**Figure 22**). This negative result can be explained by comparing it to cytoskeletal analyses performed with other cells in the past. Studies showed a remodeling of the fiber network after exposition to fluid flow in human and bovine pulmonary artery endothelial cells already after 15 min [235], in murine osteoblast cell line MC3T3-E1 after 1 h [236] as well as in HUVEC after 24 h [237]. Even a short periodic centrifugation over a time range of 16 h led to an increase of the F-actin content in cardiomyocytes by 1.6 times [238]. All these investigations had in common, that the cells were exposed to shear stress over a longer time period. In contrast, the residence time of each cell passing through the printing needle just takes some seconds or less depending on parameters like nozzle geometry, bioink rheology or pneumatic pressure [127]. For that reason, such short exposition to shear stress seems to be insufficient for a remodeling of the cytoskeleton. To further explore potential mechanotransduction, expression of the mechanoresponsive genes FOS and PTGS2 were assessed after cell processing in both bioinks. qPCR data showed an upregulation of FOS and a downregulation of PTGS2 for both bioinks, which were more pronounced for Pluronic F127 and in case of only mixing with the polymer solution (**Figure 23A**). In literature, bone-related cells are well known for their mechanosensitivity as normal bone formation needs mechanical stimulation [239]. Murine osteoblasts (MC3T3-E1) revealed an ongoing upregulation of PTGS2 after 1 h exposition to fluid flow positively correlated with the shear intensity [240]. Primary hMSC as precursors also showed an increased gene expression of FOS and PTGS2 already after 15 min cyclic stretching of cell layer grown in elastic polyurethane well plates [241]. Considering the different exposition times to shear stress again, the upregulation of FOS in this project surprises despite the high variances when using Pluronic F127. It might be possible that FOS-mediated mechanotransduction is more sensitive to mechanical loads than PTGS2 lacking any activation independent of the processing step or the bioink. However, applying less harsh printing conditions in terms of cytocompatibility (30 % of cell concentration, conical nozzle with 2.6-fold wider aperture and 4 % of pneumatic pressure) showed no increased FOS gene expression (results by Maria Danz from the work group of Prof. Dr. Regina

Ebert) (**Figure 23B**). This opposed result clearly demonstrates the impact of printing conditions and how cells respond to them. To investigate, if the mechanotransduction finally leads to a coupled cell response by protein expression, hMSC-TERT-AP1 were assessed the same way. This cell system features a luciferase gene construct whose AP1-responsive promoter element gets activated upon FOS expression and subsequent formation of the AP1 transcription factor complex [26]. In contrast to the gene analyses, cells treated with POx-POzi showed significantly more luciferase activity (up to 1.7-fold), which were higher when only mixed with the polymer solution (**Figure 23C**). The lower luciferase activity deriving from Pluronic F127-treated cells is indeed unexpected. However, literature raises questions about its sensitivity as Seefried *et al*. did not find consequent protein expression during their characterization when applying cyclic stretching to hMSC-TERT-AP1 layer grown in polyurethane well plates [26]. Though luciferase activity correlated neither with applied strain intensity nor with exposition time in a consequent manner. While it was almost 4-fold higher than the unstretched control at 1 % extension or at 1 Hz after 30 min cyclic stretching, a later study by the same group showed lesser luciferase expression (below 1.5-fold) of hMSC-TERT-AP1 even after 60 min exposition to cyclic stretching [241].

In summary, it seems that hMSC-TERT did not experience shear stress provoking remarkable cell responses when used in thermoresponsive bioinks. A closer look at the type of shear loads could deliver additional answers. Most of the studies characterizing cell or glycocalyx behavior subjected to shear stress focus on immobilized cells. Weinbaum *et al*. modeled mechanotransduction of shear forces through glycocalyx components based on the glycocalyx model proposed by Squire *et al*. [35] featuring bush-like structures comprising proteoglycan-chains linked to anchored core proteins. According to their calculations, shear forces bend the proteoglycan bushes, which in turn transmits a torque to the rigid core proteins acting as a leverage. Furthermore, they assume that a more rigid structure of the glycocalyx supports the molecular sieving function and dissipates shear loads in a way that fluid velocity close to the cell membrane diminishes to 0.2 % of the edge velocity [242]. Comparing these conditions to the situation in a printing needle, it is obvious that axial shear forces are minimized as cells are floating within the polymer solution. However, this still depends on the radial position within the needle as shear stress linearly increases with the distance from the center [127]. In addition to potential shear loads deriving from fluid flow, the cell concentration adds another important aspect as mentioned earlier.

Conclusion

Concerning the numerous application possibilities for metabolic glycoengineering due to the feasibility of introducing any target molecule into the cell glycocalyx, it is important to know which modified monosaccharides provide the best outcomes in terms of viability and incorporation efficiency. In particular, if animals or patients were involved in the study, cell modification should be optimized for the respective purposes. The characterization of glycoengineering in hMSC and hMSC-TERT in this project compared with other cell types from literature revealed quite different outcomes, especially in terms of the incorporation efficiency. Since glycosylation represents an ubiquitous pathway in every cell, one would expect similar metabolic fluxes for certain monosaccharides. However, the partly opposed results clearly demonstrate that glycosylation depends on much more than just conditions of sugar supplementation. They further legitimate if not demand preliminary testing of click sugars prior to functional approaches using metabolic glycoengineering just as a tool. Although some studies showed cell engineering by use of modified sialic acids, the inferior incorporation efficiency due to a worse uptake into the cell impairs their potential deriving from the possibility for multiple functionalization. In that light, studies elucidating the cell's interaction with exogenous sialic acids are necessary to dissect possible uptake mechanisms and clarify their role at all, as eukaryotic cells usually cover their demand for sialic acids by intracellular production and recycling of glycocalyx components. Most applications of glycocalyx modification in cell based research aim for biological responses like among others differentiation, immunomodulation or homing, but rarely for biophysical cell features perhaps of missing applications. Based on that situation, the approach of this project to enhance cell stiffness using metabolic glycoengineering seems quite unusual at the first glance, but extends the room for possibilities and demonstrate the flexibility of this technique. As the mechanical characteristics of the glycocalyx are not fully understood yet, the small stiffness increases of hMSC-TERT after glycoengineering in this work were indeed surprising if considering the cell type. Almost every study investigating the cell glycocalyx focuses on endothelial cells, which *in vivo* are constantly exposed to fluid flow and regulate the extravasation of leukocytes. These conditions clearly define its characteristics demanding more structural integrity and flexibility to withstand the persistent shear stress. It might be this difference, which revealed a small stiffening effect in hMSC-TERT; thus cells residing an *in vivo* niche scarcely subjected to shear stress prior to differentiation into osteoblasts. Regarding the conjugated target molecules and their similar impact on cell stiffness, further questions need to be investigated regarding the molecular interactions within the glycocalyx and the impact of the molecular structure. Resulting answers are important in particular for the design process of potential target molecules. Nevertheless, a functional proof of concept to show a protective effect deriving from stiffer glycoengineered cells abides and would demonstrate, if

successful, that biophysical glycocalyx characteristics do not only play a role for endothelial cells when exposed to shear stress. Based on the printing results, the hypothesis needs to be specified as shear stress during bioprinting highly depends on the conditions. Although long-term surveillance of printed cells regarding phenotypic cell features and viability were not performed in this project, the analyses directly after processing with thermoresponsive bioinks did not show damaged cells that need to compensate lasting adverse effects. One can conclude that the physicochemical properties of both POx-POzi and Pluronic F127 (especially the shear-thinning behavior) compensate conditions, which increase shear stress like higher cell concentrations or pneumatic pressures. This strength is really beneficial for the printing process, but at the same time their greatest weakness as the lacking possibility of cross-linking the polymer network for permanent stability does not allow long-term cultivation of these printed constructs yet, which are necessary for their maturation. So the application of stiffer glycoengineered cells in cross-linkable and more viscous bioinks like alginate might be more fruitful. However, the experimental setting as such influences the type, intensity, and duration of shear stress projected on the cells and shear stress can be minimized by use of conical nozzles, highly shear-thinning bioinks, and low pneumatic pressures. Even though these indeed reasonable experimental actions are narrowing the application window for this glycoengineering approach, its advantage of implementing transient cell modifications vanishing after certain time offers several other possibilities to improve and control cell behavior in biofabrication processes.

The part of this work addressing the characterization of galectin 1 ligands and their impact on cells was a first step into the direction of applied glycoengineering using glycoconjugates in biofabrication. This molecule class was chosen due to its advantages in terms of cytocompatibility. It seems trivial but the incorporation of molecules that are highly similar to glycocalyx components minimizes unwanted chemical side-reactions. Furthermore, it might be easier to predict their behavior and impact on the cells while several natural functional groups allow specific chemical modifications broadening the tool box. For the galectin 1 ligands, successful and valid cell-based binding assays will open up more possibilities for biofabrication approaches including control of adhesion, immunomodulation or biophysical cell features as slightly indicated by the investigation of cell stiffness in this work. However, all the advantages of glycoengineered cells for biofabrication processes can be tied up by the physicochemical bioink properties impairing any expected beneficial effect. Even though true for any use of altered cells, the bioink selection as well as the printing conditions for the final application should be taken into account when designing glycocalyx modifications.

Bibliography

1 Colter, D. C., Sekiya, I. & Prockop, D. J. Identification of a subpopulation of rapidly self-renewing and multipotential adult stem cells in colonies of human marrow stromal cells. *Proc Natl Acad Sci USA* **98**, 7841-7845, doi:10.1073/pnas.141221698 (2001).

2 Dominici, M. *et al.* Minimal criteria for defining multipotent mesenchymal stromal cells. The International Society for Cellular Therapy position statement. *Cytotherapy* **8**, 315-317, doi:10.1080/14653240600855905 (2006).

3 Pittenger, M. F. *et al.* Multilineage potential of adult human mesenchymal stem cells. *Science* **284**, 143-147, doi:10.1126/science.284.5411.143 (1999).

4 Mamidi, M. K. *et al.* Comparative cellular and molecular analyses of pooled bone marrow multipotent mesenchymal stromal cells during continuous passaging and after successive cryopreservation. *J Cell Biochem* **113**, 3153-3164, doi:10.1002/jcb.24193 (2012).

5 Zheng, Y. H., Xiong, W., Su, K., Kuang, S. J. & Zhang, Z. G. Multilineage differentiation of human bone marrow mesenchymal stem cells in vitro and in vivo. *Exp Ther Med* **5**, 1576-1580, doi:10.3892/etm.2013.1042 (2013).

6 Okolicsanyi, R. K. *et al.* Human Mesenchymal Stem Cells Retain Multilineage Differentiation Capacity Including Neural Marker Expression after Extended In Vitro Expansion. *PloS one* **10**, e0137255-e0137255, doi:10.1371/journal.pone.0137255 (2015).

7 Rehman, J. *et al.* Secretion of angiogenic and antiapoptotic factors by human adipose stromal cells. *Circulation* **109**, 1292-1298, doi:10.1161/01.Cir.0000121425.42966.F1 (2004).

8 Eirin, A. *et al.* Comparative proteomic analysis of extracellular vesicles isolated from porcine adipose tissue-derived mesenchymal stem/stromal cells. *Scientific reports* **6**, 36120-36120, doi:10.1038/srep36120 (2016).

9 Samsonraj, R. M. *et al.* Concise Review: Multifaceted Characterization of Human Mesenchymal Stem Cells for Use in Regenerative Medicine. *Stem Cells Transl Med* **6**, 2173-2185, doi:10.1002/sctm.17-0129 (2017).

10 Le Blanc, K. *et al.* Mesenchymal stem cells for treatment of steroid-resistant, severe, acute graft-versus-host disease: a phase II study. *Lancet* **371**, 1579-1586, doi:10.1016/s0140-6736(08)60690-x (2008).

11 Ringdén, O. *et al.* Mesenchymal stem cells for treatment of therapy-resistant graft-versus-host disease. *Transplantation* **81**, 1390-1397, doi:10.1097/01.tp.0000214462.63943.14 (2006).

12 Koç, O. N. *et al.* Allogeneic mesenchymal stem cell infusion for treatment of metachromatic leukodystrophy (MLD) and Hurler syndrome (MPS-IH). *Bone Marrow Transplant* **30**, 215-222, doi:10.1038/sj.bmt.1703650 (2002).

13 Gieseke, F. *et al.* Human multipotent mesenchymal stromal cells use galectin-1 to inhibit immune effector cells. *Blood* **116**, 3770-3779, doi:10.1182/blood-2010-02-270777 (2010).

14 Ortiz, L. A. *et al.* Interleukin 1 receptor antagonist mediates the antiinflammatory and antifibrotic effect of mesenchymal stem cells during lung injury. *Proceedings of the National Academy of Sciences of the United States of America* **104**, 11002-11007, doi:10.1073/pnas.0704421104 (2007).

15 Bonfield, T. L. *et al.* Human mesenchymal stem cells suppress chronic airway inflammation in the murine ovalbumin asthma model. *Am J Physiol Lung Cell Mol Physiol* **299**, L760-770, doi:10.1152/ajplung.00182.2009 (2010).

16 Tu, C. *et al.* Human Umbilical Cord Mesenchymal Stem Cells Promote Macrophage PD-L1 Expression and Attenuate Acute Lung Injury in Mice. *Curr Stem Cell Res Ther*, doi:10.2174/1574888x17666220127110332 (2022).

17 Kossl, J. *et al.* Antiapoptotic Properties of Mesenchymal Stem Cells in a Mouse Model of Corneal Inflammation. *Stem Cells Dev* **30**, 418-427, doi:10.1089/scd.2020.0195 (2021).

18 Buono, L. *et al.* Mesenchymal Stem Cell-Derived Extracellular Vesicles Protect Human Corneal Endothelial Cells from Endoplasmic Reticulum Stress-Mediated Apoptosis. *Int J Mol Sci* **22**, doi:10.3390/ijms22094930 (2021).
19 Chen, J. *et al.* Human mesenchymal stromal cells small extracellular vesicles attenuate sepsis-induced acute lung injury in a mouse model: the role of oxidative stress and the mitogen-activated protein kinase/nuclear factor kappa B pathway. *Cytotherapy* **23**, 918-930, doi:10.1016/j.jcyt.2021.05.009 (2021).
20 Arutyunyan, I. *et al.* Role of VEGF-A in angiogenesis promoted by umbilical cord-derived mesenchymal stromal/stem cells: in vitro study. *Stem Cell Res Ther* **7**, 46, doi:10.1186/s13287-016-0305-4 (2016).
21 Samsonraj, R. M. *et al.* Establishing criteria for human mesenchymal stem cell potency. *Stem cells (Dayton, Ohio)* **33**, 1878-1891, doi:10.1002/stem.1982 (2015).
22 Digirolamo, C. M. *et al.* Propagation and senescence of human marrow stromal cells in culture: a simple colony-forming assay identifies samples with the greatest potential to propagate and differentiate. *Br J Haematol* **107**, 275-281, doi:10.1046/j.1365-2141.1999.01715.x (1999).
23 Schellenberg, A. *et al.* Replicative senescence of mesenchymal stem cells causes DNA-methylation changes which correlate with repressive histone marks. *Aging (Albany NY)* **3**, 873-888, doi:10.18632/aging.100391 (2011).
24 Bonab, M. M. *et al.* Aging of mesenchymal stem cell in vitro. *BMC Cell Biol* **7**, 14, doi:10.1186/1471-2121-7-14 (2006).
25 Twine, N. A. *et al.* Molecular Phenotyping of Telomerized Human Bone Marrow Skeletal Stem Cells Reveals a Genetic Program of Enhanced Proliferation and Maintenance of Differentiation Responses. *JBMR Plus* **2**, 257-267, doi:10.1002/jbm4.10050 (2018).
26 Seefried, L. *et al.* A small scale cell culture system to analyze mechanobiology using reporter gene constructs and polyurethane dishes. *Eur Cell Mater* **20**, 344-355, doi:10.22203/ecm.v020a28 (2010).
27 Kokenyesi, R. & Bernfield, M. Core protein structure and sequence determine the site and presence of heparan sulfate and chondroitin sulfate on syndecan-1. *J Biol Chem* **269**, 12304-12309 (1994).
28 Rapraeger, A., Jalkanen, M., Endo, E., Koda, J. & Bernfield, M. The cell surface proteoglycan from mouse mammary epithelial cells bears chondroitin sulfate and heparan sulfate glycosaminoglycans. *J Biol Chem* **260**, 11046-11052 (1985).
29 Meyer, K., Smyth, E. M. & Dawson, M. H. THE ISOLATION OF A MUCOPOLYSACCHARIDE FROM SYNOVIAL FLUID. *Journal of Biological Chemistry* **128**, 319-327, doi:10.1016/S0021-9258(18)73756-3 (1939).
30 Hoffman, P., Linker, A., Lippman, V. & Meyer, K. The Structure of Chondroitin Sulfate B from Studies with Flavobacterium Enzymes. *Journal of Biological Chemistry* **235**, 3066-3069, doi:10.1016/S0021-9258(20)81310-6 (1960).
31 Cifonelli, J. A. & Dorfman, A. Structural studies on heparin and heparitin sulfate. *Biochemical and Biophysical Research Communications* **4**, 328-331, doi:10.1016/0006-291X(61)90212-1 (1961).
32 Hopwood, J. J. & Robinson, H. C. The structure and composition of cartilage keratan sulphate. *Biochem J* **141**, 517-526, doi:10.1042/bj1410517 (1974).
33 Oohira, A., Wight, T. N. & Bornstein, P. Sulfated proteoglycans synthesized by vascular endothelial cells in culture. *Journal of Biological Chemistry* **258**, 2014-2021, doi:10.1016/S0021-9258(18)33090-4 (1983).
34 Nandi, A., Estess, P. & Siegelman, M. H. Hyaluronan anchoring and regulation on the surface of vascular endothelial cells is mediated through the functionally active form of CD44. *J Biol Chem* **275**, 14939-14948, doi:10.1074/jbc.275.20.14939 (2000).

35 Squire, J. M. *et al.* Quasi-Periodic Substructure in the Microvessel Endothelial Glycocalyx: A Possible Explanation for Molecular Filtering? *Journal of Structural Biology* **136**, 239-255, doi:10.1006/jsbi.2002.4441 (2001).
36 Gao, L. & Lipowsky, H. H. Composition of the endothelial glycocalyx and its relation to its thickness and diffusion of small solutes. *Microvasc Res* **80**, 394-401, doi:10.1016/j.mvr.2010.06.005 (2010).
37 Ebong, E. E., Macaluso, F. P., Spray, D. C. & Tarbell, J. M. Imaging the endothelial glycocalyx in vitro by rapid freezing/freeze substitution transmission electron microscopy. *Arterioscler Thromb Vasc Biol* **31**, 1908-1915, doi:10.1161/atvbaha.111.225268 (2011).
38 Targosz-Korecka, M. *et al.* AFM-based detection of glycocalyx degradation and endothelial stiffening in the db/db mouse model of diabetes. *Sci Rep* **7**, 15951, doi:10.1038/s41598-017-16179-7 (2017).
39 Mockl, L. *et al.* Quantitative Super-Resolution Microscopy of the Mammalian Glycocalyx. *Dev Cell* **50**, 57-72 e56, doi:10.1016/j.devcel.2019.04.035 (2019).
40 Marsh, G. & Waugh, R. E. Quantifying the mechanical properties of the endothelial glycocalyx with atomic force microscopy. *J Vis Exp*, e50163, doi:10.3791/50163 (2013).
41 O'Callaghan, R., Job, K. M., Dull, R. O. & Hlady, V. Stiffness and heterogeneity of the pulmonary endothelial glycocalyx measured by atomic force microscopy. *Am J Physiol Lung Cell Mol Physiol* **301**, L353-360, doi:10.1152/ajplung.00342.2010 (2011).
42 Job, K. M., Dull, R. O. & Hlady, V. Use of reflectance interference contrast microscopy to characterize the endothelial glycocalyx stiffness. *Am J Physiol Lung Cell Mol Physiol* **302**, L1242-1249, doi:10.1152/ajplung.00341.2011 (2012).
43 Chen, J. *et al.* Revealing the carbohydrate pattern on a cell surface by super-resolution imaging. *Nanoscale* **7**, 3373-3380, doi:10.1039/c4nr05970k (2015).
44 Kramer, J. R., Onoa, B., Bustamante, C. & Bertozzi, C. R. Chemically tunable mucin chimeras assembled on living cells. *Proc Natl Acad Sci USA* **112**, 12574-12579, doi:10.1073/pnas.1516127112 (2015).
45 Harding, I. C. *et al.* Endothelial barrier reinforcement relies on flow-regulated glycocalyx, a potential therapeutic target. *Biorheology* **56**, 131-149, doi:10.3233/BIR-180205 (2019).
46 Houser, J. R. *et al.* The impact of physiological crowding on the diffusivity of membrane bound proteins. *Soft Matter* **12**, 2127-2134, doi:10.1039/c5sm02572a (2016).
47 Chang, P. S. *et al.* Cell Surface Access Is Modulated by Tethered Bottlebrush Proteoglycans. *Biophys J* **110**, 2739-2750, doi:10.1016/j.bpj.2016.05.027 (2016).
48 Gromnicova, R. *et al.* Transport of Gold Nanoparticles by Vascular Endothelium from Different Human Tissues. *PLoS One* **11**, e0161610, doi:10.1371/journal.pone.0161610 (2016).
49 Möckl, L. *et al.* The glycocalyx regulates the uptake of nanoparticles by human endothelial cells in vitro. *Nanomedicine (Lond)* **12**, 207-217, doi:10.2217/nnm-2016-0332 (2017).
50 Uhl, B. *et al.* The Endothelial Glycocalyx Controls Interactions of Quantum Dots with the Endothelium and Their Translocation across the Blood-Tissue Border. *ACS Nano* **11**, 1498-1508, doi:10.1021/acsnano.6b06812 (2017).
51 Shurer, C. R. *et al.* Genetically Encoded Toolbox for Glycocalyx Engineering: Tunable Control of Cell Adhesion, Survival, and Cancer Cell Behaviors. *ACS Biomater Sci Eng* **4**, 388-399, doi:10.1021/acsbiomaterials.7b00037 (2018).
52 Xu, G. K., Qian, J. & Hu, J. The glycocalyx promotes cooperative binding and clustering of adhesion receptors. *Soft Matter* **12**, 4572-4583, doi:10.1039/c5sm03139g (2016).
53 Soler, M. *et al.* Adhesion-related glycocalyx study: quantitative approach with imaging-spectrum in the energy filtering transmission electron microscope (EFTEM). *FEBS Lett* **429**, 89-94, doi:10.1016/s0014-5793(98)00570-5 (1998).
54 Gandhi, J. G., Koch, D. L. & Paszek, M. J. Equilibrium Modeling of the Mechanics and Structure of the Cancer Glycocalyx. *Biophys J* **116**, 694-708, doi:10.1016/j.bpj.2018.12.023 (2019).

55 Henry, C. B. & Duling, B. R. TNF-alpha increases entry of macromolecules into luminal endothelial cell glycocalyx. *Am J Physiol Heart Circ Physiol* **279**, H2815-2823, doi:10.1152/ajpheart.2000.279.6.H2815 (2000).
56 Blaum, B. S. *et al.* Structural basis for sialic acid-mediated self-recognition by complement factor H. *Nat Chem Biol* **11**, 77-82, doi:10.1038/nchembio.1696 (2015).
57 Jandus, C. *et al.* Interactions between Siglec-7/9 receptors and ligands influence NK cell-dependent tumor immunosurveillance. *J Clin Invest* **124**, 1810-1820, doi:10.1172/jci65899 (2014).
58 Läubli, H. *et al.* Engagement of myelomonocytic Siglecs by tumor-associated ligands modulates the innate immune response to cancer. *Proc Natl Acad Sci USA* **111**, 14211-14216, doi:10.1073/pnas.1409580111 (2014).
59 Thi, M. M., Tarbell, J. M., Weinbaum, S. & Spray, D. C. The role of the glycocalyx in reorganization of the actin cytoskeleton under fluid shear stress: a "bumper-car" model. *Proc Natl Acad Sci USA* **101**, 16483-16488, doi:10.1073/pnas.0407474101 (2004).
60 Pahakis, M. Y., Kosky, J. R., Dull, R. O. & Tarbell, J. M. The role of endothelial glycocalyx components in mechanotransduction of fluid shear stress. *Biochem Biophys Res Commun* **355**, 228-233, doi:10.1016/j.bbrc.2007.01.137 (2007).
61 Florian, J. A. *et al.* Heparan sulfate proteoglycan is a mechanosensor on endothelial cells. *Circ Res* **93**, e136-142, doi:10.1161/01.Res.0000101744.47866.D5 (2003).
62 Lopez-Quintero, S. V., Amaya, R., Pahakis, M. & Tarbell, J. M. The endothelial glycocalyx mediates shear-induced changes in hydraulic conductivity. *Am J Physiol Heart Circ Physiol* **296**, H1451-1456, doi:10.1152/ajpheart.00894.2008 (2009).
63 Park, D. *et al.* Enterocyte glycosylation is responsive to changes in extracellular conditions: implications for membrane functions. *Glycobiology* **27**, 847-860, doi:10.1093/glycob/cwx041 (2017).
64 Mahmoud, M., Cancel, L. & Tarbell, J. M. Matrix Stiffness Affects Glycocalyx Expression in Cultured Endothelial Cells. *Front Cell Dev Biol* **9**, 731666, doi:10.3389/fcell.2021.731666 (2021).
65 Mueckler, M. *et al.* Sequence and Structure of a Human Glucose Transporter. *Science* **229**, 941-945, doi:doi:10.1126/science.3839598 (1985).
66 Hediger, M. A., Coady, M. J., Ikeda, T. S. & Wright, E. M. Expression cloning and cDNA sequencing of the Na+/glucose co-transporter. *Nature* **330**, 379-381, doi:10.1038/330379a0 (1987).
67 Sommers, L. W. & Hirschberg, C. B. Transport of sugar nucleotides into rat liver Golgi. A new Golgi marker activity. *Journal of Biological Chemistry* **257**, 10811-10817, doi:10.1016/S0021-9258(18)33897-3 (1982).
68 Eckhardt, M., Mühlenhoff, M., Bethe, A. & Gerardy-Schahn, R. Expression cloning of the Golgi CMP-sialic acid transporter. *Proceedings of the National Academy of Sciences of the United States of America* **93**, 7572-7576, doi:10.1073/pnas.93.15.7572 (1996).
69 Miura, N. *et al.* Human UDP-Galactose Translocator: Molecular Cloning of a Complementary DNA That Complements the Genetic Defect of a Mutant Cell Line Deficient in UDP-Galactose Translocator1. *The Journal of Biochemistry* **120**, 236-241, doi:10.1093/oxfordjournals.jbchem.a021404 (1996).
70 Jones, M. B. *et al.* Characterization of the cellular uptake and metabolic conversion of acetylated N-acetylmannosamine (ManNAc) analogues to sialic acids. *Biotechnol Bioeng* **85**, 394-405, doi:10.1002/bit.10901 (2004).
71 Kim, E. J. *et al.* Characterization of the metabolic flux and apoptotic effects of O-hydroxyl- and N-acyl-modified N-acetylmannosamine analogs in Jurkat cells. *J Biol Chem* **279**, 18342-18352, doi:10.1074/jbc.M400205200 (2004).
72 Bertram, J. & Krisch, K. Hydrolysis of Vitamin A Acetate by Unspecific Carboxylesterases from Liver and Kidney. *European Journal of Biochemistry* **11**, 122-126, doi:10.1111/j.1432-1033.1969.tb00748.x (1969).

73 Harms, E. & Reutter, W. Half-life of N-acetylneuraminic acid in plasma membranes of rat liver and Morris hepatoma 7777. *Cancer Res* **34**, 3165-3172 (1974).
74 Münster, A. K. *et al.* Mammalian cytidine 5'-monophosphate N-acetylneuraminic acid synthetase: a nuclear protein with evolutionarily conserved structural motifs. *Proceedings of the National Academy of Sciences of the United States of America* **95**, 9140-9145, doi:10.1073/pnas.95.16.9140 (1998).
75 Beyer, T. A. *et al.* Biosynthesis of mammalian glycoproteins. Glycosylation pathways in the synthesis of the nonreducing terminal sequences. *Journal of Biological Chemistry* **254**, 12531-12541, doi:10.1016/S0021-9258(19)86347-0 (1979).
76 Holt, G. D. & Hart, G. W. The subcellular distribution of terminal N-acetylglucosamine moieties. Localization of a novel protein-saccharide linkage, O-linked GlcNAc. *Journal of Biological Chemistry* **261**, 8049-8057, doi:10.1016/S0021-9258(19)57510-X (1986).
77 Hinderlich, S., Stäsche, R., Zeitler, R. & Reutter, W. A Bifunctional Enzyme Catalyzes the First Two Steps in N-Acetylneuraminic Acid Biosynthesis of Rat Liver. *Journal of Biological Chemistry* **272**, 24313-24318, doi:10.1074/jbc.272.39.24313 (1997).
78 Watson, D. R., Jourdian, G. W. & Roseman, S. The Sialic Acids: VIII. SIALIC ACID 9-PHOSPHATE SYNTHETASE. *Journal of Biological Chemistry* **241**, 5627-5636, doi:10.1016/S0021-9258(18)96390-8 (1966).
79 Jacobs, C. L. *et al.* Substrate Specificity of the Sialic Acid Biosynthetic Pathway. *Biochemistry* **40**, 12864-12874, doi:10.1021/bi010862s (2001).
80 Layek, B., Sadhukha, T. & Prabha, S. Glycoengineered mesenchymal stem cells as an enabling platform for two-step targeting of solid tumors. *Biomaterials* **88**, 97-109, doi:10.1016/j.biomaterials.2016.02.024 (2016).
81 Saeui, C. T. *et al.* Integration of genetic and metabolic features related to sialic acid metabolism distinguishes human breast cell subtypes. *PLoS One* **13**, e0195812, doi:10.1371/journal.pone.0195812 (2018).
82 Rostovtsev, V. V., Green, L. G., Fokin, V. V. & Sharpless, K. B. A Stepwise Huisgen Cycloaddition Process: Copper(I)-Catalyzed Regioselective "Ligation" of Azides and Terminal Alkynes. *Angewandte Chemie International Edition* **41**, 2596-2599, doi:10.1002/1521-3773(20020715)41:14<2596::AID-ANIE2596>3.0.CO;2-4 (2002).
83 Hong, V., Presolski, S. I., Ma, C. & Finn, M. G. Analysis and optimization of copper-catalyzed azide-alkyne cycloaddition for bioconjugation. *Angew Chem Int Ed Engl* **48**, 9879-9883, doi:10.1002/anie.200905087 (2009).
84 Seth, R., Yang, S., Choi, S., Sabean, M. & Roberts, E. A. In vitro assessment of copper-induced toxicity in the human hepatoma line, Hep G2. *Toxicol In Vitro* **18**, 501-509, doi:10.1016/j.tiv.2004.01.006 (2004).
85 Ning, X., Guo, J., Wolfert, M. A. & Boons, G.-J. Visualizing metabolically labeled glycoconjugates of living cells by copper-free and fast huisgen cycloadditions. *Angewandte Chemie (International ed. in English)* **47**, 2253-2255, doi:10.1002/anie.200705456 (2008).
86 Codelli, J. A., Baskin, J. M., Agard, N. J. & Bertozzi, C. R. Second-generation difluorinated cyclooctynes for copper-free click chemistry. *J Am Chem Soc* **130**, 11486-11493, doi:10.1021/ja803086r (2008).
87 Gutmann, M., Bechold, J., Seibel, J., Meinel, L. & Lühmann, T. Metabolic Glycoengineering of Cell-Derived Matrices and Cell Surfaces: A Combination of Key Principles and Step-by-Step Procedures. *ACS Biomaterials Science & Engineering* **5**, 215-233, doi:10.1021/acsbiomaterials.8b00865 (2019).
88 Laughlin Scott, T., Baskin Jeremy, M., Amacher Sharon, L. & Bertozzi Carolyn, R. In Vivo Imaging of Membrane-Associated Glycans in Developing Zebrafish. *Science* **320**, 664-667, doi:10.1126/science.1155106 (2008).
89 Hao, Y. *et al.* Next-generation unnatural monosaccharides reveal that ESRRB O-GlcNAcylation regulates pluripotency of mouse embryonic stem cells. *Nat Commun* **10**, 4065, doi:10.1038/s41467-019-11942-y (2019).

90 Gutmann, M., Braun, A., Seibel, J. & Lühmann, T. Bioorthogonal Modification of Cell Derived Matrices by Metabolic Glycoengineering. *ACS Biomaterials Science & Engineering* **4**, 1300-1306, doi:10.1021/acsbiomaterials.8b00264 (2018).
91 Bodnar, E. *et al.* Mass spectrometric analysis of products of metabolic glycan engineering with azido-modification of sialic acids. *Anal Bioanal Chem* **407**, 8945-8958, doi:10.1007/s00216-015-9010-x (2015).
92 Lee, S. Y. *et al.* Non-invasive stem cell tracking in hindlimb ischemia animal model using bio-orthogonal copper-free click chemistry. *Biochem Biophys Res Commun* **479**, 779-786, doi:10.1016/j.bbrc.2016.09.132 (2016).
93 Mao, D. *et al.* Bio-orthogonal click reaction-enabled highly specific in situ cellularization of tissue engineering scaffolds. *Biomaterials* **230**, 119615, doi:10.1016/j.biomaterials.2019.119615 (2020).
94 Memmel, E., Homann, A., Oelschlaeger, T. A. & Seibel, J. Metabolic glycoengineering of Staphylococcus aureus reduces its adherence to human T24 bladder carcinoma cells. *Chem Commun (Camb)* **49**, 7301-7303, doi:10.1039/c3cc43424a (2013).
95 Wang, X. *et al.* Equipping Natural Killer Cells with Cetuximab through Metabolic Glycoengineering and Bioorthogonal Reaction for Targeted Treatment of KRAS Mutant Colorectal Cancer. *ACS Chem Biol* **16**, 724-730, doi:10.1021/acschembio.1c00022 (2021).
96 Zhao, Z. *et al.* Cytosolic protein delivery via metabolic glycoengineering and bioorthogonal click reactions. *Biomater Sci* **9**, 4639-4647, doi:10.1039/d1bm00548k (2021).
97 Ruther, F., Distler, T., Boccaccini, A. R. & Detsch, R. Biofabrication of vessel-like structures with alginate di-aldehyde—gelatin (ADA-GEL) bioink. *Journal of Materials Science: Materials in Medicine* **30**, 8, doi:10.1007/s10856-018-6205-7 (2018).
98 Gao, G. *et al.* Tissue-engineering of vascular grafts containing endothelium and smooth-muscle using triple-coaxial cell printing. *Applied Physics Reviews* **6**, 041402, doi:10.1063/1.5099306 (2019).
99 Ooi, H. W. *et al.* Thiol-Ene Alginate Hydrogels as Versatile Bioinks for Bioprinting. *Biomacromolecules* **19**, 3390-3400, doi:10.1021/acs.biomac.8b00696 (2018).
100 Hauptstein, J. *et al.* Hyaluronic Acid-Based Bioink Composition Enabling 3D Bioprinting and Improving Quality of Deposited Cartilaginous Extracellular Matrix. *Advanced Healthcare Materials* **9**, 2000737, doi:10.1002/adhm.202000737 (2020).
101 Russell, C. S. *et al.* In Situ Printing of Adhesive Hydrogel Scaffolds for the Treatment of Skeletal Muscle Injuries. *ACS Applied Bio Materials* **3**, 1568-1579, doi:10.1021/acsabm.9b01176 (2020).
102 Lechner, A., Trossmann, V. T. & Scheibel, T. Impact of Cell Loading of Recombinant Spider Silk Based Bioinks on Gelation and Printability. *Macromolecular Bioscience* **n/a**, 2100390, doi:10.1002/mabi.202100390 (2021).
103 Lorson, T. *et al.* A Thermogelling Supramolecular Hydrogel with Sponge-Like Morphology as a Cytocompatible Bioink. *Biomacromolecules* **18**, 2161-2171, doi:10.1021/acs.biomac.7b00481 (2017).
104 Bednarzig, V. *et al.* Advanced ADA-GEL bioink for bioprinted artificial cancer models. *Bioprinting* **23**, e00145, doi:10.1016/j.bprint.2021.e00145 (2021).
105 Hauptstein, J. *et al.* Bioink Platform Utilizing Dual-Stage Crosslinking of Hyaluronic Acid Tailored for Chondrogenic Differentiation of Mesenchymal Stromal Cells. *Macromolecular Bioscience* **22**, 2100331, doi:10.1002/mabi.202100331 (2022).
106 Reakasame, S. *et al.* Development of alginate dialdehyde-gelatin based bioink with methylcellulose for improving printability. *Materials Science and Engineering: C* **128**, 112336, doi:10.1016/j.msec.2021.112336 (2021).
107 Cai, F.-F., Heid, S. & Boccaccini, A. R. Potential of Laponite® incorporated oxidized alginate–gelatin (ADA-GEL) composite hydrogels for extrusion-based 3D printing. *Journal of Biomedical Materials Research Part B: Applied Biomaterials* **109**, 1090-1104, doi:10.1002/jbm.b.34771 (2021).

108 Hu, C. *et al.* Improving printability of a thermoresponsive hydrogel biomaterial ink by nanoclay addition. *Journal of Materials Science* **56**, 691-705, doi:10.1007/s10853-020-05190-5 (2021).

109 Sonnleitner, D., Schrüfer, S., Berglund, L., Schubert, D. W. & Lang, G. Correlating rheology and printing performance of fiber-reinforced bioinks to assess predictive modelling for biofabrication. *Journal of Materials Research* **36**, 3821-3832, doi:10.1557/s43578-021-00276-5 (2021).

110 Hazur, J. *et al.* Improving alginate printability for biofabrication: establishment of a universal and homogeneous pre-crosslinking technique. *Biofabrication* **12**, 045004, doi:10.1088/1758-5090/ab98e5 (2020).

111 Saravanan, S., Vimalraj, S. & Anuradha, D. Chitosan based thermoresponsive hydrogel containing graphene oxide for bone tissue repair. *Biomed Pharmacother* **107**, 908-917, doi:10.1016/j.biopha.2018.08.072 (2018).

112 Schmid, R. *et al.* A New Printable Alginate/Hyaluronic Acid/Gelatin Hydrogel Suitable for Biofabrication of In Vitro and In Vivo Metastatic Melanoma Models. *Advanced Functional Materials* **32**, 2107993, doi:10.1002/adfm.202107993 (2022).

113 Roshanbinfar, K. *et al.* Electroconductive Biohybrid Hydrogel for Enhanced Maturation and Beating Properties of Engineered Cardiac Tissues. *Advanced Functional Materials* **28**, 1803951, doi:10.1002/adfm.201803951 (2018).

114 Bakhtiiari, A., Khorshidi, R., Yazdian, F., Rashedi, H. & Omidi, M. A bioprinted composite hydrogel with controlled shear stress on cells. *Proc Inst Mech Eng H* **235**, 314-322, doi:10.1177/0954411920976682 (2021).

115 Lueckgen, A. *et al.* Enzymatically-degradable alginate hydrogels promote cell spreading and in vivo tissue infiltration. *Biomaterials* **217**, 119294, doi:10.1016/j.biomaterials.2019.119294 (2019).

116 Böck, T. *et al.* TGF-β1-Modified Hyaluronic Acid/Poly(glycidol) Hydrogels for Chondrogenic Differentiation of Human Mesenchymal Stromal Cells. *Macromolecular Bioscience* **18**, 1700390, doi:10.1002/mabi.201700390 (2018).

117 Hauptstein, J. *et al.* Tethered TGF-β1 in a Hyaluronic Acid-Based Bioink for Bioprinting Cartilaginous Tissues. *Int J Mol Sci* **23**, doi:10.3390/ijms23020924 (2022).

118 Zhang, J., Wehrle, E., Rubert, M. & Müller, R. 3D Bioprinting of Human Tissues: Biofabrication, Bioinks, and Bioreactors. *International journal of molecular sciences* **22**, 3971, doi:10.3390/ijms22083971 (2021).

119 Berg, J. *et al.* Optimization of cell-laden bioinks for 3D bioprinting and efficient infection with influenza A virus. *Sci Rep* **8**, 13877, doi:10.1038/s41598-018-31880-x (2018).

120 Berg, J. *et al.* Bioprinted Multi-Cell Type Lung Model for the Study of Viral Inhibitors. *Viruses* **13**, doi:10.3390/v13081590 (2021).

121 Horder, H. *et al.* Bioprinting and Differentiation of Adipose-Derived Stromal Cell Spheroids for a 3D Breast Cancer-Adipose Tissue Model. *Cells* **10**, doi:10.3390/cells10040803 (2021).

122 Yang, H. *et al.* Three-dimensional bioprinted hepatorganoids prolong survival of mice with liver failure. *Gut* **70**, 567-574, doi:10.1136/gutjnl-2019-319960 (2021).

123 Hao, L. *et al.* Biofabrication of cell-free dual drug-releasing biomimetic scaffolds for meniscal regeneration. *Biofabrication* **14**, doi:10.1088/1758-5090/ac2cd7 (2021).

124 Aldrich, A., Kuss, M. A., Duan, B. & Kielian, T. 3D Bioprinted Scaffolds Containing Viable Macrophages and Antibiotics Promote Clearance of Staphylococcus aureus Craniotomy-Associated Biofilm Infection. *ACS Appl Mater Interfaces* **11**, 12298-12307, doi:10.1021/acsami.9b00264 (2019).

125 Dogan, L. *et al.* Human iPSC-derived mesodermal progenitor cells preserve their vasculogenesis potential after extrusion and form hierarchically organized blood vessels. *Biofabrication* **13**, doi:10.1088/1758-5090/ac26ac (2021).

126 Yu, Y., Zhang, Y., Martin, J. A. & Ozbolat, I. T. Evaluation of cell viability and functionality in vessel-like bioprintable cell-laden tubular channels. *J Biomech Eng* **135**, 91011, doi:10.1115/1.4024575 (2013).
127 Paxton, N. *et al.* Proposal to assess printability of bioinks for extrusion-based bioprinting and evaluation of rheological properties governing bioprintability. *Biofabrication* **9**, 044107, doi:10.1088/1758-5090/aa8dd8 (2017).
128 Müller, S. J. *et al.* Flow and hydrodynamic shear stress inside a printing needle during biofabrication. *PLoS One* **15**, e0236371, doi:10.1371/journal.pone.0236371 (2020).
129 Chang, R., Nam, J. & Sun, W. Effects of dispensing pressure and nozzle diameter on cell survival from solid freeform fabrication-based direct cell writing. *Tissue Eng Part A* **14**, 41-48, doi:10.1089/ten.a.2007.0004 (2008).
130 Nair, K. *et al.* Characterization of cell viability during bioprinting processes. *Biotechnol J* **4**, 1168-1177, doi:10.1002/biot.200900004 (2009).
131 Han, S., Kim, C. M., Jin, S. & Kim, T. Y. Study of the process-induced cell damage in forced extrusion bioprinting. *Biofabrication* **13**, doi:10.1088/1758-5090/ac0415 (2021).
132 Lin, S. *et al.* New method for reducing viscosity and shear stress in hydrogel 3D printing via multidimension vibration. *Comput Methods Biomech Biomed Engin*, 1-16, doi:10.1080/10255842.2022.2039129 (2022).
133 Distler, T. *et al.* 3D printed oxidized alginate-gelatin bioink provides guidance for C2C12 muscle precursor cell orientation and differentiation via shear stress during bioprinting. *Biofabrication* **12**, 045005, doi:10.1088/1758-5090/ab98e4 (2020).
134 Kim, H. *et al.* Shear-induced alignment of collagen fibrils using 3D cell printing for corneal stroma tissue engineering. *Biofabrication* **11**, 035017, doi:10.1088/1758-5090/ab1a8b (2019).
135 Blaeser, A. *et al.* Controlling Shear Stress in 3D Bioprinting is a Key Factor to Balance Printing Resolution and Stem Cell Integrity. *Adv Healthc Mater* **5**, 326-333, doi:10.1002/adhm.201500677 (2016).
136 Ning, L., Betancourt, N., Schreyer, D. J. & Chen, X. Characterization of Cell Damage and Proliferative Ability during and after Bioprinting. *ACS Biomaterials Science & Engineering* **4**, 3906-3918, doi:10.1021/acsbiomaterials.8b00714 (2018).
137 Kim, S. *et al.* Photocrosslinkable chitosan hydrogels functionalized with the RGD peptide and phosphoserine to enhance osteogenesis. *J Mater Chem B* **4**, 5289-5298, doi:10.1039/C6TB01154C (2016).
138 Park, H., Kim, D. & Lee, K. Y. Interaction-tailored cell aggregates in alginate hydrogels for enhanced chondrogenic differentiation. *J Biomed Mater Res A* **105**, 42-50, doi:10.1002/jbm.a.35865 (2017).
139 Oda, Y. & Kasai, K.-I. Purification and characterization of β-galactoside-binding lectin from chick embryonic skin. *Biochimica et Biophysica Acta (BBA) - General Subjects* **761**, 237-245, doi:10.1016/0304-4165(83)90071-5 (1983).
140 Stowell, S. R. *et al.* Galectin-1, -2, and -3 exhibit differential recognition of sialylated glycans and blood group antigens. *J Biol Chem* **283**, 10109-10123, doi:10.1074/jbc.M709545200 (2008).
141 Rapoport, E. M. *et al.* Localization of Galectins within Glycocalyx. *Biochemistry (Mosc)* **83**, 727-737, doi:10.1134/S000629791806010X (2018).
142 Vasta, G. R. *et al.* Galectins as self/non-self recognition receptors in innate and adaptive immunity: an unresolved paradox. *Front Immunol* **3**, 199, doi:10.3389/fimmu.2012.00199 (2012).
143 Ahmed, H., Du, S. J. & Vasta, G. R. Knockdown of a galectin-1-like protein in zebrafish (Danio rerio) causes defects in skeletal muscle development. *Glycoconj J* **26**, 277-283, doi:10.1007/s10719-008-9178-9 (2009).
144 Georgiadis, V. *et al.* Lack of galectin-1 results in defects in myoblast fusion and muscle regeneration. *Dev Dyn* **236**, 1014-1024, doi:10.1002/dvdy.21123 (2007).

145 Cerri, D. G. *et al.* Degeneration of dystrophic or injured skeletal muscles induces high expression of Galectin-1. *Glycobiology* **18**, 842-850, doi:10.1093/glycob/cwn079 (2008).
146 Moiseeva, E. P., Javed, Q., Spring, E. L. & de Bono, D. P. Galectin 1 is involved in vascular smooth muscle cell proliferation. *Cardiovasc Res* **45**, 493-502, doi:10.1016/s0008-6363(99)00276-x (2000).
147 Jouve, N. *et al.* The involvement of CD146 and its novel ligand Galectin-1 in apoptotic regulation of endothelial cells. *J Biol Chem* **288**, 2571-2579, doi:10.1074/jbc.M112.418848 (2013).
148 Perillo, N. L., Pace, K. E., Seilhamer, J. J. & Baum, L. G. Apoptosis of T cells mediated by galectin-1. *Nature* **378**, 736-739, doi:10.1038/378736a0 (1995).
149 Brandt, B. *et al.* Galectin-1 induced activation of the apoptotic death-receptor pathway in human Jurkat T lymphocytes. *Histochem Cell Biol* **129**, 599-609, doi:10.1007/s00418-008-0395-x (2008).
150 Martinez, V. G. *et al.* Galectin-1, a cell adhesion modulator, induces apoptosis of rat Leydig cells in vitro. *Glycobiology* **14**, 127-137, doi:10.1093/glycob/cwh025 (2004).
151 Sanchez-Ruderisch, H. *et al.* Galectin-1 sensitizes carcinoma cells to anoikis via the fibronectin receptor α5β1-integrin. *Cell Death Differ* **18**, 806-816, doi:10.1038/cdd.2010.148 (2011).
152 Andersen, H., Jensen, O. N., Moiseeva, E. P. & Eriksen, E. F. A proteome study of secreted prostatic factors affecting osteoblastic activity: galectin-1 is involved in differentiation of human bone marrow stromal cells. *J Bone Miner Res* **18**, 195-203, doi:10.1359/jbmr.2003.18.2.195 (2003).
153 Freitag, N. *et al.* Interfering with Gal-1-mediated angiogenesis contributes to the pathogenesis of preeclampsia. *Proc Natl Acad Sci USA* **110**, 11451-11456, doi:10.1073/pnas.1303707110 (2013).
154 Pacienza, N. *et al.* The immunoregulatory glycan-binding protein galectin-1 triggers human platelet activation. *Faseb j* **22**, 1113-1123, doi:10.1096/fj.07-9524com (2008).
155 Romaniuk, M. A. *et al.* Binding of galectin-1 to $\alpha IIb\beta_3$ integrin triggers "outside-in" signals, stimulates platelet activation, and controls primary hemostasis. *Faseb j* **26**, 2788-2798, doi:10.1096/fj.11-197541 (2012).
156 Vyakarnam, A., Dagher, S. F., Wang, J. L. & Patterson, R. J. Evidence for a role for galectin-1 in pre-mRNA splicing. *Mol Cell Biol* **17**, 4730-4737, doi:10.1128/mcb.17.8.4730 (1997).
157 Endharti, A. T., Zhou, Y. W., Nakashima, I. & Suzuki, H. Galectin-1 supports survival of naive T cells without promoting cell proliferation. *Eur J Immunol* **35**, 86-97, doi:10.1002/eji.200425340 (2005).
158 Stowell, S. R. *et al.* Differential roles of galectin-1 and galectin-3 in regulating leukocyte viability and cytokine secretion. *J Immunol* **180**, 3091-3102, doi:10.4049/jimmunol.180.5.3091 (2008).
159 van der Leij, J. *et al.* Dimeric galectin-1 induces IL-10 production in T-lymphocytes: an important tool in the regulation of the immune response. *J Pathol* **204**, 511-518, doi:10.1002/path.1671 (2004).
160 Tribulatti, M. V., Figini, M. G., Carabelli, J., Cattaneo, V. & Campetella, O. Redundant and antagonistic functions of galectin-1, -3, and -8 in the elicitation of T cell responses. *J Immunol* **188**, 2991-2999, doi:10.4049/jimmunol.1102182 (2012).
161 Anginot, A., Espeli, M., Chasson, L., Mancini, S. J. & Schiff, C. Galectin 1 modulates plasma cell homeostasis and regulates the humoral immune response. *J Immunol* **190**, 5526-5533, doi:10.4049/jimmunol.1201885 (2013).
162 Thijssen, V. L. *et al.* Galectin-1 is essential in tumor angiogenesis and is a target for antiangiogenesis therapy. *Proc Natl Acad Sci USA* **103**, 15975-15980, doi:10.1073/pnas.0603883103 (2006).

163 Paz, A., Haklai, R., Elad-Sfadia, G., Ballan, E. & Kloog, Y. Galectin-1 binds oncogenic H-Ras to mediate Ras membrane anchorage and cell transformation. *Oncogene* **20**, 7486-7493, doi:10.1038/sj.onc.1204950 (2001).
164 Soldati, R. *et al.* Neuroblastoma triggers an immunoevasive program involving galectin-1-dependent modulation of T cell and dendritic cell compartments. *Int J Cancer* **131**, 1131-1141, doi:10.1002/ijc.26498 (2012).
165 Dalotto-Moreno, T. *et al.* Targeting galectin-1 overcomes breast cancer-associated immunosuppression and prevents metastatic disease. *Cancer Res* **73**, 1107-1117, doi:10.1158/0008-5472.Can-12-2418 (2013).
166 Moiseeva, E. P., Spring, E. L., Baron, J. H. & de Bono, D. P. Galectin 1 modulates attachment, spreading and migration of cultured vascular smooth muscle cells via interactions with cellular receptors and components of extracellular matrix. *J Vasc Res* **36**, 47-58, doi:10.1159/000025625 (1999).
167 Moiseeva, E. P., Williams, B., Goodall, A. H. & Samani, N. J. Galectin-1 interacts with beta-1 subunit of integrin. *Biochem Biophys Res Commun* **310**, 1010-1016, doi:10.1016/j.bbrc.2003.09.112 (2003).
168 Reynolds, N. M. *et al.* Galectin-1 Influences Breast Cancer Cell Adhesion to E-selectin Via Ligand Intermediaries. *Cell Mol Bioeng* **11**, 37-52, doi:10.1007/s12195-017-0512-9 (2018).
169 Rabinovich, G. A. *et al.* Specific inhibition of T-cell adhesion to extracellular matrix and proinflammatory cytokine secretion by human recombinant galectin-1. *Immunology* **97**, 100-106, doi:10.1046/j.1365-2567.1999.00746.x (1999).
170 van den Brûle, F. A. *et al.* Galectin-1 modulates human melanoma cell adhesion to laminin. *Biochem Biophys Res Commun* **209**, 760-767, doi:10.1006/bbrc.1995.1564 (1995).
171 Jing, L. *et al.* Differential expression of galectin-1 and its interactions with cells and laminins in the intervertebral disc. *J Orthop Res* **30**, 1923-1931, doi:10.1002/jor.22158 (2012).
172 Ramkumar, R. & Podder, S. K. Elucidation of the mechanism of interaction of sheep spleen galectin-1 with splenocytes and its role in cell-matrix adhesion. *J Mol Recognit* **13**, 299-309, doi:10.1002/1099-1352(200009/10)13:5<299::Aid-jmr504>3.0.Co;2-o (2000).
173 van den Brûle, F. *et al.* Galectin-1 accumulation in the ovary carcinoma peritumoral stroma is induced by ovary carcinoma cells and affects both cancer cell proliferation and adhesion to laminin-1 and fibronectin. *Lab Invest* **83**, 377-386, doi:10.1097/01.lab.0000059949.01480.40 (2003).
174 Horiguchi, N. *et al.* Galectin-1 induces cell adhesion to the extracellular matrix and apoptosis of non-adherent human colon cancer Colo201 cells. *J Biochem* **134**, 869-874, doi:10.1093/jb/mvg213 (2003).
175 Tsai, M. S. *et al.* Galectin-1 Restricts Vascular Smooth Muscle Cell Motility Via Modulating Adhesion Force and Focal Adhesion Dynamics. *Sci Rep* **8**, 11497, doi:10.1038/s41598-018-29843-3 (2018).
176 Mercier, S. *et al.* Galectin-1 promotes HIV-1 infectivity in macrophages through stabilization of viral adsorption. *Virology* **371**, 121-129, doi:10.1016/j.virol.2007.09.034 (2008).
177 Reynolds, J. L. *et al.* Morphine and galectin-1 modulate HIV-1 infection of human monocyte-derived macrophages. *J Immunol* **188**, 3757-3765, doi:10.4049/jimmunol.1102276 (2012).
178 Tamai, R., Kobayashi-Sakamoto, M. & Kiyoura, Y. Extracellular galectin-1 enhances adhesion to and invasion of oral epithelial cells by Porphyromonas gingivalis. *Can J Microbiol* **64**, 465-471, doi:10.1139/cjm-2017-0461 (2018).
179 Nita-Lazar, M. *et al.* Desialylation of airway epithelial cells during influenza virus infection enhances pneumococcal adhesion via galectin binding. *Mol Immunol* **65**, 1-16, doi:10.1016/j.molimm.2014.12.010 (2015).
180 Abdallah, B. M. *et al.* Maintenance of differentiation potential of human bone marrow mesenchymal stem cells immortalized by human telomerase reverse transcriptase gene despite [corrected] extensive proliferation. *Biochem Biophys Res Commun* **326**, 527-538, doi:10.1016/j.bbrc.2004.11.059 (2005).

181 Simonsen, J. L. *et al.* Telomerase expression extends the proliferative life-span and maintains the osteogenic potential of human bone marrow stromal cells. *Nat Biotechnol* **20**, 592-596, doi:10.1038/nbt0602-592 (2002).
182 Fernandez-Rebollo, E. *et al.* Human Platelet Lysate versus Fetal Calf Serum: These Supplements Do Not Select for Different Mesenchymal Stromal Cells. *Sci Rep* **7**, 5132, doi:10.1038/s41598-017-05207-1 (2017).
183 Ebert, R. *et al.* Selenium supplementation restores the antioxidative capacity and prevents cell damage in bone marrow stromal cells in vitro. *Stem Cells* **24**, 1226-1235, doi:10.1634/stemcells.2005-0117 (2006).
184 Pfaffl, M. W. A new mathematical model for relative quantification in real-time RT-PCR. *Nucleic Acids Res* **29**, e45, doi:10.1093/nar/29.9.e45 (2001).
185 Wolf, N., Kersting, L., Herok, C., Mihm, C. & Seibel, J. High-Yielding Water-Soluble Asymmetric Cyanine Dyes for Labeling Applications. *J Org Chem* **85**, 9751-9760, doi:10.1021/acs.joc.0c01084 (2020).
186 Schindelin, J. *et al.* Fiji: an open-source platform for biological-image analysis. *Nat Methods* **9**, 676-682, doi:10.1038/nmeth.2019 (2012).
187 Gerum, R. *et al.* Viscoelastic properties of suspended cells measured with shear flow deformation cytometry. *bioRxiv*, 2022.2001.2011.475843, doi:10.1101/2022.01.11.475843 (2022).
188 Aigouy, B. & Mirouse, V. ScientiFig: a tool to build publication-ready scientific figures. *Nat Methods* **10**, 1048, doi:10.1038/nmeth.2692 (2013).
189 Han, S. S. *et al.* Safety and Optimization of Metabolic Labeling of Endothelial Progenitor Cells for Tracking. *Sci Rep* **8**, 13212, doi:10.1038/s41598-018-31594-0 (2018).
190 Qin, W. *et al.* Artificial Cysteine S-Glycosylation Induced by Per-O-Acetylated Unnatural Monosaccharides during Metabolic Glycan Labeling. *Angew Chem Int Ed Engl* **57**, 1817-1820, doi:10.1002/anie.201711710 (2018).
191 Gutmann, M. *et al.* Biocompatible Azide-Alkyne "Click" Reactions for Surface Decoration of Glyco-Engineered Cells. *Chembiochem* **17**, 866-875, doi:10.1002/cbic.201500582 (2016).
192 Bai, K. & Wang, W. Shear stress-induced redistribution of the glycocalyx on endothelial cells in vitro. *Biomech Model Mechanobiol* **13**, 303-311, doi:10.1007/s10237-013-0502-3 (2014).
193 Montini, E. *et al.* Hematopoietic stem cell gene transfer in a tumor-prone mouse model uncovers low genotoxicity of lentiviral vector integration. *Nat Biotechnol* **24**, 687-696, doi:10.1038/nbt1216 (2006).
194 Montini, E. *et al.* The genotoxic potential of retroviral vectors is strongly modulated by vector design and integration site selection in a mouse model of HSC gene therapy. *J Clin Invest* **119**, 964-975, doi:10.1172/jci37630 (2009).
195 Liu, X., Kim, C. N., Yang, J., Jemmerson, R. & Wang, X. Induction of apoptotic program in cell-free extracts: requirement for dATP and cytochrome c. *Cell* **86**, 147-157, doi:10.1016/s0092-8674(00)80085-9 (1996).
196 Leist, M., Single, B., Castoldi, A. F., Kühnle, S. & Nicotera, P. Intracellular adenosine triphosphate (ATP) concentration: a switch in the decision between apoptosis and necrosis. *J Exp Med* **185**, 1481-1486, doi:10.1084/jem.185.8.1481 (1997).
197 Zou, H., Li, Y., Liu, X. & Wang, X. An APAF-1.cytochrome c multimeric complex is a functional apoptosome that activates procaspase-9. *J Biol Chem* **274**, 11549-11556, doi:10.1074/jbc.274.17.11549 (1999).
198 Seyrek, K., Richter, M. & Lavrik, I. N. Decoding the sweet regulation of apoptosis: the role of glycosylation and galectins in apoptotic signaling pathways. *Cell Death Differ* **26**, 981-993, doi:10.1038/s41418-019-0317-6 (2019).
199 Besanceney-Webler, C. *et al.* Increasing the efficacy of bioorthogonal click reactions for bioconjugation: a comparative study. *Angew Chem Int Ed Engl* **50**, 8051-8056, doi:10.1002/anie.201101817 (2011).

200 Neufeld, E. F. Formation and epimerization of dTDP-D-galactose catalyzed by plant enzymes. *Biochemical and Biophysical Research Communications* **7**, 461-466, doi:10.1016/0006-291X(62)90336-4 (1962).
201 Rose, I. A., O'Connell, E. L. & Schray, K. J. Mannose 6-Phosphate: Anomeric Form Used by Phosphomannose Isomerase and Its l-Epimerization by Phosphoglucose Isomerase. *Journal of Biological Chemistry* **248**, 2232-2234, doi:10.1016/S0021-9258(19)44210-5 (1973).
202 Barber, G. A. Observations on the mechanism of the reversible epimerization of GDP-D-mannose to GDP-L-galactose by an enzyme from Chlorella pyrenoidosa. *Journal of Biological Chemistry* **254**, 7600-7603, doi:10.1016/S0021-9258(18)35986-6 (1979).
203 Du, J. *et al.* Metabolic glycoengineering: sialic acid and beyond. *Glycobiology* **19**, 1382-1401, doi:10.1093/glycob/cwp115 (2009).
204 Yarema, K. J., Mahal, L. K., Bruehl, R. E., Rodriguez, E. C. & Bertozzi, C. R. Metabolic Delivery of Ketone Groups to Sialic Acid Residues: APPLICATION TO CELL SURFACE GLYCOFORM ENGINEERING*. *Journal of Biological Chemistry* **273**, 31168-31179, doi:10.1074/jbc.273.47.31168 (1998).
205 Chen, S. C. *et al.* Mechanism and inhibition of human UDP-GlcNAc 2-epimerase, the key enzyme in sialic acid biosynthesis. *Sci Rep* **6**, 23274, doi:10.1038/srep23274 (2016).
206 Homann, A., Qamar, R. U., Serim, S., Dersch, P. & Seibel, J. Bioorthogonal metabolic glycoengineering of human larynx carcinoma (HEp-2) cells targeting sialic acid. *Beilstein J Org Chem* **6**, 24, doi:10.3762/bjoc.6.24 (2010).
207 Letschert, S. *et al.* Super-resolution imaging of plasma membrane glycans. *Angew Chem Int Ed Engl* **53**, 10921-10924, doi:10.1002/anie.201406045 (2014).
208 Dold, J. & Wittmann, V. Metabolic Glycoengineering with Azide- and Alkene-Modified Hexosamines: Quantification of Sialic Acid Levels. *Chembiochem*, doi:10.1002/cbic.202000715 (2020).
209 Almaraz, R. T. *et al.* Metabolic oligosaccharide engineering with N-Acyl functionalized ManNAc analogs: cytotoxicity, metabolic flux, and glycan-display considerations. *Biotechnol Bioeng* **109**, 992-1006, doi:10.1002/bit.24363 (2012).
210 Chang, P. V. *et al.* Metabolic labeling of sialic acids in living animals with alkynyl sugars. *Angew Chem Int Ed Engl* **48**, 4030-4033, doi:10.1002/anie.200806319 (2009).
211 Wang, G. *et al.* Shear Stress Regulation of Endothelial Glycocalyx Structure Is Determined by Glucobiosynthesis. *Arterioscler Thromb Vasc Biol* **40**, 350-364, doi:10.1161/atvbaha.119.313399 (2020).
212 Feng, L. *et al.* Bifunctional unnatural sialic acids for dual metabolic labeling of cell-surface sialylated glycans. *J Am Chem Soc* **135**, 9244-9247, doi:10.1021/ja402326z (2013).
213 Bardor, M., Nguyen, D. H., Diaz, S. & Varki, A. Mechanism of uptake and incorporation of the non-human sialic acid N-glycolylneuraminic acid into human cells. *J Biol Chem* **280**, 4228-4237, doi:10.1074/jbc.M412040200 (2005).
214 Mancini, G. M., de Jonge, H. R., Galjaard, H. & Verheijen, F. W. Characterization of a proton-driven carrier for sialic acid in the lysosomal membrane. Evidence for a group-specific transport system for acidic monosaccharides. *J Biol Chem* **264**, 15247-15254 (1989).
215 Aula, N., Jalanko, A., Aula, P. & Peltonen, L. Unraveling the molecular pathogenesis of free sialic acid storage disorders: altered targeting of mutant sialin. *Mol Genet Metab* **77**, 99-107, doi:10.1016/s1096-7192(02)00124-5 (2002).
216 Oetke, C. *et al.* Evidence for efficient uptake and incorporation of sialic acid by eukaryotic cells. *Eur J Biochem* **268**, 4553-4561, doi:10.1046/j.1432-1327.2001.02379.x (2001).
217 Bulai, T., Bratosin, D., Artenie, V. & Montreuil, J. Uptake of sialic acid by human erythrocyte. Characterization of a transport system. *Biochimie* **85**, 241-244, doi:10.1016/s0300-9084(03)00059-2 (2003).
218 Qin, L. *et al.* Sialin (SLC17A5) functions as a nitrate transporter in the plasma membrane. *Proc Natl Acad Sci USA* **109**, 13434-13439, doi:10.1073/pnas.1116633109 (2012).

219 Oetke, C. *et al.* Versatile biosynthetic engineering of sialic acid in living cells using synthetic sialic acid analogues. *J Biol Chem* **277**, 6688-6695, doi:10.1074/jbc.M109973200 (2002).
220 Lehmann, J., Wright, M. H. & Sieber, S. A. Making a Long Journey Short: Alkyne Functionalization of Natural Product Scaffolds. *Chemistry* **22**, 4666-4678, doi:10.1002/chem.201504419 (2016).
221 Wiesinger, A. *et al.* Nanomechanics of the endothelial glycocalyx in experimental sepsis. *PLoS One* **8**, e80905, doi:10.1371/journal.pone.0080905 (2013).
222 Kadri, T. *et al.* Proteomic study of Galectin-1 expression in human mesenchymal stem cells. *Stem Cells Dev* **14**, 204-212, doi:10.1089/scd.2005.14.204 (2005).
223 Zhang, Y. *et al.* Bone Marrow Mesenchymal Stem Cells Inhibit the Function of Dendritic Cells by Secreting Galectin-1. *Biomed Res Int* **2017**, 3248605, doi:10.1155/2017/3248605 (2017).
224 Bertleff-Zieschang, N. *et al.* Exploring the Structural Space of the Galectin-1-Ligand Interaction. *Chembiochem* **18**, 1477-1481, doi:10.1002/cbic.201700251 (2017).
225 Suzuki, O., Nozawa, Y. & Abe, M. The regulatory roles of cell surface sialylation and N-glycans in human B cell lymphoma cell adhesion to galectin-1. *Int J Oncol* **28**, 155-160 (2006).
226 Suzuki, O. & Abe, M. Galectin-1-mediated cell adhesion, invasion and cell death in human anaplastic large cell lymphoma: regulatory roles of cell surface glycans. *Int J Oncol* **44**, 1433-1442, doi:10.3892/ijo.2014.2319 (2014).
227 Dabelsteen, E., Vedtofte, P., Hakomori, S. & Young, W. W., Jr. Accumulation of a blood group antigen precursor in oral premalignant lesions. *Cancer Res* **43**, 1451-1454 (1983).
228 Fernandes, B., Sagman, U., Auger, M., Demetrio, M. & Dennis, J. W. β1–6 Branched Oligosaccharides as a Marker of Tumor Progression in Human Breast and Colon Neoplasia. *Cancer Research* **51**, 718-723 (1991).
229 Miyake, M., Taki, T., Hitomi, S. & Hakomori, S. Correlation of expression of H/Le(y)/Le(b) antigens with survival in patients with carcinoma of the lung. *N Engl J Med* **327**, 14-18, doi:10.1056/nejm199207023270103 (1992).
230 Dings, R. P. M., Kumar, N., Mikkelson, S., Gabius, H. J. & Mayo, K. H. Simulating cellular galectin networks by mixing galectins in vitro reveals synergistic activity. *Biochem Biophys Rep* **28**, 101116, doi:10.1016/j.bbrep.2021.101116 (2021).
231 Haider, M. S. *et al.* Tuning the Thermogelation and Rheology of Poly(2-Oxazoline)/Poly(2-Oxazine)s Based Thermosensitive Hydrogels for 3D Bioprinting. *Gels* **7**, doi:10.3390/gels7030078 (2021).
232 Thonhoff, J. R., Lou, D. I., Jordan, P. M., Zhao, X. & Wu, P. Compatibility of human fetal neural stem cells with hydrogel biomaterials in vitro. *Brain Res* **1187**, 42-51, doi:10.1016/j.brainres.2007.10.046 (2008).
233 Mortensen, K. & Talmon, Y. Cryo-TEM and SANS Microstructural Study of Pluronic Polymer Solutions. *Macromolecules* **28**, 8829-8834, doi:10.1021/ma00130a016 (1995).
234 Bonné, T. B., Lüdtke, K., Jordan, R., Štěpánek, P. & Papadakis, C. M. Aggregation behavior of amphiphilic poly(2-alkyl-2-oxazoline) diblock copolymers in aqueous solution studied by fluorescence correlation spectroscopy. *Colloid and Polymer Science* **282**, 833-843, doi:10.1007/s00396-004-1131-2 (2004).
235 Birukov, K. G. *et al.* Shear stress-mediated cytoskeletal remodeling and cortactin translocation in pulmonary endothelial cells. *Am J Respir Cell Mol Biol* **26**, 453-464, doi:10.1165/ajrcmb.26.4.4725 (2002).
236 Pavalko, F. M. *et al.* Fluid shear-induced mechanical signaling in MC3T3-E1 osteoblasts requires cytoskeleton-integrin interactions. *Am J Physiol* **275**, C1591-1601 (1998).
237 Raasch, M. *et al.* Microfluidically supported biochip design for culture of endothelial cell layers with improved perfusion conditions. *Biofabrication* **7**, 015013, doi:10.1088/1758-5090/7/1/015013 (2015).
238 Zhao, L., Li, X., Niu, P. & Li, L. The effect of shear on the cytoskeleton remodeling and physiological performance of myocardium cells through Tmod1. *RSC Advances* **8**, 33347-33353, doi:10.1039/C8RA05982A (2018).

239 Sharir, A., Stern, T., Rot, C., Shahar, R. & Zelzer, E. Muscle force regulates bone shaping for optimal load-bearing capacity during embryogenesis. *Development* **138**, 3247-3259, doi:10.1242/dev.063768 (2011).

240 Ogasawara, A. *et al.* Fluid Shear Stress-induced Cyclooxygenase-2 Expression Is Mediated by C/EBP β, cAMP-response Element-binding Protein, and AP-1 in Osteoblastic MC3T3-E1 Cells*. *Journal of Biological Chemistry* **276**, 7048-7054, doi:10.1074/jbc.M008070200 (2001).

241 Ziouti, F. *et al.* NOTCH Signaling Is Activated through Mechanical Strain in Human Bone Marrow-Derived Mesenchymal Stromal Cells. *Stem Cells Int* **2019**, 5150634, doi:10.1155/2019/5150634 (2019).

242 Weinbaum, S., Zhang, X., Han, Y., Vink, H. & Cowin, S. C. Mechanotransduction and flow across the endothelial glycocalyx. *Proc Natl Acad Sci USA* **100**, 7988-7995, doi:10.1073/pnas.1332808100 (2003).

Annex

List of Figures

Figure 1: Mesenchymal Stromal Cells (MSC) as Interface between Tissue Maturation, Regeneration, and Repair. 1
Figure 2: Schematic Model of the Cell Glycocalyx. 3
Figure 3: Principle of Metabolic Glycoengineering. 5
Figure 4: Principle of Azide-Alkyne 1,3-dipolar Cycloaddition (AAC) Click Reaction. 6
Figure 5: Biofabrication Steps in Tissue Engineering. 8
Figure 6: Shear Forces in a cylindrical Bioprinter Nozzle. 10
Figure 7: Binding Sites for Galectins and possible Functions. 11
Figure 8: Modified Monosaccharides and Target Molecules for Metabolic Glycoengineering used in this Project. 19
Figure 9: Bioinks used in this Project. 21
Figure 10: Cell Viability of human Mesenchymal Stromal Cells (hMSC) and Telomerase-immortalized hMSC after Treatment with peracetylated modified Monosaccharides. ... 24
Figure 11: Cell Viability of human Mesenchymal Stromal Cells (hMSC) and Telomerase-immortalized hMSC after Treatment with non-acetylated modified Monosaccharides. . 25
Figure 12: Cell Viability of human Mesenchymal Stromal Cells (hMSC) and Telomerase-immortalized hMSC after Treatment with Cu. 26
Figure 13: Differentiation Capacity and Gene Expression of Telomerase-immortalized human Mesenchymal Stromal Cells (hMSC-TERT) after 72 h Incubation with peracetylated *N*-azidoacetylmannosamine (Ac_4ManNAz) or peracetylated *N*-alkyneacetylmannosamine (Ac_4ManNAl). 28
Figure 14: Incorporation of peracetylated *N*-azidoacetylmannosamine (Ac_4ManNAz) (25 μM) into the Glycocalyx of primary human Mesenchymal Stromal Cells (hMSC) and Telomerase-immortalized hMSC after 48 h Incubation. 29
Figure 15: Incorporation of peracetylated Azido/Alkyne Monosaccharides into the Glycocalyx of Telomerase-immortalized human Mesenchymal Stromal Cells (hMSC-TERT) after 72 h Incubation ... 30
Figure 16: Temporal Course of the Decline of Glycocalyx Modification in Telomerase-immortalized human Mesenchymal Stromal Cells (hMSC-TERT) after 72 h Incubation with peracetylated *N*-azidoacetylmannosamine (Ac_4ManNAz) or peracetylated *N*-alkyneacetylmannosamine (Ac_4ManNAl) (20 μM). 31
Figure 17: Incorporation of Azido/Alkyne Monosaccharides into the Glycocalyx of primary human Mesenchymal Stromal Cells (hMSC) after 72 h Incubation. 33

Figure 18: Incorporation of Azido/Alkyne Monosaccharides into the Glycocalyx of Telomerase-immortalized human Mesenchymal Stromal Cells (hMSC-TERT) after 72 h Incubation. 34
Figure 19: Galectin 1 Expression in human Mesenchymal Stromal Cells (hMSC) and Telomerase-immortalized hMSC (hMSC-TERT). 35
Figure 20: Biomechanical Features of Telomerase-immortalized human Mesenchymal Stromal Cells (hMSC-TERT) after Introduction of Target Molecules Coumarin Derivative AG13 or Galectin 1 Ligand JM139 into the Glycocalyx via Copper-catalyzed Azide–Alkyne Cycloaddition (CuAAC) Click Reaction. 36
Figure 21: Viability of Telomerase-immortalized human Mesenchymal Stromal Cells (hMSC-TERT) after Processing in Pluronic F127 or POx-POzi Bioink. 37
Figure 22: Cytoskeleton Formation in Telomerase-immortalized human Mesenchymal Stromal Cells (hMSC-TERT) after Processing in Pluronic F127 or POx-POzi Bioink. 38
Figure 23: Expression of mechanoresponsive Genes in Telomerase-immortalized human Mesenchymal Stromal Cells (hMSC-TERT) or Luciferase Activity in hMSC-TERT-AP1 after Processing in Pluronic F127 or POx-POzi Bioink. 40

List of Tables

Table 1: Antibodies (class G) used for immunocytochemical Analyses. 16
Table 2: Primers used for Gene Expression Analyses. 18
Table 3: Composition of Luciferase Buffer. 22

Statement on Copyright & Self-Plagiarism

Parts of this work were published earlier in the original article “Metabolic Glycoengineering in hMSC-TERT as a Model for Skeletal Precursors by Using Modified Azide/Alkyne Monosaccharides” in the peer-reviewed International Journal of Molecular Sciences by the Multidisciplinary Digital Publishing Institute. Its content is distributed under an open access Creative Commons Attribution License and copyright was retained by the authors. Text and figures from this article were partly reused in this thesis in identical or modified form, as I, Stephan Altmann, was mainly responsible for the generation, evaluation and visualization of data as well as writing the manuscript.

Altmann, S., Mut, J., Wolf, N., Meißner-Weigl, J., Rudert, M., Jakob, F., Gutmann, M., Lühmann, T., Seibel, J., Ebert, R. Metabolic Glycoengineering in hMSC-TERT as a Model for Skeletal Precursors by Using Modified Azide/Alkyne Monosaccharides. *Int J Mol Sci* **22**, 2820, doi:10.3390/ijms22062820 (2021).

Affidavit

Affidavit

I hereby confirm that my thesis entitled “Characterization of Metabolic Glycoengineering in Mesenchymal Stromal Cells for its Application in thermoresponsive Bioinks” is the result of my own work. I did not receive any help or support from commercial consultants. All sources and materials applied are listed and specified in the thesis.

Furthermore, I confirm that this thesis has not yet been submitted as part of another examination process neither in identical nor in similar form.

Place, Date Signature

Eidesstattliche Erklärung

Hiermit erkläre ich an Eides statt, die Dissertation “Charakterisierung von *Metabolic Glycoengineering* in mesenchymalen Stromazellen für die Anwendung in thermoresponsiven Biotinten” eigenständig, d. h. insbesondere selbstständig und ohne Hilfe eines kommerziellen Promotionsberaters, angefertigt und keine anderen als die von mir angegebenen Quellen und Hilfsmittel verwendet zu haben.

Ich erkläre außerdem, dass die Dissertation weder in gleicher noch in ähnlicher Form bereits in einem anderen Prüfungsverfahren vorgelegen hat.

Ort, Datum Unterschrift

Acknowledgements

First of all, I would like to thank Prof. Dr. Regina Ebert and Prof. Dr. Jürgen Seibel for giving me the opportunity to be part of this really interesting project. This particular combination of glycobiology and biofabrication caught my attention and finally motivated me to break new grounds.

My biggest and warmest appreciation belongs to my supervisor Prof. Dr. Regina Ebert, who believed in me from the first day. Our work relationship felt almost like a friendship and that trustful freedom allowed me not only to explore my own scientific skills, but also to implement own ideas regarding the project contents. I really appreciated that I received fast feedback from her whenever I needed it, even if she was busy with other projects. Although scientifically new for both of us in the beginning, we grew as a team with this project and demonstrated within the biofabrication consortium that also unusual project ideas can be fruitful in one way or another. We shared something that is often being forgotten in the success-driven and competitive science: staying down to earth and remembering that scientists are only humans as well. Thank you, Regina, for all your optimism and smiles that I was grateful to return!

Further, I would like to thank my two other supervisors, Prof. Dr. Jürgen Seibel and Prof. Dr. Stephan Gekle, for their scientific support by sharing their knowledge and providing me helpful advices.

A big thanks must be given to Dr. Stephanie Graser and PD Dr. Marietta Herrmann as both had always an open ear for my questions and more importantly very helpful answers. We had nice talks and I remember a funny rainy city trip during our visit of the ECTS conference in Budapest!

In the lab, I received a nice introduction and good support when needed from Sabine Zeck, Jutta Meißner-Weigl, Doris Schneider, and Melanie Krug, while Dr. Sigrid Müller-Deubert and Martin Kuric occasionally helped me with scientific questions. Thank you all for the nice working atmosphere and the lively and interesting talks during our lunch breaks!

Among many PhD peers I met during my thesis time within the biofabrication consortium, I would like to thank Jürgen Mut, Lukas Hahn, Ruben Scheuring and Sebastian Müller for their support, especially in form of interesting discussions adding new aspects from their scientific background to my point of view.

Furthermore, I would like to thank Jennifer Elsterer for her support with the cell stiffness measurements and Maria Danz for her support with the printing experiments.

Finally, I was glad to be part of such wonderful and well-planned research consortium (TRR 225 'From the Fundamentals of Biofabrication toward functional Tissue Models') providing their PhD candidates a nice research environment including regular retreats, interesting summer schools, travel fundings, the possibility to request student research helpers and much more. Although the 17 subprojects were distributed over three cities, being united at the retreats felt somehow like a big family reunion and was fun as well!

This structured program was well supported and supervised by the Graduate School of Life Sciences and I really liked their transferable skill courses which helped me to improve the management of all research-related tasks outside of the lab. Toward the end of the promotion time, I had a lot of questions during the submission process and was thankful for the fast and great support I received at that time.